

# From low-momentum interactions to nuclear structure

S.K. Bogner<sup>1</sup>, R.J. Furnstahl<sup>2</sup>, A. Schwenk<sup>3,4,5</sup>

<sup>1</sup> National Superconducting Cyclotron Laboratory and  
Department of Physics and Astronomy,

Michigan State University, East Lansing, MI 48844, USA

<sup>2</sup> Department of Physics, The Ohio State University, Columbus, OH 43210, USA

<sup>3</sup> TRIUMF, 4004 Wesbrook Mall, Vancouver, BC, V6T 2A3, Canada

<sup>4</sup> ExtreMe Matter Institute EMMI,

GSI Helmholtzzentrum für Schwerionenforschung GmbH,  
64291 Darmstadt, Germany

<sup>5</sup> Institut für Kernphysik, Technische Universität Darmstadt,  
64289 Darmstadt, Germany

April 15, 2019

## Abstract

We present an overview of low-momentum two-nucleon and many-body interactions and their use in calculations of nuclei and infinite matter. The softening of phenomenological and effective field theory (EFT) potentials by renormalization group (RG) transformations that decouple low and high momenta leads to greatly enhanced convergence in few- and many-body systems while maintaining a decreasing hierarchy of many-body forces. This review surveys the RG-based technology and results, discusses the connections to chiral EFT, and clarifies various misconceptions.

*Keywords:* Nuclear forces, nuclear structure, renormalization group

## Contents

<b>1</b>	<b>Introduction</b>	<b>2</b>
1.1	Nuclear forces . . . . .	3
1.2	Nuclear structure challenges . . . . .	8
1.3	Renormalization group approaches . . . . .	11
1.4	Scope of the review . . . . .	13
<b>2</b>	<b>Renormalization group: motivation and principles</b>	<b>13</b>
2.1	Decoupling . . . . .	13
2.2	Connections to effective field theory . . . . .	15
2.3	Universality . . . . .	17
2.4	Perturbativeness . . . . .	17
2.5	Many-body interactions and operators . . . . .	22
2.6	Cutoff dependence as a tool . . . . .	24

<b>3</b>	<b>Low-momentum technology for two-nucleon interactions</b>	<b>25</b>
3.1	Sharp cutoff $V_{\text{low } k}$ . . . . .	25
3.2	Smooth regulators for $V_{\text{low } k}$ . . . . .	26
3.3	Similarity renormalization group (SRG) . . . . .	29
3.4	$V_{\text{low } k}$ from SRG flow equations . . . . .	32
3.5	Related methods . . . . .	33
<b>4</b>	<b>Many-body interactions and operators</b>	<b>35</b>
4.1	Three-nucleon interactions . . . . .	36
4.2	Three-nucleon force evolution . . . . .	38
4.3	In-medium SRG . . . . .	41
4.4	Effective operators . . . . .	44
<b>5</b>	<b>Applications to infinite matter</b>	<b>47</b>
5.1	Nuclear matter . . . . .	47
5.2	Neutron matter . . . . .	50
5.3	Pairing . . . . .	51
<b>6</b>	<b>Applications to finite nuclei</b>	<b>54</b>
6.1	Ab initio calculations . . . . .	54
6.2	Scattering and reactions . . . . .	57
6.3	Shell-model approaches . . . . .	58
6.4	Density functional theory . . . . .	60
<b>7</b>	<b>Summary and outlook</b>	<b>61</b>
7.1	Misconceptions and clarifications . . . . .	62
7.2	Open problems and opportunities . . . . .	65

# 1 Introduction

A new era is dawning for the theory of nuclear structure and reactions. Renewed interest in the physics of nuclei is fueled by experiments at rare isotope beam facilities, which open the door to new regions of exotic nuclei; by astrophysical observations and simulations of neutron stars and supernovae, which require controlled extrapolations of the equation of state of nucleonic matter in density, temperature, and proton fraction; and by studies of universal physics, which unite cold atom and dilute neutron physics [1–4]. The interplay and coalescence of different threads: rapidly increasing computational power, effective field theory (EFT), and renormalization group (RG) transformations are enabling the development of new many-body methods and the revival of old ones to successfully attack these problems.

A key to optimizing computational power for describing nuclei is a proper choice of degrees of freedom. While there is little doubt that quantum chromodynamics (QCD) is the correct underlying theory of strong interactions, the *efficient* low-energy degrees of freedom for nuclear structure are not quarks and gluons, but the colorless hadrons of traditional nuclear phenomenology. But this realization is not enough. For low-energy calculations to be computationally efficient (or even feasible in some cases) we need to exclude or, more generally, to *decouple* the high-energy degrees of freedom.

Progress on the nuclear many-body problem has been slowed for decades because nucleon-nucleon (NN) potentials that reproduce elastic scattering phase shifts typically have strong short-range repulsion and strong short-range tensor forces. The consequence is substantial coupling to high-energy modes, which is manifested as highly correlated many-body wave functions and highly nonperturbative few- and many-body systems. In recent years, new approaches to nuclear forces grounded in RG ideas

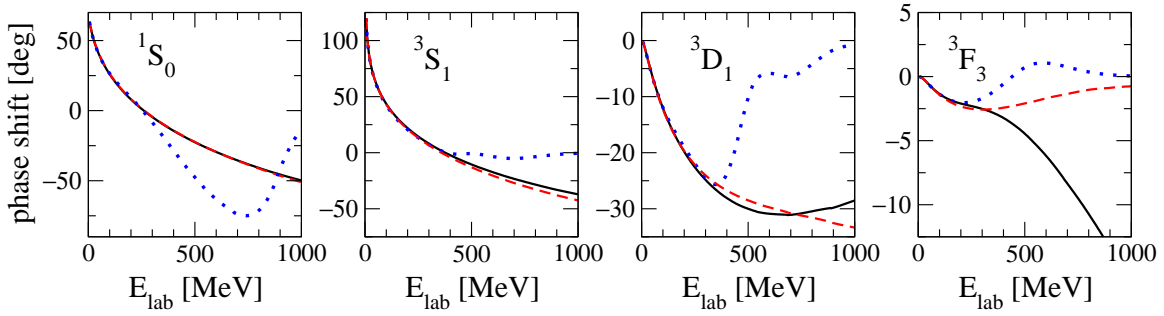


Figure 1: NN phase shifts for the Argonne  $v_{18}$  [18] (solid), CD-Bonn [19] (dashed), and one of the chiral  $N^3\text{LO}$  [20] (dotted) potentials in selected channels (using nonrelativistic kinematics). All agree with experiment up to about 300 MeV.

and techniques have been developed. The RG allows continuous changes in “resolution” that decouple the troublesome high-momentum modes and can be used to evolve interactions to nuclear structure energy and momentum scales while preserving low-energy observables [5–7]. Such potentials, known generically as “low-momentum interactions,” are more perturbative and generate much less correlated wave functions [8–17]. This greatly simplifies the nuclear many-body problem, making structure and reaction calculations more convergent, while variations of the resolution provide new tools to assess theoretical errors.

In this review, we survey the technical and phenomenological aspects of the low-momentum methods. Although there are multiple paths to low-momentum interactions, we focus on the RG-based techniques (known as “ $V_{\text{low } k}$ ” or “SRG” potentials), which provide new perspectives that mesh constructively with the developments of EFT for nuclear forces. When combined with advances in many-body methods and the increases in computer power, EFT and RG make feasible a controlled description, grounded in QCD symmetries, of nuclei across the nuclear many-body landscape. At the same time, the RG approach leads to reinterpretations of the physics or the role of different parts of the physics, such as what causes nuclear saturation. An unintended consequence is that many misconceptions or misinterpretations have arisen. A principal goal of this review is to address these.

## 1.1 Nuclear forces

Establishing an interparticle Hamiltonian, which is the most basic precursor to many-body calculations, is a difficult and on-going challenge for low-energy nuclear physics. The two-body sector has been “solved” in the sense that various interactions are available that reproduce phase shifts with  $\chi^2/\text{dof} \approx 1$  in the elastic regime (up to roughly 300–350 MeV energy in the laboratory frame, see Fig. 1). The unsettled frontier is three- and higher-body forces, although there remain important open questions about the systematic construction of NN potentials using EFT.

Figure 2(a) shows nuclear interactions in the  $^1S_0$  channel for several phenomenological NN potentials. The longest range feature is one-pion exchange, which is justified by quantum chromodynamics (via the spontaneous breaking of chiral symmetry) and is a common feature of most potentials. The midrange part, which has a net attraction, has usually been associated with two-pion and/or heavy meson exchange ( $\rho$ ,  $\omega$ , “ $\sigma$ ”). The short-range part of the potentials in Fig. 2(a) is a repulsive core (often called a “hard core”).

Nuclear structure calculations are complicated due to the *coupling* of low to high momenta by these potentials. This is made clear by the Fourier transform (that is, the Bessel transform in a given partial wave), as shown in Fig. 2(b). We feature the Argonne  $v_{18}$  potential [18] because it is used in the most successful high precision ( $\lesssim 1\%$  accuracy) nuclear structure calculations of nuclei with mass number  $A \leq 12$  [22–24]. For our purposes, the equivalent contour plot in Fig. 3(a) is a clearer representation

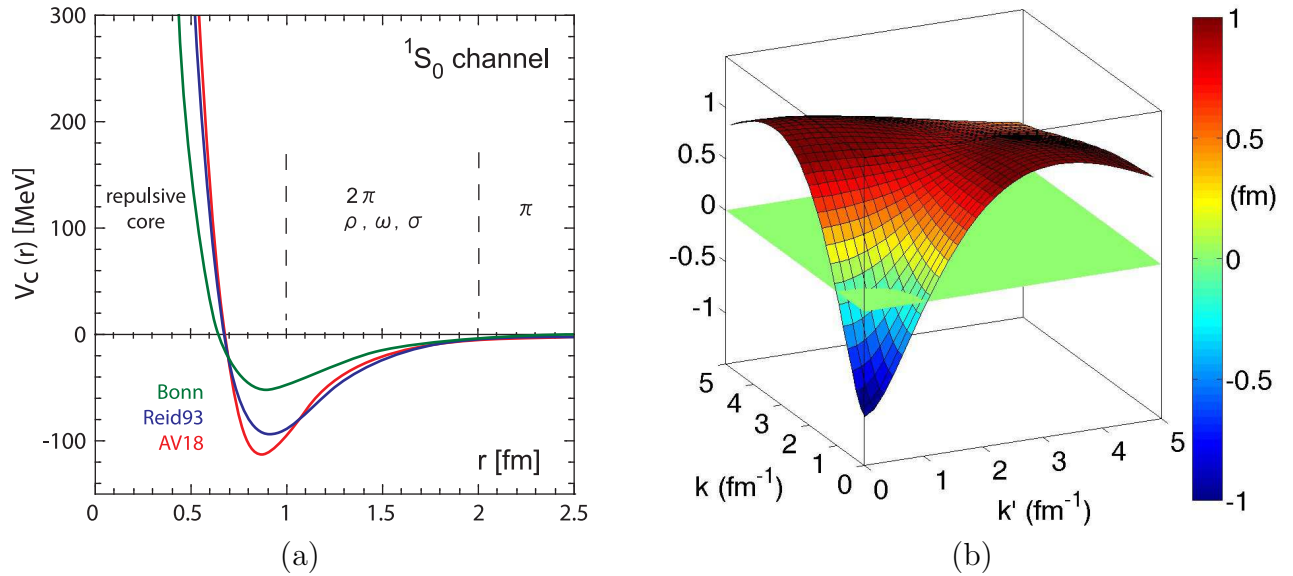


Figure 2: (a) Several phenomenological NN potentials in the  $^1S_0$  channel from Ref. [21]. (b) Momentum-space matrix elements of the Argonne  $v_{18}$  (AV18)  $^1S_0$  potential after Fourier (Bessel) transformation.<sup>1</sup>

and we use such plots throughout this review.<sup>1</sup> The elastic regime for NN scattering corresponds to relative momenta  $k \lesssim 2 \text{ fm}^{-1}$ . The strong low- to high-momentum coupling driven by the short-range repulsion is manifested in Fig. 3(a) by the large regions of non-zero off-diagonal matrix elements. A consequence is a suppression of probability in the relative wave function (“short-range correlations”), as seen for the deuteron in Fig. 3(b).

The potentials in Fig. 2(a) are partial-wave local; that is, in each partial wave they are functions of the separation  $r$  alone. This condition, which simplifies certain types of numerical calculations,<sup>2</sup> constrains the radial dependence to be similar to Fig. 2(a) if the potential is to reproduce elastic phase shifts, and in particular necessitates a strong short-range repulsion in the S-waves. The similarity of all such potentials, perhaps combined with experience from the Coulomb potential, has led to the (often implicit) misconception that the nuclear potential must have this form. This prejudice has been reinforced recently by QCD lattice calculations that apparently validate a repulsive core [25–28].

For finite-mass composite particles, locality is a feature we expect at long distances, but non-local interactions would be more natural at short distances. In fact, the potential at short range is far removed from an observable, and locality is imposed on potentials for convenience, not because of physical necessity. Recall that we are free to apply a short-range unitary transformation  $U$  to the Hamiltonian (and to other operators at the same time),

$$E_n = \langle \Psi_n | H | \Psi_n \rangle = (\langle \Psi_n | U^\dagger) U H U^\dagger (U | \Psi_n \rangle) = \langle \tilde{\Psi}_n | \tilde{H} | \tilde{\Psi}_n \rangle, \quad (1)$$

and the physics described by  $H$  and  $\tilde{H}$  is indistinguishable by experiment. Thus there are an *infinite* number of equally valid potentials, and once we allow non-locality, a repulsive core and the strong low- to high-momentum coupling is no longer inevitable.

The EFT approach uses this freedom to construct a systematic expansion of the Hamiltonian. A particular EFT is associated with a momentum scale  $\Lambda_b$  that is the dividing point between resolved,

<sup>1</sup>In units where  $\hbar = c = m = 1$  (with nucleon mass  $m$ ), the momentum-space potential is given in fm. In addition, we typically express momenta in  $\text{fm}^{-1}$  (the conversion to MeV is using  $\hbar c \approx 197 \text{ MeV fm}$ ).

<sup>2</sup>For example, in current implementations of Green’s Function Monte Carlo (GFMC) calculations [22], the potential must be (almost) diagonal in coordinate space, such as the Argonne  $v_{18}$  potential.

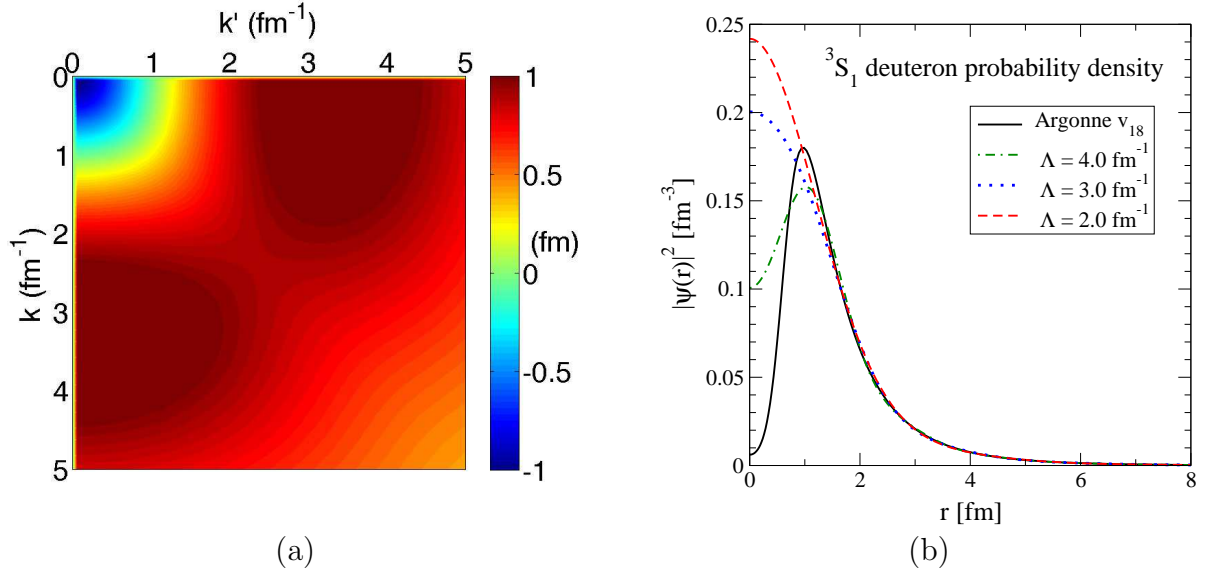


Figure 3: (a) Momentum-space matrix elements of the Argonne  $v_{18}$   $^1S_0$  potential. (b) Probability density for the S-wave part of the deuteron wave function for Argonne  $v_{18}$  and smooth  $V_{\text{low } k}$  potentials with several cutoffs  $\Lambda$ . The probability suppression at short distances is called “short-range correlation”.

long-range physics, which is treated explicitly, and unresolved, short-range physics, which is expanded in contact interactions. Results are given order-by-order in  $Q/\Lambda_b$ , where  $Q$  is a generic momentum (or light mass) scale of the process being calculated. There is also a cutoff  $\Lambda$  needed to regulate the theory, which suppresses high momenta. Thus  $\Lambda$  acts as a resolution scale for the theory. If  $\Lambda$  is chosen to be less than  $\Lambda_b$ , then the truncation error for the EFT will be dominated by powers of  $Q/\Lambda$  rather than  $Q/\Lambda_b$ . In principle one could take  $\Lambda$  as large as desired but in practice this only works if the renormalization and the numerics involved in matching to data are sufficiently under control [29].

In general, the forces between nucleons depend on the resolution scale  $\Lambda$  and are given by an effective theory for scale-dependent two-nucleon  $V_{\text{NN}}(\Lambda)$  and corresponding many-nucleon interactions  $V_{3\text{N}}(\Lambda)$ ,  $V_{4\text{N}}(\Lambda)$  and so on [5, 30, 31]. This scale dependence is analogous to the scale dependence of parton distribution functions. At very low momenta  $Q \ll m_\pi$ , the details of pion exchanges are not resolved and nuclear forces can be systematically expanded in contact interactions and their derivatives [30]. The corresponding pionless EFT (for which  $\Lambda_b \sim m_\pi$ ) is very successful in capturing universal large scattering-length physics (with improvements by including effective range and higher-order terms) in dilute neutron matter and reactions at astrophysical energies [30, 32–35].

For most nuclei, the typical momenta are  $Q \sim m_\pi$  and therefore pion exchanges are included explicitly in nuclear forces. The corresponding chiral EFT has been developed for over fifteen years as a systematic approach to nuclear interactions [30, 31, 36, 37]. This provides a unified approach to NN and many-body forces, and a pathway to direct connections with QCD through lattice calculations (see, for example, Ref. [38]). Examples of order-by-order improved calculations of observables are shown in Figs. 4(b), 5(a), and 5(b). However, some open questions remain [31]: understanding the power counting with singular pion exchanges [39–41], including  $\Delta$  degrees of freedom, the counting of relativistic  $1/m$  corrections. Resolving these questions is important for improving the starting Hamiltonian for low-momentum interactions, but does not affect our discussion of RG technology.

In chiral EFT [30, 31, 36, 37], the expansion in powers of  $Q/\Lambda_b$  has roughly  $\Lambda_b \lesssim m_\rho$ . As shown in Fig. 4(a), at a given order this includes contributions from one- or multi-pion exchanges and from contact interactions, with scale-dependent short-range couplings that are fit to low-energy data for each  $\Lambda$  (experiment captures all short-range effects). There are natural sizes to many-body force contributions that are made manifest in the EFT power counting and which explain the phenomenological hierarchy

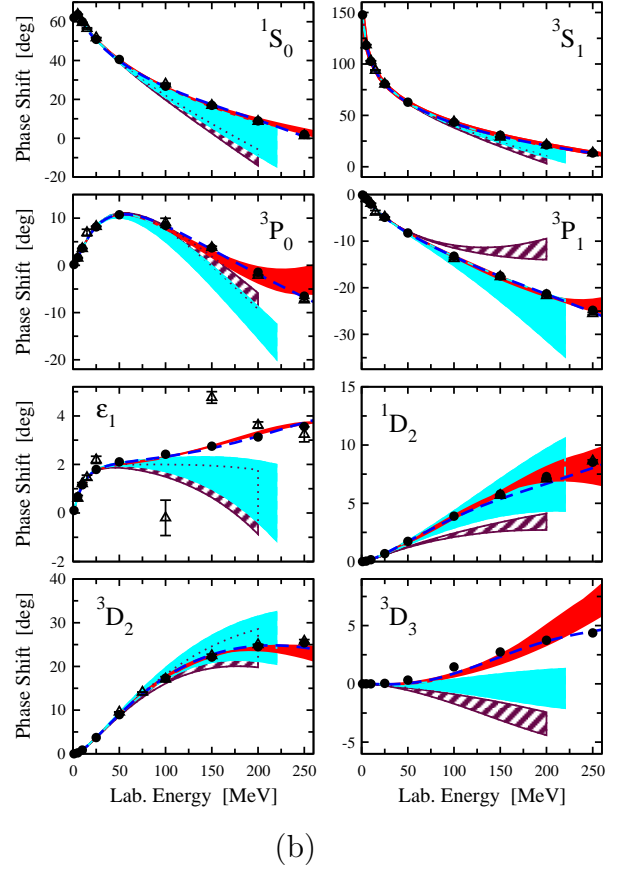
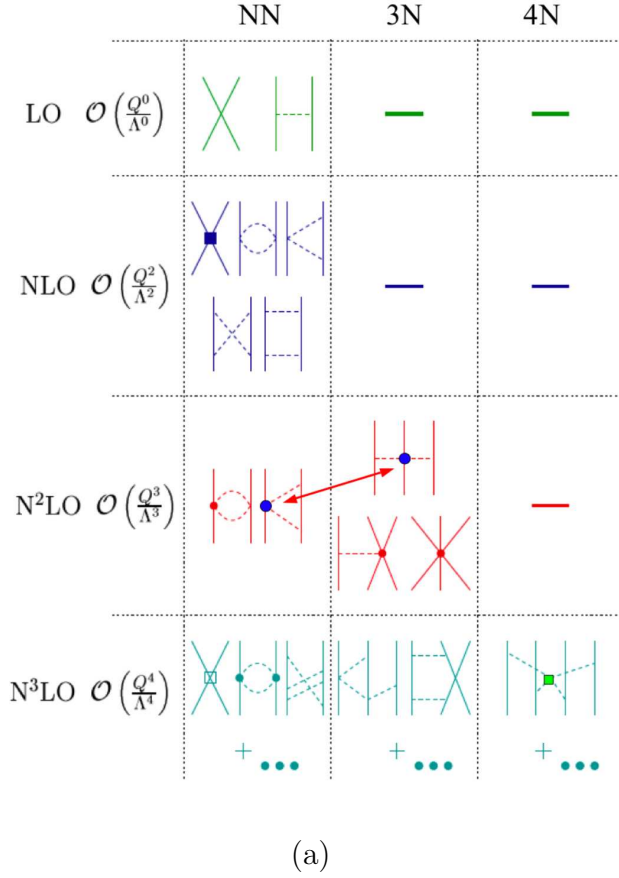


Figure 4: (a) Chiral EFT for nuclear forces. (b) Improvement in neutron-proton phase shifts shown by shaded bands from cutoff variation at NLO (dashed), N<sup>2</sup>LO (light), and N<sup>3</sup>LO (dark) compared to extractions from experiment (points) [31]. The dashed line is from the N<sup>3</sup>LO potential of Ref. [20].

of many-body forces. In addition, the EFT (extended to include chiral perturbation theory) provides a consistent theory for multi-pion and pion-nucleon systems and electroweak operators, as well as for hyperon-nucleon interactions [31, 42, 43].

The highest-order NN interactions available to date are at next-to-next-to-next-to-leading order, N<sup>3</sup>LO or  $(Q/\Lambda_b)^3$ , for several different cutoffs ( $\Lambda = 450\text{--}600$  MeV) and two different regulator schemes [20, 44]. Representative results for NN phase shifts at NLO, N<sup>2</sup>LO, and N<sup>3</sup>LO are shown in Fig. 4(b), where error bands are determined by the spread in predictions for different  $\Lambda \sim \Lambda_b$ . Contour plots of momentum-space matrix elements for the softest, most commonly used N<sup>3</sup>LO potential and one with a higher cutoff are shown in Fig. 6. While they are much softer than Argonne  $v_{18}$  in the  $^1S_0$  channel, there is still considerable off-diagonal strength above  $k = 2\text{ fm}^{-1}$ , which remains problematic for nuclear structure calculations (and the coupled  $^3S_1\text{--}^3D_1$  channel is generally worse).<sup>3</sup> One might think the solution is to simply fit with a smaller  $\Lambda$ , but then the fit worsens significantly as the truncation error grows with  $Q/\Lambda$ .

Instead we can use RG transformations to evolve to lower  $\Lambda$  while preserving the truncation error of the original Hamiltonian. We will roughly define “low-momentum interactions” as potentials that do not couple  $k \lesssim 2\text{ fm}^{-1}$  to larger momenta. This is a relatively small (but significant) evolution for chiral potentials and a large one for phenomenological potentials. Low-momentum interactions are sometimes categorized as phenomenological interactions or regarded as an alternative to EFT interactions. Instead

<sup>3</sup>Note that the cutoff associated with the potential in Fig. 6(a) is  $\Lambda = 500$  MeV, which might lead one to expect no strength above  $k \approx 2.5\text{ fm}^{-1}$ . However, the regulator does not sharply cut off relative momenta.



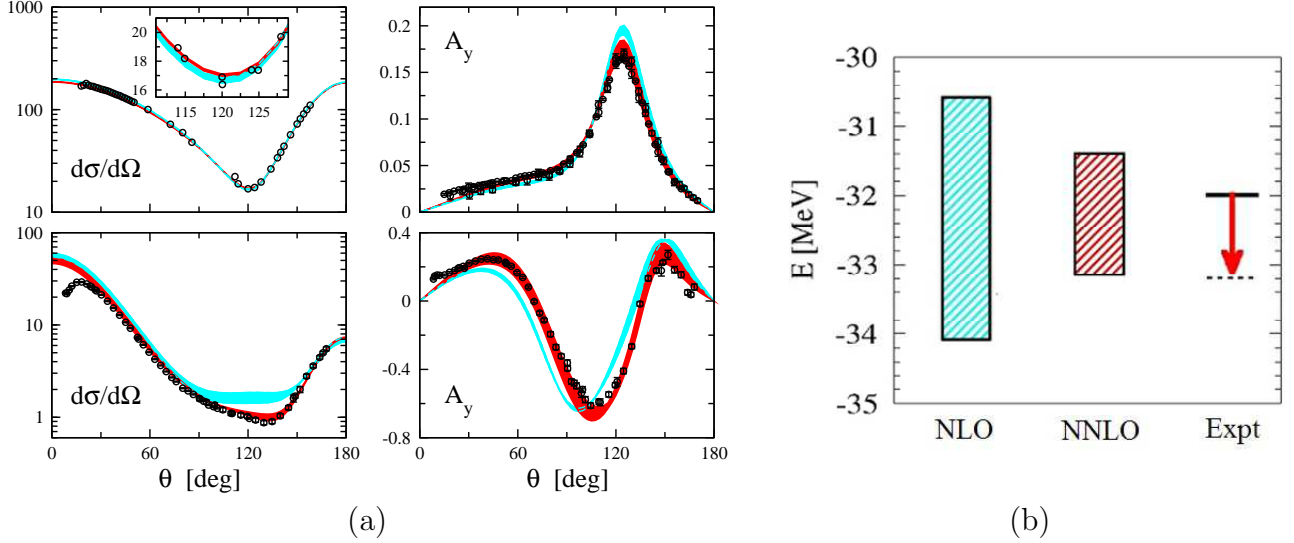


Figure 5: (a) Differential cross section (in mb/sr) and vector analyzing power for elastic neutron-deuteron scattering at 10 MeV (top) and 65 MeV (bottom) at NLO (light) and N<sup>2</sup>LO (dark) from Ref. [36]. (b) Ground-state energy of  ${}^6\text{Li}$  at NLO and N<sup>2</sup>LO with bands corresponding to the  $\Lambda$  variation over 500–600 MeV compared to experiment (solid line, see Ref. [36] for details).

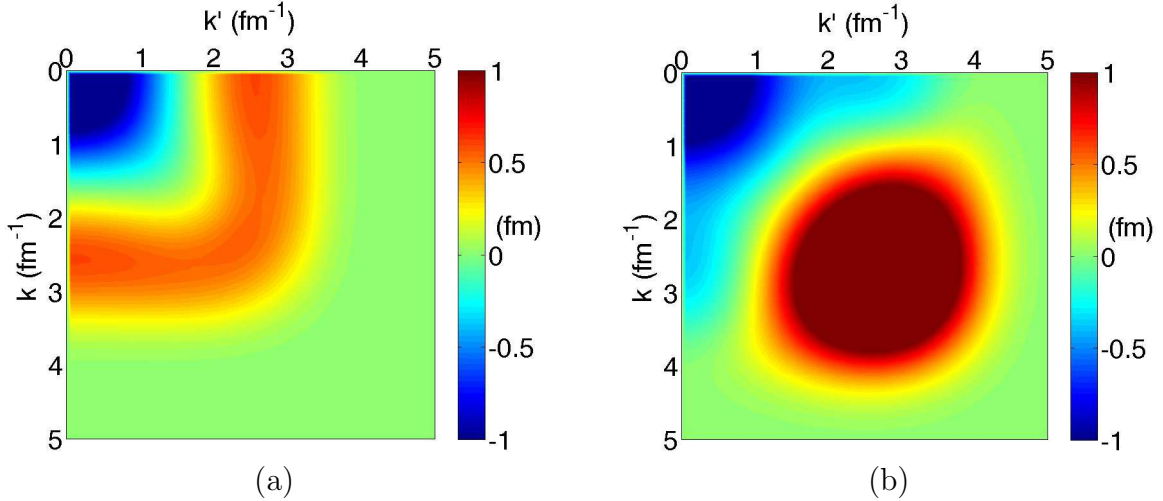
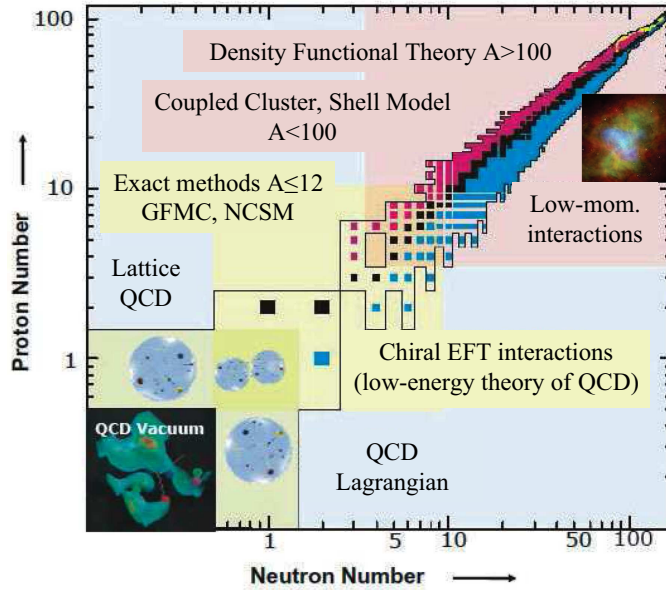


Figure 6: Two N<sup>3</sup>LO  ${}^1S_0$  potentials with (a) 500 MeV and (b) 600 MeV cutoffs [20].

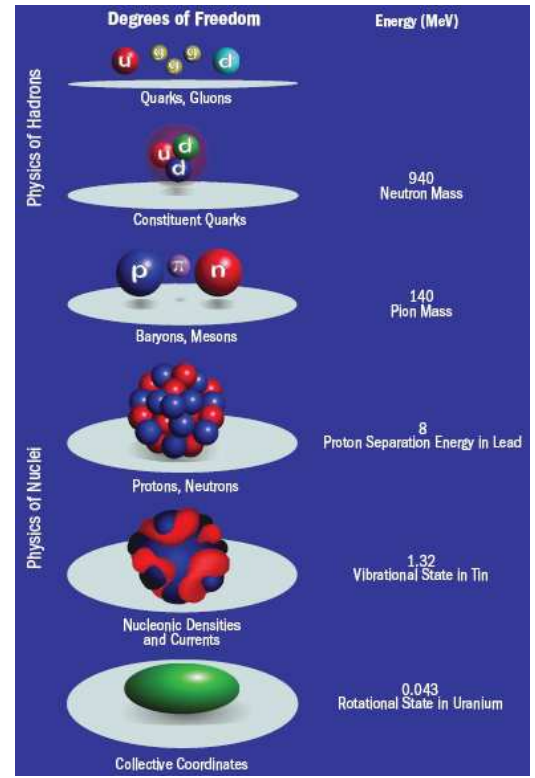
they are an entire class of potentials associated with an initial Hamiltonian. There is no prejudice in the RG methods as to the starting Hamiltonian, but we favor the chiral EFT framework because of the consistent organization of many-body forces and operators and the capacity for systematic improvements. We emphasize that precision tests of all currently available Hamiltonians have only been made in few-body systems. Details of three-body forces and the four-body strength, for example, are quite uncertain.<sup>4</sup>

In the past, unitary transformations were used to soften NN potentials, which were then applied to calculations of few-body systems and nuclear matter. Results for observables depended on the transformations and this was often the context for discussing “off-shell” effects and which was the “true potential”. From the modern perspective, this approach is misleading at best. These transformations

<sup>4</sup>An exploratory calculation for  ${}^4\text{He}$  suggested a contribution of order 100 keV to the binding energy from the long-range four-body force at N<sup>3</sup>LO, but with substantial uncertainty [45, 46].



(a)



(b)

Figure 7: (a) Nuclear many-body landscape and (b) degrees of freedom and corresponding scales in nuclei [48].

*always* lead to many-body interactions, even if absent in the initial Hamiltonian.<sup>5</sup> While this fact was clearly recognized in past investigations [47], many-body forces were usually neglected, which is what led to the different results. In contrast, we account for three-body forces, but we also stress that maintaining *exact* equivalence is not required, because the original Hamiltonian already contains truncation errors.

## 1.2 Nuclear structure challenges

The nuclear many-body landscape is illustrated in Fig. 7(a), where each square represents a nucleus. The challenge of contemporary nuclear structure physics is to describe this entire range of nuclei and beyond to neutron stars and supernovae in a controlled and unified way. The logarithmic scale in proton and neutron number emphasizes the different regions in  $A$  where different many-body methods are applicable. Also shown is the theoretical hierarchy that we propose to exploit: QCD  $\rightarrow$  chiral EFT  $\rightarrow$  low-momentum interactions, which then feed into (most of) the many-body methods, including some not listed. Within the broader challenge there are many more specific challenges, for example, mapping out the drip-lines (the boundaries of nuclear existence), the description of halo nuclei, the evolution of shell structure, the characteristics of pairing, and the description of nuclear decays and spontaneous fission. An intertwined challenge to controlled calculations of binding energies and spectra are nuclear reactions. This includes the interaction with external electroweak probes, which require the consistent

<sup>5</sup>It is possible to find NN potentials that come close to the binding energy of  $^3\text{H}$  and  $^4\text{He}$  and other few-body nuclei without three-body forces. Beyond the problem of constructing consistent electroweak currents for these interactions, this entails a fine tuning to avoid the natural size of many-body forces, which may not persist when these interactions are applied elsewhere.



calculation of electroweak currents.

These challenges are increased by the wide range of scales for strongly interacting particles, illustrated schematically in Fig. 7(b). In particular, we highlight the weak binding of nuclei compared to typical QCD energy scales. For nuclear structure physics, we need methods appropriate to the energy and momentum scales of nuclei, which means isolating the relevant degrees of freedom. As we emphasize throughout this review, the decoupling of scales is at the heart of EFT and RG approaches, and leads us to the low-momentum interaction technology to be documented.

Each of the many-body methods faces computational challenges, principally to the rapid growth of resources needed with increasing  $A$ . For methods such as the No-Core Shell Model and coupled-cluster methods, the key is to improve convergence within the spaces accessible. For heavier nuclei, density functional theory methods offer favorable scaling, but are challenged to reach reliable accuracy such as the sub-MeV level for binding energies. Improved accuracy is needed in the shell model and other methods to realize the use of nuclei as laboratories for fundamental symmetries, such as for isospin-symmetry-breaking corrections to superallowed decays, for neutrinoless double-beta decay, or for octupole enhancement factors of electric dipole moments. In all cases, we seek theoretical error estimates, particularly for extrapolations to systems where measurements will be limited or non-existent.

Progress toward such controlled nuclear calculations has long been hindered by the difficulty of the nuclear many-body problem when conventional nuclear potentials are used. This has historically been accepted as an unavoidable reality. Indeed, conventional wisdom among nuclear physicists, as summarized by Bethe in his review of over 30 years ago [49], holds that successful nuclear matter calculations must be highly nonperturbative in the potential. This is in contrast to the Coulomb many-body problem, for which Hartree-Fock is a useful starting point and (possibly resummed) many-body perturbation theory is an effective tool. The possibility of a soft potential providing a more perturbative solution to the nuclear matter problem was discarded at that time, and saturation firmly identified with the density dependence due to the tensor force [49]. Until recent RG-based calculations [9, 16, 17], subsequent work on the nuclear matter problem [50–53] had not significantly altered the general perspective or conclusions of Bethe’s review (although the role of three-nucleon (3N) forces has been increasingly emphasized).

As already noted, nonperturbative behavior in the particle-particle channel for nuclear forces arises from several sources. First is the strong short-range repulsion, which requires at least a summation of particle-particle ladder diagrams [49]. Second is the tensor force, for example, from pion exchanges, which is highly singular at short distances, and requires iteration in the triplet channels [54, 55]. Third is the presence of low-energy bound states or nearly-bound states in the S-waves. These states imply poles in the scattering  $T$  matrix that render the perturbative Born series divergent. All of these nonperturbative features are present in conventional high-precision NN potentials.

The philosophy behind the standard approach to nuclear matter is to attack these features head-on. This attitude was succinctly stated by Bethe [49]:

“The theory must be such that it can deal with any NN force, including hard or ‘soft’ core, tensor forces, and other complications. It ought not to be necessary to tailor the NN force for the sake of making the computation of nuclear matter (or finite nuclei) easier, but the force should be chosen on the basis of NN experiments (and possibly subsidiary experimental evidence, like the binding energy of  $^3\text{H}$ ).”

In contrast, the EFT and RG perspective has a completely different underlying philosophy, which stresses that the potential is not an observable to be fixed from experiment (there is no “true potential”), but that an infinite number of potentials are capable of accurately describing low-energy physics [56]. In order to be predictive and systematic, an organization (“power counting”) must be present to permit a truncation of possible terms in the potential. If a complete Hamiltonian is used (including many-body

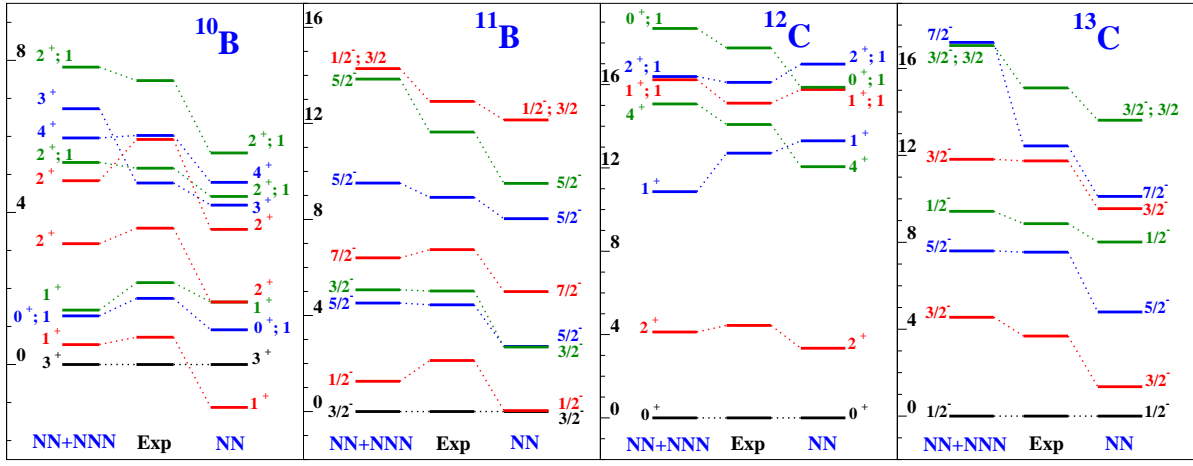


Figure 8: Excitation energies (in MeV) in light nuclei calculated using the No-Core Shell Model (NCSM) with chiral EFT interactions (NN to  $N^3\text{LO}$  and 3N to  $N^2\text{LO}$ ) compared to experiment [57]. Reprinted with permission from P. Navratil et al. [57], copyright (2007) by the American Physical Society.

forces), then all observables should be equivalent up to truncation errors. The EFT philosophy implies using this freedom to choose a convenient and efficient potential for the problems of interest.

The use of energy-independent low-momentum interactions is a direct implementation of these ideas. Varying the cutoff can be used as a powerful tool to study the underlying physics scales, to evaluate the completeness of approximate calculations, and to estimate truncation errors from omitted higher-order contributions. These variable-cutoff interactions reveal the resolution or scale dependence of the first two sources of nonperturbative behavior, which are tamed as high momenta are decoupled. In free space, the third source of nonperturbative behavior remains independent of the cutoff because the pole positions of weakly and nearly bound states that necessitate fine tuning are physical observables. However, this fine tuning is eliminated in the medium at sufficiently high density. In short, a repulsive core is not constrained by phase shifts and is essentially removed by even a moderately low-momentum cutoff (note the  $\Lambda$  dependence in Fig. 3(b)), the short-range tensor force is tamed by a sufficiently low cutoff, and the weakly and nearly bound states become perturbative as a result of Pauli blocking. For cutoffs around  $2\text{ fm}^{-1}$ , which preserve phase shifts up to 330 MeV laboratory energy, the Born series in nuclear matter is well converged at second order in the potential, bringing the nuclear and Coulomb many-body problems closer together [9].

While *evolving* a soft potential from higher momentum is a new development in nuclear physics [5,58], attempts to use soft potentials for nuclear matter were made in the mid sixties and early seventies [47, 59]. It had long been observed that a strongly repulsive core is not resolved until eight times nuclear saturation density [49]. Thus, saturation is *not* driven by a hard core (unlike liquid  $^3\text{He}$ ). However, these soft potentials were abandoned because they seemed incapable of quantitatively reproducing nuclear matter properties. Their requiem was given by Bethe [49]:

“Very soft potentials must be excluded because they do not give saturation; they give too much binding and too high density. In particular, a substantial tensor force is required.”

From the EFT perspective, a failure to reproduce nuclear matter observables should not be interpreted as showing that the low-energy potential is wrong, but that it is incomplete. This misconception still persists and has led to the conclusion that low-momentum NN interactions are “wrong” because they do not give saturation in nuclear matter and finite nuclei are overbound for lower cutoffs. The missing physics that invalidates this conclusion is many-body forces.

In a low-energy effective theory, many-body forces are inevitable; the relevant question is how large they are. It is established beyond doubt that 3N forces are required to describe light nuclei [22–24, 57,

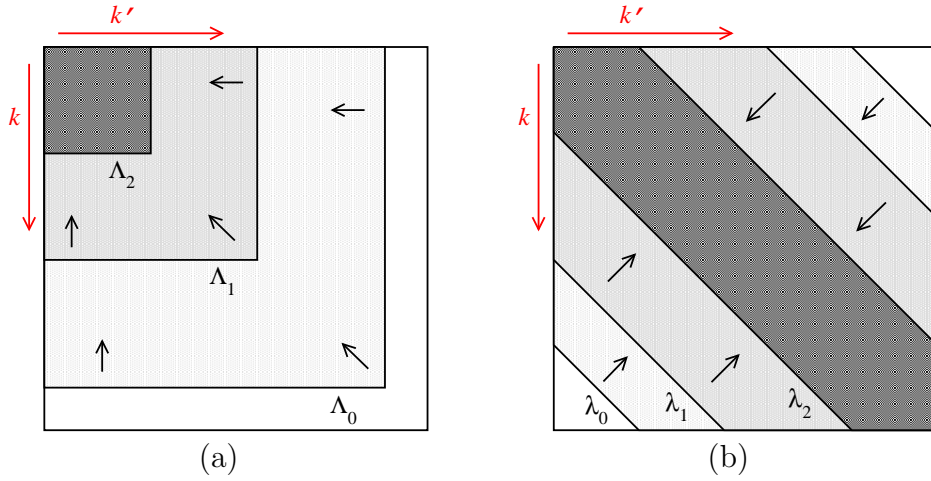


Figure 9: Schematic illustration of two types of RG evolution for NN potentials in momentum space: (a)  $V_{\text{low } k}$  running in  $\Lambda$ , and (b) SRG running in  $\lambda$ . At each  $\Lambda_i$  or  $\lambda_i$ , the matrix elements outside of the corresponding lines are zero, so that high- and low-momentum states are decoupled.

60, 61], as shown, for example, in Fig. 8. For variable-cutoff potentials, three-body (and higher-body) interactions evolve naturally with the resolution scale.

### 1.3 Renormalization group approaches

A fundamental tenet of renormalization theory is that the *relevant* details of high-energy physics for calculating low-energy observables can be captured in the scale-dependent coefficients of operators in a low-energy Hamiltonian [29]. This principle does not mean that high-energy and low-energy physics is automatically decoupled in every effective theory. In fact, it implies that we can include as much irrelevant coupling to *incorrect* high-energy physics as we want by using a large cutoff, with no consequence to low-energy predictions (assuming we can calculate accurately). But this freedom also offers the possibility of decoupling, which makes practical calculations more tractable by restricting the necessary degrees of freedom. This decoupling can be efficiently achieved by evolving nuclear interactions using RG transformations designed to handle similar problems in relativistic field theories and critical phenomena in condensed matter systems.<sup>6</sup>

The general purpose of the RG when dealing with the large range of scales in physical systems was eloquently explained by David Gross [63]:

“At each scale, we have different degrees of freedom and different dynamics. Physics at a larger scale (largely) decouples from the physics at a smaller scale. ... Thus, a theory at a larger scale remembers only finitely many parameters from the theories at smaller scales, and throws the rest of the details away. More precisely, when we pass from a smaller scale to a larger scale, we average over irrelevant degrees of freedom. ... The general aim of the RG method is to explain how this decoupling takes place and why exactly information is transmitted from scale to scale through finitely many parameters.”

The common features of RG for critical phenomena and high-energy scattering are discussed by Steven Weinberg in an essay in Ref. [64]. He summarizes:

“The method in its most general form can I think be understood as a way to arrange in various theories that the degrees of freedom that you’re talking about are the relevant degrees of freedom for the problem at hand.”

<sup>6</sup>For an early discussion of decoupling based on Okubo unitary transformations, see Ref. [62].

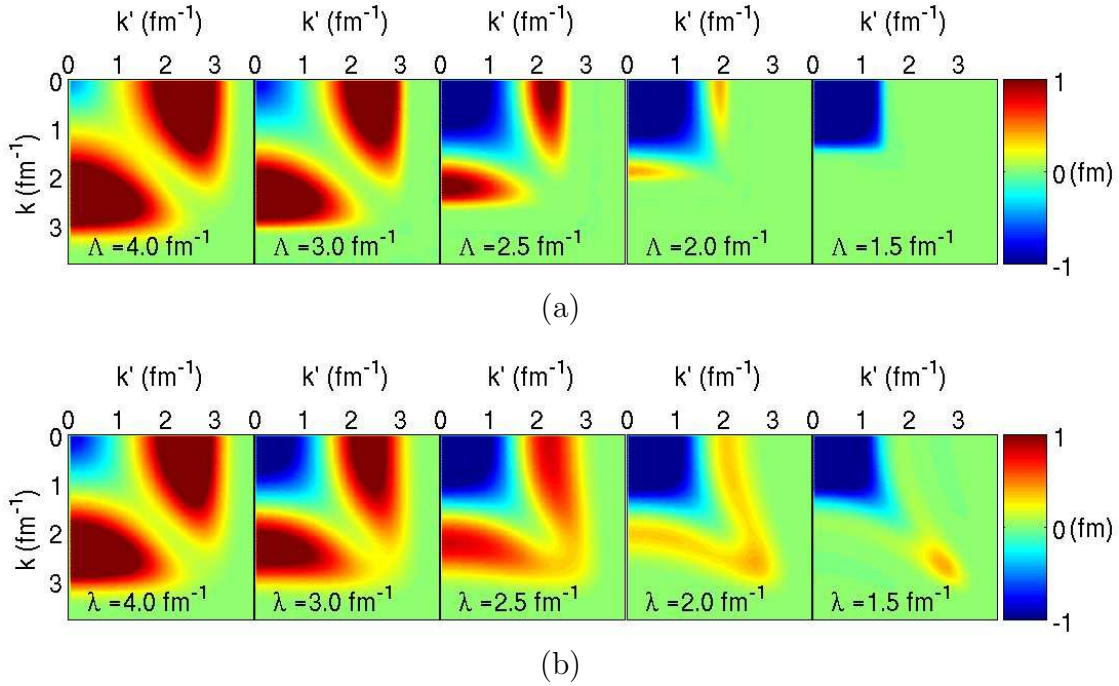


Figure 10: Two types of RG evolution applied to one of the chiral N<sup>3</sup>LO NN potentials (550/600 MeV) of Ref. [44] in the <sup>3</sup>S<sub>1</sub> channel: (a)  $V_{\text{low } k}$  running in  $\Lambda$ , and (b) SRG running in  $\lambda$  (see Fig. 27 for plots in  $k^2$ , which show the diagonal width of order  $\lambda^2$ ).

This is the heart of what is done with low-momentum interaction approaches: arrange for the degrees of freedom for nuclear structure to be the relevant ones. This does not mean that other degrees of freedom cannot be used, but to again quote Weinberg [64]: “You can use any degrees of freedom you want, but if you use the wrong ones, you’ll be sorry.”

There are two major classes of RG transformations used to construct low-momentum interactions, which are illustrated schematically in Fig. 9. In the  $V_{\text{low } k}$  approach, decoupling is achieved by lowering a momentum cutoff  $\Lambda$  above which matrix elements go to zero. In the SRG approach, decoupling is achieved by lowering a cutoff  $\lambda$  (in energy differences  $\lambda^2$ ) using flow equations, which means evolving toward the diagonal in momentum space. The technology for carrying these out is outlined in Section 3, but the effects can be readily seen in the series of contour plots in Figs. 10(a) and 10(b).

With either approach, lowering the cutoff leaves low-energy observables unchanged by construction, but shifts contributions between the interaction strengths and the sums over intermediate states in loop integrals. The evolution of phenomenological or chiral EFT interactions to lower resolution is beneficial because these shifts can weaken or largely eliminate sources of nonperturbative behavior, and because lower cutoffs require smaller bases in many-body calculations, leading to improved convergence for nuclei. The RG cutoff variation estimates theoretical uncertainties due to higher-order contributions, to neglected many-body interactions or to an incomplete many-body treatment. When initialized with different orders of chiral EFT interactions, we have a powerful tool for extrapolations to the extremes and for assessing the uncertainties of key matrix elements needed in fundamental symmetry tests.

The idea of effective interactions in a limited model space is an old and well-exploited one in nuclear physics. However, we will emphasize the flexibility of the RG compared to effective interaction methods. The continuous “cutoff” variation (in quotes because it may not be an explicit cutoff) is a valuable new tool for nuclear physics (see Section 2.6). The RG methods are versatile and suggest new ways to make progress (for example, using the in-medium SRG, discussed in Section 4.3). In addition, RG combined with EFT is a natural framework for uncovering universal behavior.

We note that the RG is an integral part of any EFT. Matching of the EFT at a given truncation

level (to data or to an underlying theory) but at different regulator cutoffs establishes the RG evolution (or “running”) of the EFT couplings. This includes the shift of strength between loop integrals and couplings and between two and many-body interactions. However, because the EFT basis is truncated, the error at the initial cutoff is not preserved with the running, in contrast to the momentum-space RG evolution using  $V_{\text{low } k}$  or SRG techniques, which keep all orders.

## 1.4 Scope of the review

This review focuses on the use of RG methods to derive low-momentum interactions. There are other approaches to softened interactions that share many of the same advantages and issues, which we do not address in detail. Fortunately there are recent reviews to cover these omissions, for example, Ref. [31] on nuclear forces, Refs. [65] and [66] on ab initio and shell-model applications, and Ref. [67] on density functional theory.

In Section 2, we discuss general principles of the RG as applied to nuclear forces. The various technologies for evolving NN potentials are outlined in Section 3. Many-body interactions and operators are addressed in Section 4. Sections 5 and 6 review many-body advances with applications to infinite matter and finite nuclei. We conclude in Section 7 with a summary of the main points, through a consideration of misconceptions and clarifications, on-going developments, and important open questions.

# 2 Renormalization group: motivation and principles

## 2.1 Decoupling

High-momentum degrees of freedom do not automatically decouple from low-energy observables, especially for NN potentials that have significant high-momentum off-diagonal strength (typically beyond  $k \gtrsim 2 \text{ fm}^{-1}$ ). The coupling between low- and high-momentum states is a consequence of quantum fluctuations, as manifested in intermediate state summations in perturbation theory, e.g.,

$$T(k', k; E) = \langle k' | V^\Lambda | k \rangle + \sum_{q=0}^{\Lambda} \frac{\langle k' | V^\Lambda | q \rangle \langle q | V^\Lambda | k \rangle}{E - \varepsilon_q} + \dots \quad (2)$$

This coupling is regulated by the cutoff or resolution scale  $\Lambda$  that is present in all NN interactions.

A central theme of this review is that nonperturbative features of nuclear forces can be radically altered by explicitly decoupling low- and high-momentum degrees of freedom. As we will see, many-body calculations become more perturbative, basis expansions converge more rapidly, and strong short-range correlations are smeared out, rendering variational methods more effective. However, if NN potentials at a large scale  $\Lambda$  are simply truncated at some  $k_{\text{max}} \ll \Lambda$ , the calculated low-energy observables (such as phase shifts and the deuteron binding energy) are drastically changed, as shown in Figs. 11 and 12. Such a brute-force cutoff does not disentangle high-energy (short-range) features from low-energy (long-range) observables. To do so, it is necessary to integrate out (and thus decouple) irrelevant high-momentum details from their effects on low-energy observables. This is achieved by the two classes of RG transformations illustrated in Fig. 9 and described in greater detail in Section 3.

A practical test for decoupling is whether changing high-momentum matrix elements of a given potential changes low-energy observables. The SRG allows for particularly convincing demonstrations of decoupling, because the unitary evolution of the Hamiltonian preserves the deuteron binding energy and phase shifts for *all* energies. The SRG-evolved potential  $V_s$  explicitly decouples high-energy dynamics from low-energy observables, which means that we can set to zero the high-momentum parts (so that we have a potential like  $V_{\text{low } k}$ ) with no significant changes in the low-energy physics.

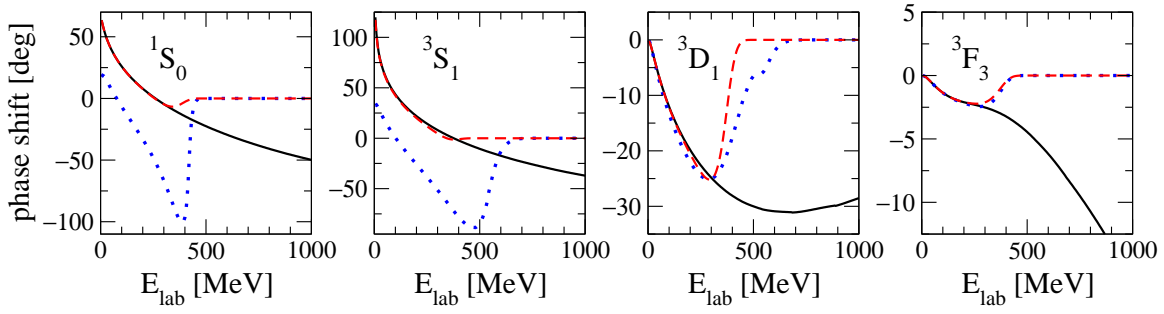


Figure 11: NN phase shifts for the Argonne  $v_{18}$  potential [18] and the SRG-evolved potential for  $\lambda = 2 \text{ fm}^{-1}$  with all momenta included (two indistinguishable solid lines) and with the exclusion of momenta  $k > k_{\text{max}} = 2.2 \text{ fm}^{-1}$  (Argonne  $v_{18}$  dotted, SRG-evolved dashed) [68].

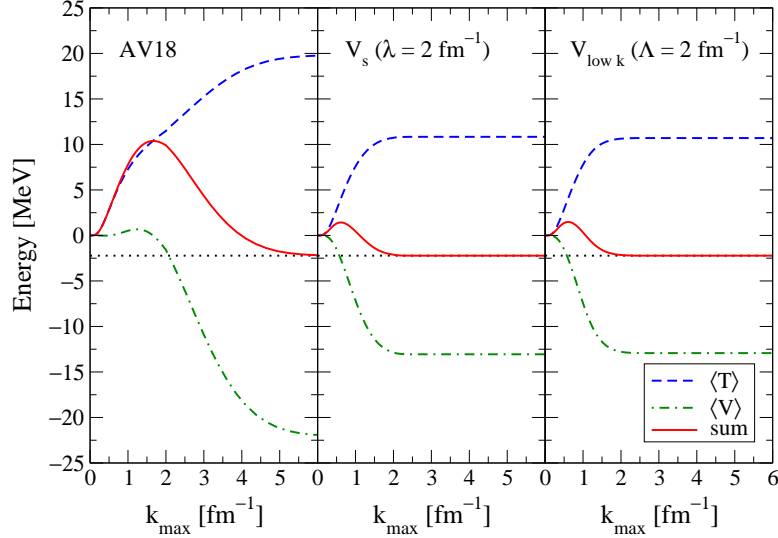


Figure 12: Expectation values in the deuteron of the kinetic  $\langle T \rangle$  (dashed), potential  $\langle V \rangle$  (dot-dashed), and total energy (solid) evaluated in momentum space as a function of the maximum momentum  $k_{\text{max}}$ , see Eq. (3). Results are shown for the Argonne  $v_{18}$  potential [18] (left), the SRG-evolved potential  $V_s$  for  $\lambda = 2 \text{ fm}^{-1}$  (middle), and the smooth-cutoff  $V_{\text{low } k}$  interaction with  $\Lambda = 2 \text{ fm}^{-1}$  (right) [68].

In Ref. [68], the decoupling of high-energy details from low-energy phase shifts and the deuteron binding energy was demonstrated by setting  $V_s(k, k')$  to zero for all  $k, k'$  above a specified momentum  $k_{\text{max}}$  (using a smooth regulator function). Phase shifts for  $k_{\text{max}} = 2.2 \text{ fm}^{-1}$  are shown in Fig. 11 for the initial Argonne  $v_{18}$  potential and for the SRG-evolved  $V_s$  with  $\lambda = 2 \text{ fm}^{-1}$ . The phase shifts for the initial potential in the lower partial waves bear no relation to the result without a  $k_{\text{max}}$  cutoff. In contrast, the low-energy phase shifts for the SRG-evolved potential are unchanged, even though the high-energy phase shifts above  $k_{\text{max}}$  are now zero.

The deuteron binding energy provides another clear example of how the contributions of different momentum components to a low-energy observable depend on the resolution scale (as measured by  $\Lambda$  or  $\lambda$ , see Fig. 9). In Fig. 12, we show the kinetic, potential, and total energy from an integration in momentum space including momenta up to  $k_{\text{max}}$ . That is, we plot

$$E_d(k < k_{\text{max}}) = \int_0^{k_{\text{max}}} d\mathbf{k} \int_0^{k_{\text{max}}} d\mathbf{k}' \psi_d^\dagger(\mathbf{k}; \lambda) (k^2 \delta^3(\mathbf{k} - \mathbf{k}') + V_s(\mathbf{k}, \mathbf{k}')) \psi_d(\mathbf{k}'; \lambda), \quad (3)$$

where  $\psi_d(\mathbf{k}; \lambda)$  is the momentum-space deuteron wave function from the corresponding potential  $V_s$  (without  $k_{\text{max}}$ ). Figure 12 shows that if one excludes momenta greater than  $2 \text{ fm}^{-1}$  in the Argonne  $v_{18}$



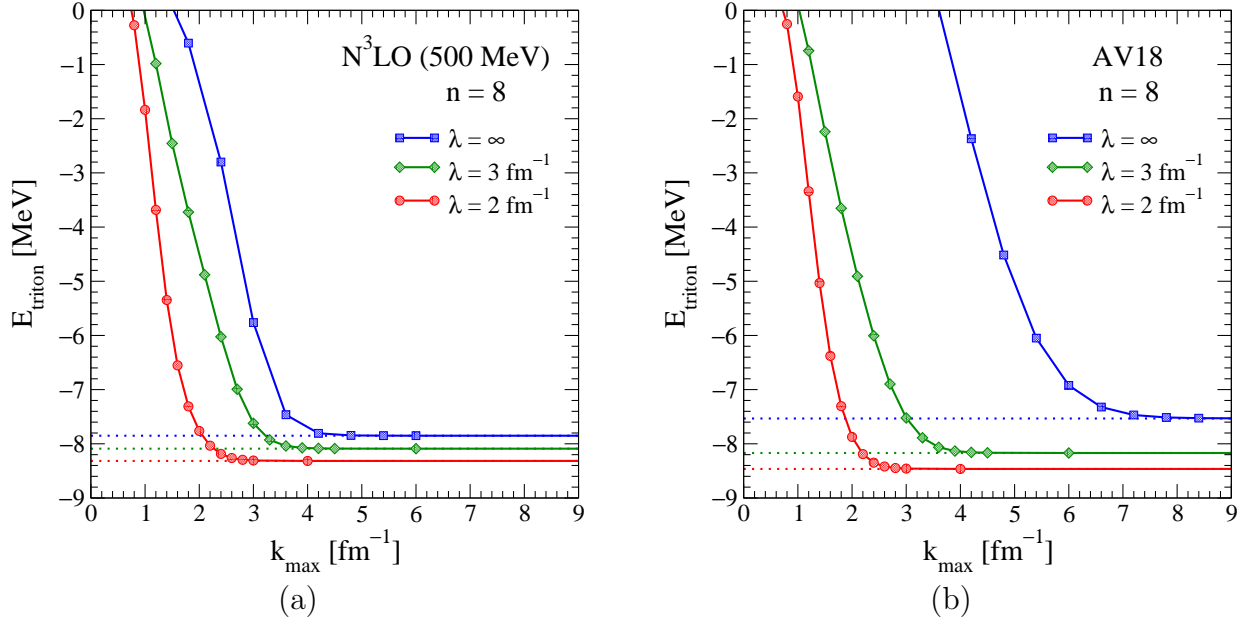


Figure 13: Ground-state energy of  ${}^3\text{H}$  as a function of the maximum momentum  $k_{\text{max}}$  for three different values of  $\lambda$  [14]. The cutoff function is  $\exp[-(k^2/k_{\text{max}}^2)^n]$  with  $n = 8$ . The initial potentials are (a) the  $\text{N}^3\text{LO}$  NN potential of Ref. [20] and (b) the Argonne  $v_{18}$  potential [18].

deuteron wave function, the deuteron is 9.9 MeV unbound (that is, the integrated kinetic energy up to  $2 \text{ fm}^{-1}$  is 11.5 MeV while the potential energy is  $-1.6 \text{ MeV}$ ). In contrast, using  $V_s$  with  $\lambda = 2 \text{ fm}^{-1}$ , one sees that the converged result is dominated by contributions from much lower momenta. Note that the  $V_s$  potential has no appreciable contributions above  $\lambda$ , even though the near-diagonal matrix elements of the potential  $V_s(k, k')$  for  $k, k' > k_{\text{max}}$  are sizable. This again validates decoupling. It is also evident that the  $V_s$  and  $V_{\text{low } k}$  results are very similar for  $\lambda \approx \Lambda$ , where  $\Lambda$  is the momentum cutoff for  $V_{\text{low } k}$ . Lastly, we mention that the decoupling carries over to few-body systems [14, 69], as shown similarly for the  ${}^3\text{H}$  ground-state energy in Fig. 13. Note that the different converged energies for each  $\lambda$  reflects the truncation of the SRG at the NN level, see Section 2.5.

## 2.2 Connections to effective field theory

The RG plays a central role in EFT. It determines the running of low-energy couplings (see, for example, Ref. [30]) and the RG scaling of operators can be used to identify power counting schemes [70, 71]. In this section, we discuss how the nonperturbative RG evolution works in the context of chiral EFT interactions. In EFT, it is optimal to fit the low-energy couplings at larger cutoffs, because this minimizes the truncation errors that can scale as rapidly as  $(Q/\Lambda)^n$ , and because larger cutoffs include maximal long-distance physics up to the given order in the EFT expansion. This is illustrated in Fig. 14 by comparing an  $\text{N}^3\text{LO}$  potential with a larger cutoff  $\Lambda = 500 \text{ MeV}$  ( $2.5 \text{ fm}^{-1}$ ) to the sharp cutoff  $\text{N}^3\text{LO}$  potential of Ref. [72] with  $\Lambda = 2.0 \text{ fm}^{-1}$ . At the same EFT order, the fit for a lower cutoff requires more fine-tuning and leads to a potential that is not very smooth in momentum space. This indicates a breakdown of the gradient expansion.

The RG evolution of EFT interactions to lower cutoffs is beneficial because the resulting low-momentum interactions preserve the truncation error of the initial potential and therefore include the advantages of fitting at larger cutoffs, while they have lower cutoffs that are advantageous for applications to nuclear structure (see Sections 5 and 6). As shown in Fig. 14, the evolved interactions are smooth without the strong momentum dependencies observed for the sharp cutoff  $\text{N}^3\text{LO}$  potential

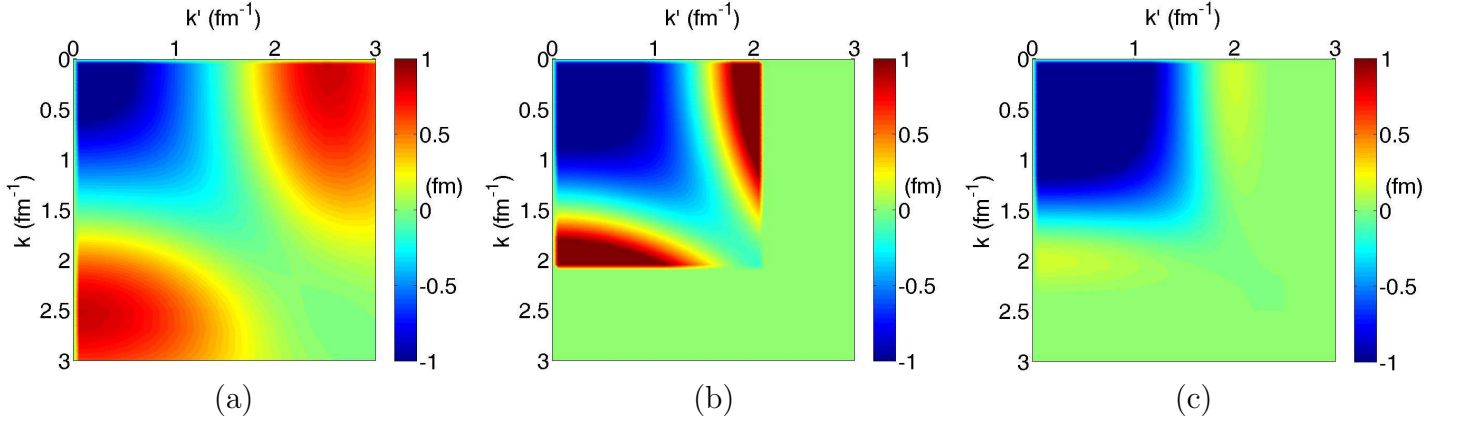


Figure 14: Momentum-space matrix elements in the  $^3S_1$  channel for (a) the N<sup>3</sup>LO potential ( $\Lambda = 500$  MeV) of Ref. [20], (b) the sharp cutoff N<sup>3</sup>LOW potential ( $\Lambda = 2.0$  fm<sup>-1</sup>) of Ref. [72], and (c) for the N<sup>3</sup>LO potential ( $\Lambda = 500$  MeV) evolved by a smooth  $V_{\text{low } k}$  to  $\Lambda = 2.0$  fm<sup>-1</sup>.

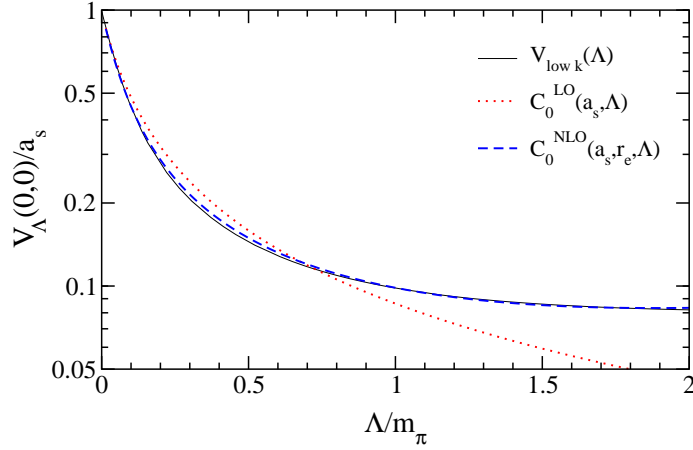


Figure 15: Flow of  $V_{\text{low } k}(k' = 0, k = 0; \Lambda)$  compared to the corresponding momentum-independent contact interaction  $C_0(\Lambda)$  at LO and NLO, where this coupling is determined entirely from RG invariance and fits to the scattering length  $a_s$  (at LO) plus effective range  $r_e$  (at NLO) [73].

at the same cutoff scale, and the NN phase shifts are reproduced with the same accuracy.

We can gain further insights into the interplay of the RG and EFT by considering chiral EFT as providing a general operator basis that can be used to expand the RG evolution. At a given order  $(Q/\Lambda_b)^n$ , chiral EFT includes contributions from one- or multi-pion exchanges and from contact interactions, with short-range couplings that depend on the resolution or cutoff scale. As part of the RG evolution, short-range couplings included in the initial potential evolve. This is illustrated in Fig. 15 by comparing the flow of  $V_{\text{low } k}(k' = 0, k = 0; \Lambda)$  with the corresponding momentum-independent contact interaction  $C_0(\Lambda)$  in subsequent orders of pionless EFT. In addition, the RG generates higher-order short-range contact interactions so that observables are exactly reproduced and the truncation error is unchanged. Consequently, the cutoff variation can be used to estimate theoretical uncertainties due to higher-order short-range many-body interactions. We will discuss using cutoff dependence as a tool in Section 2.6.

For cutoffs large compared to the pion mass, the long-range parts in the initial chiral potentials are preserved by the RG evolution. This is demonstrated in Fig. 16(a) for deuteron wave functions at different resolution scales. While the short-range behavior changes with the cutoff, the long-range parts are governed by low-energy pion physics and remain unchanged. The results discussed in Section 4 for

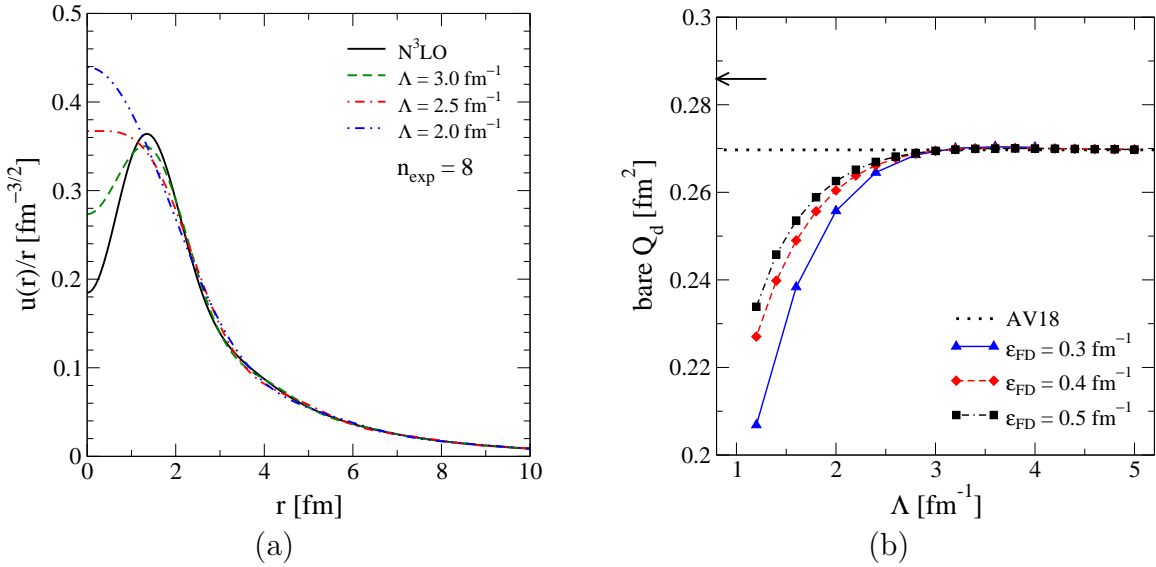


Figure 16: (a) Deuteron wave functions in coordinate space for smooth  $V_{\text{low } k}$  interactions at several different cutoffs using an exponential regulator with  $n_{\text{exp}} = 8$ . The initial interaction is the  $N^3\text{LO}$  potential of Ref. [20]. (b) Matrix element of the bare quadrupole moment operator as a function of the cutoff for several smooth  $V_{\text{low } k}$  regulators. For details see Ref. [6].

many-body interactions and operators can be explained based on the above observations.

## 2.3 Universality

Low-momentum interactions starting from different initial potentials are found to be quantitatively similar [5–7]. We use the terminology universality in this context (independent of the high-momentum details in the initial potential) and not in the sense of critical phenomena (independent of the system details). Figures 17 and 18 show various phenomenological NN potentials and different  $N^3\text{LO}$  NN interactions of Entem and Machleidt (EM) [20] and of Epelbaum et al. (EGM) [44]. Each potential accurately reproduces low-energy NN scattering, as shown in Fig. 4(b). When the potentials are evolved to lower cutoffs, the resulting low-momentum interactions become universal. In addition, the RG evolution weakens the off-diagonal coupling between low and high momenta. Section 3 reviews different low-momentum technologies for achieving this decoupling.

A similar universal behavior and decoupling is found for the low-momentum parts of SRG evolved interactions, see Fig. 28(a). We attribute the collapse to universal low-momentum interactions to the common long-range pion physics in the initial potentials, and to a similar description of low-energy NN observables up to the resolution scale, while the high-momentum parts are decoupled. This is similar to the inverse scattering problem, where the theory is restricted to the energy range set by the resolution scale. Important open problems are to understand the observed universality in terms of an RG scaling analysis, to identify eigenoperators of the RG evolution, and to extend the study of universality to 3N forces.

## 2.4 Perturbativeness

Nuclear many-body calculations are complicated by strong short-range repulsion and strong short-range tensor forces found in most NN potential models. However, both of these sources of non-perturbative

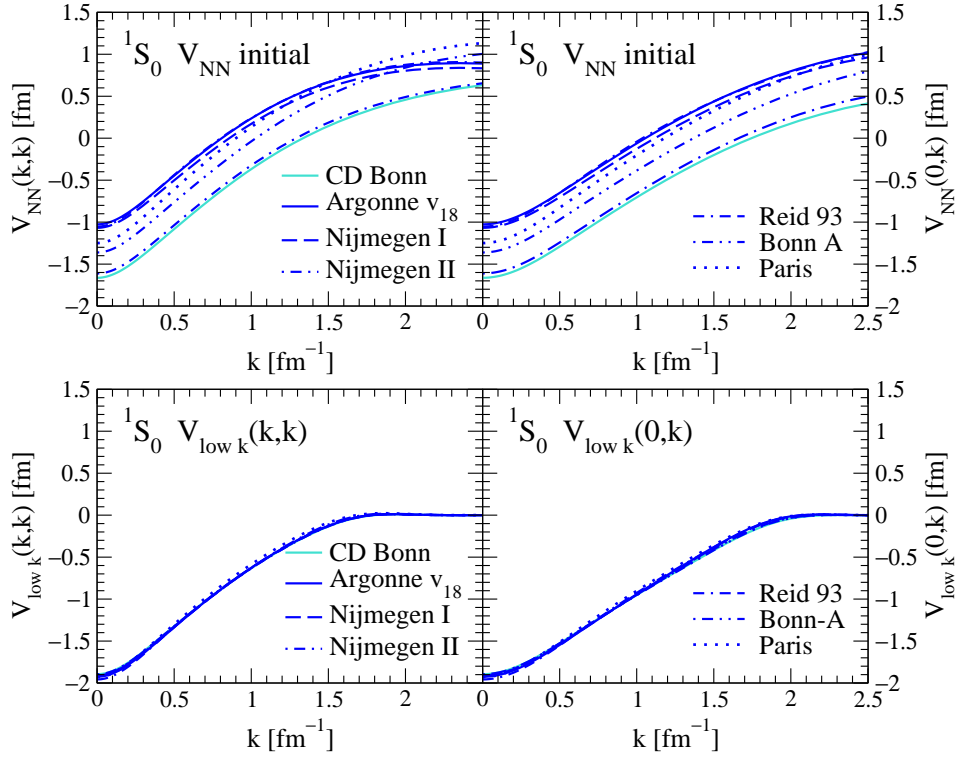


Figure 17: Diagonal (left) and off-diagonal (right) momentum-space matrix elements for various phenomenological NN potentials initially (upper figures) and after RG evolution to low-momentum interactions  $V_{\text{low } k}$  [5,6] (lower figures) for a smooth regulator with  $\Lambda = 2.0 \text{ fm}^{-1}$  and  $n_{\text{exp}} = 4$ .

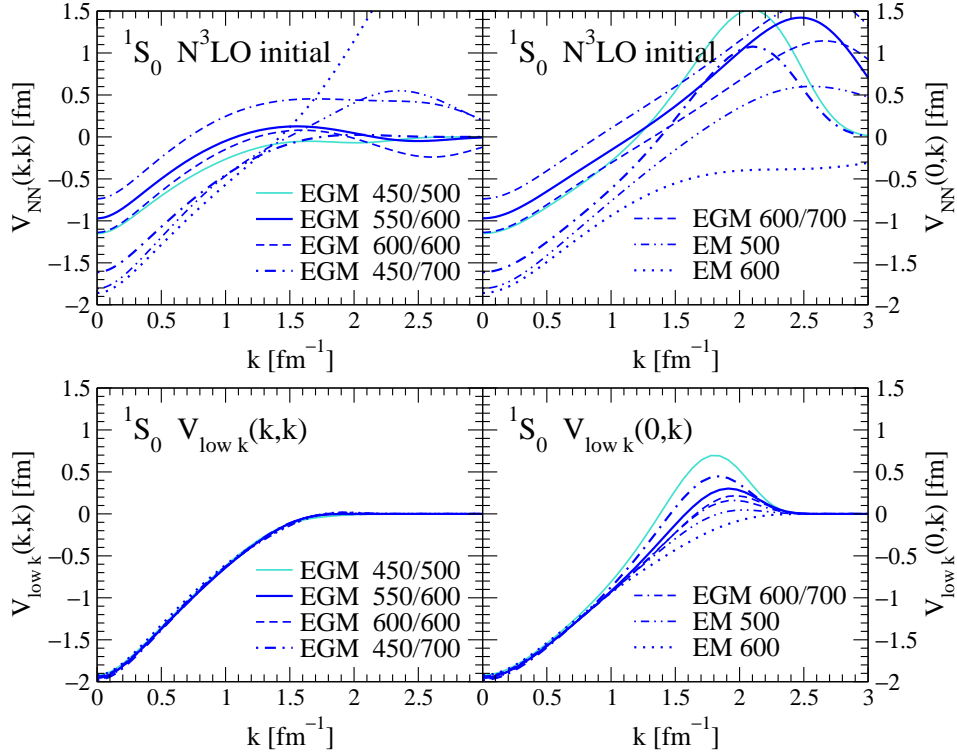


Figure 18: Diagonal (left) and off-diagonal (right) momentum-space matrix elements of different  $N^3\text{LO}$  NN interactions (EM [20] and EGM [44]) initially (upper figures) and after RG evolution to low-momentum interactions  $V_{\text{low } k}$  [5,6] (lower figures) for a smooth regulator with  $\Lambda = 2.0 \text{ fm}^{-1}$  and  $n_{\text{exp}} = 4$ .

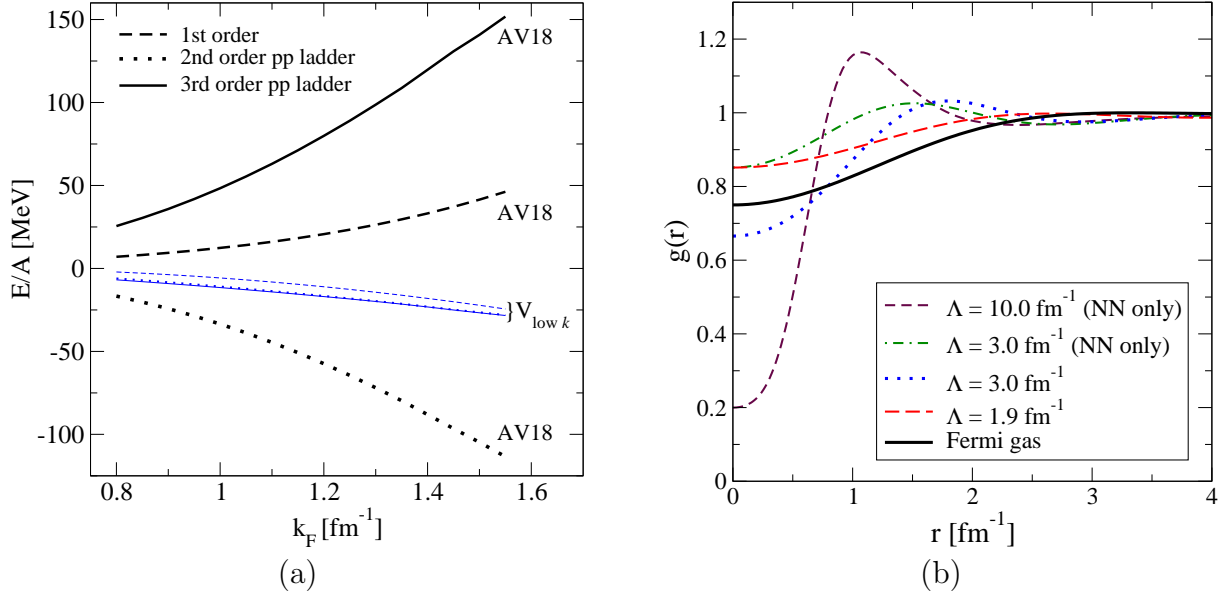


Figure 19: (a) Particle-particle contributions to the energy per nucleon in symmetric nuclear matter as a function of the Fermi momentum  $k_F$  for the initial Argonne  $v_{18}$  potential and the RG-evolved  $V_{\text{low } k}$  with  $\Lambda = 2.1 \text{ fm}^{-1}$  [9]. (b) Pair-distribution function  $g(r)$  in nuclear matter for  $k_F = 1.35 \text{ fm}^{-1}$  at different resolutions, for details see Ref. [10].

behavior are resolution-dependent,<sup>7</sup> because they depend on the degree of coupling between low- and high-momentum states [6, 7, 9, 12]. Consequently, RG methods can be used to improve perturbative convergence and reduce the short-range strength of the associated correlations in the wave functions, as shown for symmetric nuclear matter in Figs. 19(a) and 19(b), respectively.

We can quantify the perturbativeness of the potential as we evolve to lower  $\Lambda$  for  $V_{\text{low } k}$  (or  $\lambda$  for SRG) interactions by using the eigenvalue analysis introduced long ago by Weinberg [75] and applied to  $V_{\text{low } k}$  and SRG potentials in Refs. [6, 7, 9, 12]. Consider the Born series for the  $T$  matrix at energy  $E$  with Hamiltonian  $H = H_0 + V$ ,

$$T(E) = V + V \frac{1}{E - H_0} V + \dots \quad (4)$$

By finding the eigenvalues and eigenvectors of the operator  $(E - H_0)^{-1}V$ ,

$$\frac{1}{E - H_0} V |\Gamma_\nu\rangle = \eta_\nu(E) |\Gamma_\nu\rangle, \quad (5)$$

and then acting with  $T(E)$  on the eigenvectors,

$$T(E) |\Gamma_\nu\rangle = (1 + \eta_\nu(E) + \eta_\nu^2(E) + \dots) V |\Gamma_\nu\rangle, \quad (6)$$

it follows that nonperturbative behavior at energy  $E$  is signaled by one or more eigenvalues with  $|\eta_\nu(E)| \geq 1$  [75]. A rearrangement of Eq. (5) gives a simple interpretation of the eigenvalue  $\eta_\nu(E)$  as an energy-dependent coupling that must divide  $V$  to produce a solution to the Schrödinger equation at energy  $E$ . For negative energies, a purely attractive  $V$  gives positive real  $\eta_\nu(E)$  values, while a purely repulsive  $V$  gives negative eigenvalues. For this reason, we refer to negative eigenvalues as repulsive and positive ones as attractive, although the eigenvalues become complex for positive  $E$ .

<sup>7</sup>This is in contrast to non-perturbative features like low-energy bound or nearly bound states in the S-waves and the pairing instability at finite density that are insensitive to the short-distance details.

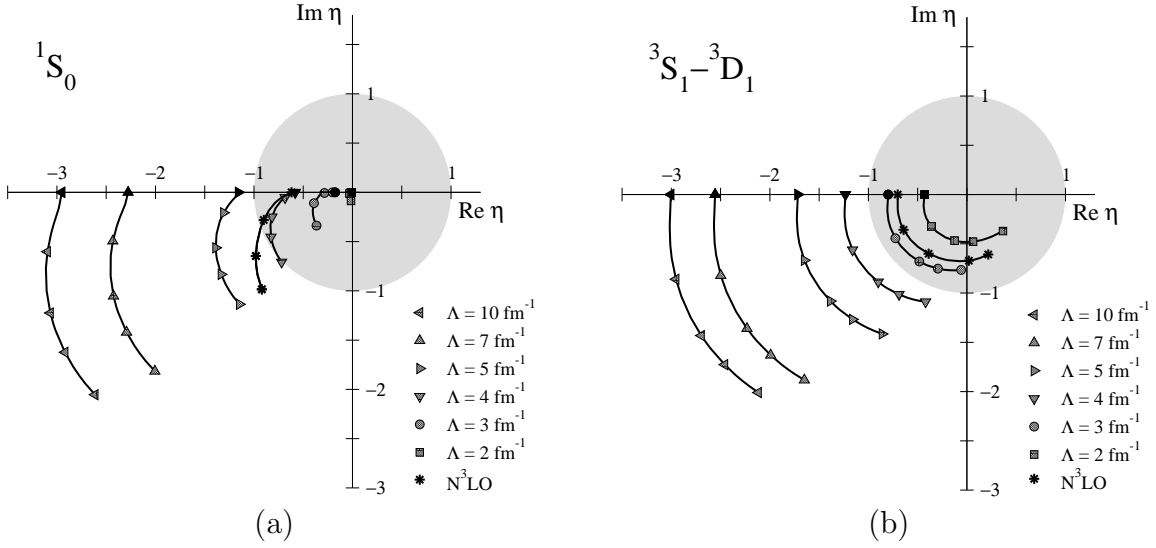


Figure 20: Trajectories of the largest repulsive Weinberg eigenvalues in the (a)  $^1S_0$  and (b)  $^3S_1$ - $^3D_1$  channels as a function of energy for  $V_{\text{low } k}$  evolved from the Argonne  $v_{18}$  potential [12]. The results for selected cutoffs are indicated by the different symbols. The positions of the symbols on each trajectory mark the eigenvalues for center-of-mass energies  $E_{\text{cm}} = 0, 25, 66, 100$  and  $150$  MeV, starting from the filled symbol at 0 MeV. The trajectory with stars are eigenvalues for the  $N^3\text{LO}$  potential of Ref. [20].

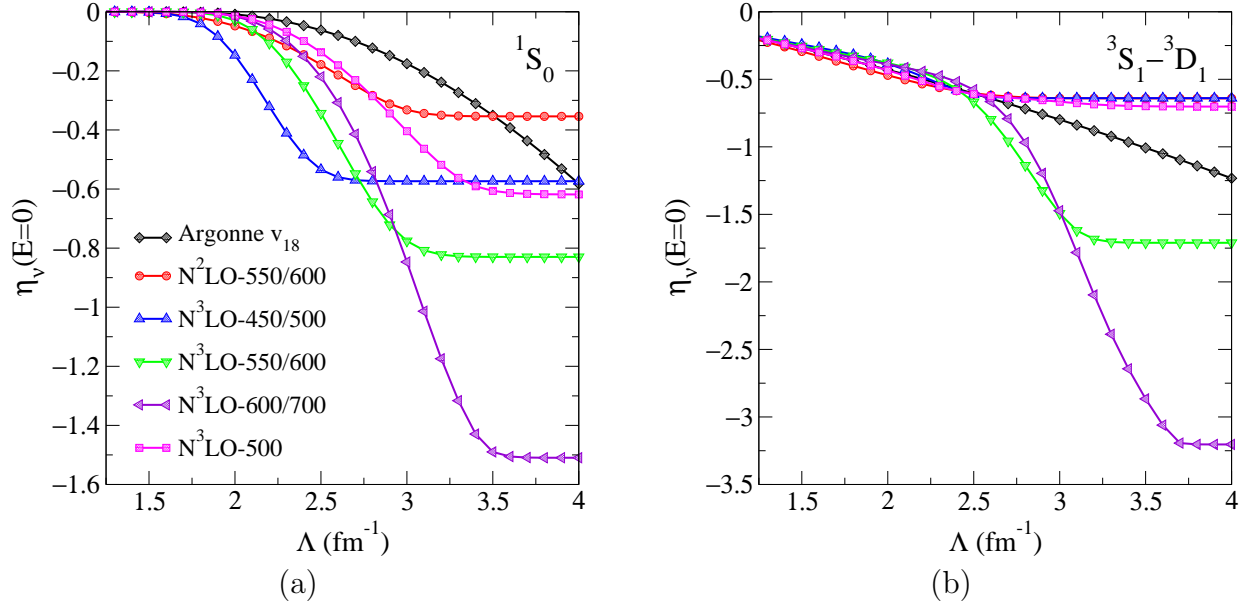


Figure 21: Largest repulsive Weinberg eigenvalues for  $E = 0$  in the (a)  $^1S_0$  and (b)  $^3S_1$ - $^3D_1$  channels as a function of cutoff for  $V_{\text{low } k}$  evolved from chiral EFT interactions [9]. Results are shown for the  $N^3\text{LO}$  potential of Entem and Machleidt [20], for  $N^3\text{LO}$  potentials of Epelbaum et al. [44] with different cutoffs  $\Lambda/\tilde{\Lambda}$  (as indicated in MeV), and for an  $N^2\text{LO}$  potential [74]. For comparison, we have plotted the largest repulsive Weinberg eigenvalues for  $V_{\text{low } k}$  evolved from the Argonne  $v_{18}$  potential.

Figure 20 shows the trajectories of the largest repulsive Weinberg eigenvalue in the  $^1S_0$  and  $^3S_1$ - $^3D_1$  channels as a function of (positive) energy for  $V_{\text{low } k}$  interactions with various cutoffs evolved from the Argonne  $v_{18}$  potential. The magnitude of the largest repulsive eigenvalue at all energies decreases rapidly as the cutoff is lowered. This reflects the decrease of the short-range repulsion present in the



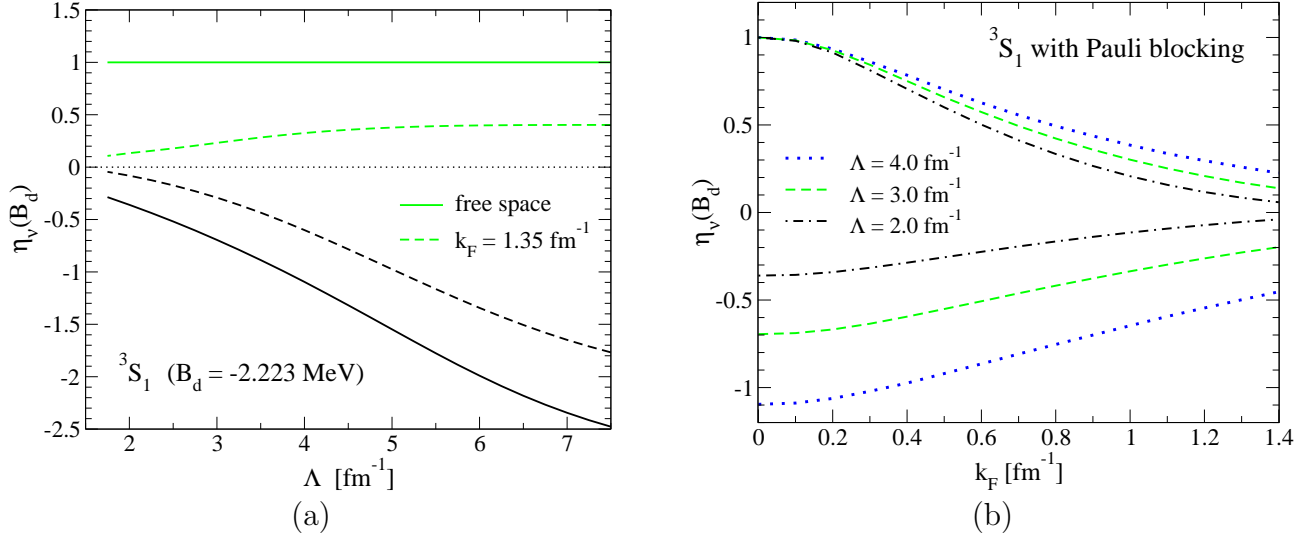


Figure 22: (a) Evolution of the two largest Weinberg eigenvalues with  $\Lambda$  in the  $^3S_1$ - $^3D_1$  channel in free-space (solid) and at saturation density (dashed). The lighter curves correspond to attractive eigenvalues and the darker curves to repulsive eigenvalues. (b) Dependence on density of the two largest Weinberg eigenvalues in the  $^3S_1$ - $^3D_1$  channel. Results are based on  $V_{\text{low } k}$  evolved from the Argonne  $v_{18}$  potential. For details see Ref. [9].

initial potential. In the  $^1S_0$  channel, the trajectory lies completely inside the shaded unit circle for cutoffs near  $4 \text{ fm}^{-1}$  and below, which implies that the Born series becomes perturbative with respect to the repulsive part of the potential. In the  $^3S_1$ - $^3D_1$  channel, the largest repulsive eigenvalues are just within the unit circle for  $\Lambda = 3 \text{ fm}^{-1}$ . The decrease from  $\Lambda = 3 \text{ fm}^{-1}$  to  $2 \text{ fm}^{-1}$  is significant for ensuring a convergence of particle-particle ladders in nuclear matter, because second-order short-range tensor contributions peak at intermediate-state momenta  $k \approx 2.5 - 3.5 \text{ fm}^{-1}$  in nuclear matter [76].

Chiral EFT interactions typically have cutoffs below  $3.5 \text{ fm}^{-1}$  and therefore are expected to be soft potentials. However, as shown in Fig. 21, the  $N^3\text{LO}$  potentials of Epelbaum et al. [44] have substantial repulsive Weinberg eigenvalues in both S-waves. These unexpected features were traced to the singular central and tensor interactions (at  $N^3\text{LO}$ ) in Ref. [12]. The results in Fig. 21 show there is a major decrease in the largest repulsive eigenvalues as the cutoff is run down from  $\Lambda = 3 \text{ fm}^{-1}$  to  $2 \text{ fm}^{-1}$ , which shows that it is advantageous to evolve chiral EFT interactions to lower cutoffs using the RG.

The systematics of the Weinberg eigenvalues in free space and at finite density are compared for the  $^3S_1$ - $^3D_1$  channel in Fig. 22(a), which shows the evolution with  $\Lambda$  of the two largest eigenvalues evaluated at the deuteron pole,  $E = B_d$ . In free space, we observe that the repulsive eigenvalue is initially large but decreases rapidly with cutoff, while the large attractive eigenvalue corresponding to the deuteron pole remains invariant,  $\eta_\nu(B_d) = 1$ . The behavior is similar at finite density, but now the attractive eigenvalue is tamed by Pauli-blocking effects. This result is general at sufficient density, as shown in Fig. 22(b). We therefore reach a promising conclusion: Large-cutoff sources of nonperturbative behavior can be eliminated using the RG, while physical sources due to weakly and nearly bound states are suppressed in the medium by Pauli-blocking. These results are qualitatively unchanged with the inclusion of low-momentum 3N interactions [9, 16] (see Section 5). Moreover, the Weinberg analysis has been applied to pairing in Ref. [77].

In addition to improving perturbative convergence, RG-evolved potentials result in more effective variational calculations [11] and rapidly converging basis expansions [14, 15], as discussed in Section 6. Finally, we mention that as a by-product of the Weinberg analysis in Ref. [12], it was found that RG-evolved interactions can be accurately described by low-rank separable expansions, a result that

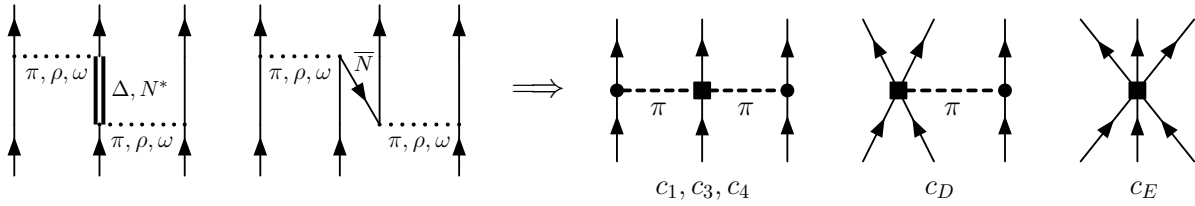


Figure 23: Eliminating degrees of freedom leads to three-body forces.

allows significant simplifications in applications ranging from few-body scattering [78] to the treatment of pairing in finite nuclei [79, 80].

## 2.5 Many-body interactions and operators

In a low-energy effective theory of finite-mass composite particles such as atoms or nucleons, three-body (or higher-body) interactions are defined as a contribution to the Hamiltonian that is not accounted for by the sum of pairwise interactions. The polarization of interacting atoms or molecules provides an intuitive example. The Axilrod-Teller potential is a three-body version of the familiar two-body long-range van der Waals force between atoms; its physical origin is triple-dipole mutual polarization [81]. Because it contributes at third order in perturbation theory and the fine structure constant is small, there is a rapidly decreasing hierarchy of many-body forces. Indeed, this contribution is usually negligible in metals and semiconductors although not in rare gas solids [82]. For solid xenon, its contribution is calculated to be about 10% of the ground-state energy [83], comparable to the typical 3N force contribution to the  ${}^3\text{H}$  binding energy. Note that polarization with additional atoms means that the Hamiltonian for an  $A$ -body system will inevitably lead to  $A$ -body forces.

The EFT perspective (see Section 1.1) confirms that operators (including the Hamiltonian) in *any* low-energy effective theory, if it is systematic rather than a model, will have many-body components. The generic origin of these many-body operators is a restriction of degrees of freedom, such as 3N forces arising from the elimination of the  $\Delta$  or anti-nucleon components, as illustrated in Fig. 23. Integrating out or decoupling high momentum modes with the RG is just another example. The EFT expansion systematically includes all such contributions as a combination of long-range (for example, due to pion exchanges) and short-range (contact) terms as on the right side of Fig. 23, even when the origin of the short-range parts is unclear. Power counting in chiral EFT establishes a decreasing hierarchy of many-body operators (see Fig. 4(a) for many-body forces) that permits truncation at a tractable level (which in present nuclear structure calculations means 3N forces and two-body current operators).

The strength of many-body components in an initial operator will shift with any change in how high-energy degrees of freedom are coupled to the low-energy degrees of freedom; particular examples are the running of a  $V_{\text{low } k}$  cutoff  $\Lambda$  or an SRG flow parameter  $\lambda$ . The correlation plot in Fig. 24(a) of  ${}^3\text{H}$  and  ${}^4\text{He}$  binding energies calculated using  $V_{\text{low } k}$  NN-only interactions shows the change in the (omitted) many-body contribution with  $\Lambda$ . This reproduces the empirical Tjon line from phenomenological potentials. The technical challenge is to carry out the evolution of many-body forces and operators in an RG implementation. The physics challenge is to establish that the EFT hierarchy of many-body components is not affected by the evolution, so that a tractable truncation is still possible. This typically means that the evolution is not extended below  $\Lambda$  or  $\lambda$  of about  $1.5\text{ fm}^{-1}$ . (For cutoffs below the pion mass, three-body forces will increase to leading order in pionless EFT [30, 32].)

The consistent RG evolution of  $V_{\text{low } k}$  many-body interactions has not yet been achieved. The underlying difficulty is that the technology used to construct  $V_{\text{low } k}$  requires the solution of the full 3N problem (bound state wave functions plus scattering wave functions in all breakup channels) to consistently evolve 3N forces (without simplifications). In  $V_{\text{low } k}$  calculations to date, the three-body evolution is therefore approximated by fitting the leading chiral EFT 3N forces at each cutoff while

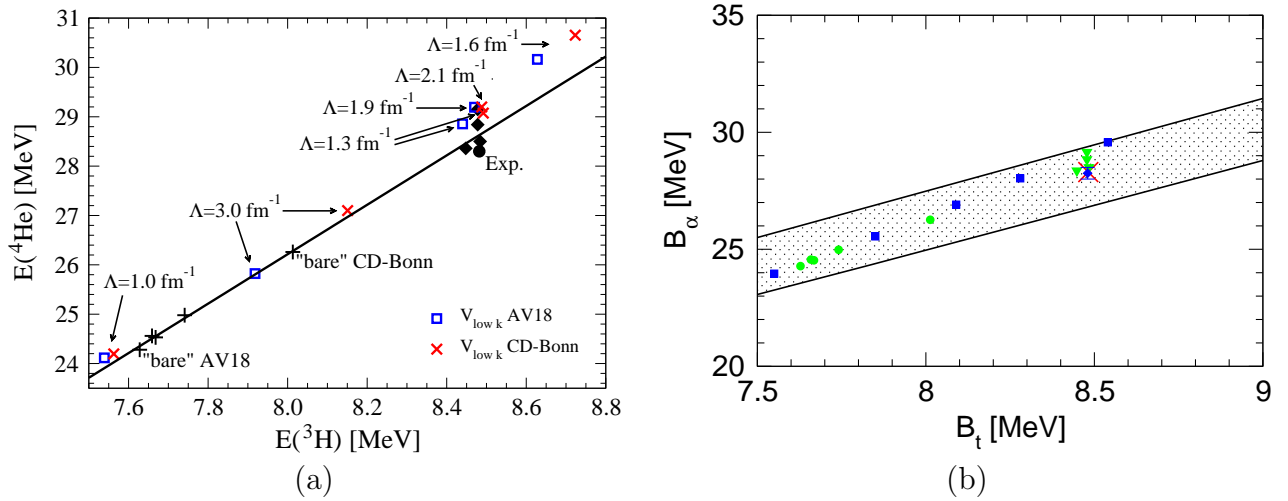


Figure 24: Correlation of  $^3\text{H}$  and  $^4\text{He}$  binding energies. (a) The cutoff dependence obtained from low-momentum NN interactions  $V_{\text{low } k}$  compared to the Tjon line [8]. (b) This correlation is driven by large scattering lengths, as demonstrated by the band obtained in pionless EFT [84].

evolving the two-body interaction exactly [8, 16]. This takes advantage of the EFT expansion being a complete operator basis for 3N forces, so that the leading effects of the evolution are simply a change in the operator coefficients (see Section 4.1 for more details).

The SRG offers a new path to the consistent running of many-body interactions and operators because they evolve through unitary transformations that require only a representation in a convenient basis. This has recently been demonstrated in practice [85]; we discuss the details in Sections 4.2 and 4.4. To see how the two-, three-, and higher-body potentials are identified and evolved, it is useful to decompose the running SRG Hamiltonian<sup>8</sup>  $H_\lambda$  in second-quantized form. Schematically (suppressing indices and sums),

$$H_\lambda = \langle T \rangle a^\dagger a + \langle V_\lambda^{(2)} \rangle a^\dagger a^\dagger a a + \langle V_\lambda^{(3)} \rangle a^\dagger a^\dagger a^\dagger a a a + \dots, \quad (7)$$

where  $a^\dagger, a$  are creation and annihilation operators with respect to the vacuum in a single-particle basis. This defines  $\langle T \rangle, \langle V_\lambda^{(2)} \rangle, \langle V_\lambda^{(3)} \rangle, \dots$  as the one-body (kinetic energy), two-body, three-body, ... matrix elements at each  $\lambda$ . The SRG evolution is dictated by commutators involving  $H_\lambda$  (see Eq. (21)); when they are evaluated using  $H_\lambda$  from Eq. (7), we see that even if initially there are only two-body potentials, higher-body interactions are generated with each step in  $\lambda$ . Thus, when applied in an  $A$ -body subspace, the SRG will “induce”  $A$ -body forces. But we also see that  $\langle T \rangle$  is fixed,  $\langle V_\lambda^{(2)} \rangle$  is determined only in the  $A = 2$  subspace with no dependence on  $\langle V_\lambda^{(3)} \rangle$ ,  $\langle V_\lambda^{(3)} \rangle$  is determined in  $A = 3$  by subtraction for given  $\langle V_\lambda^{(2)} \rangle$ , and so on. With this formulation,  $H_\lambda$  is a free-space Hamiltonian, independent of  $A$ . It is also possible to normal order in the medium, which changes the definition of the creation and annihilation in Eq. (7) and shifts higher-body pieces to the zero-, one-, and two-body levels (see Section 4.3).

Although one often characterizes the changes with  $\Lambda$  or  $\lambda$  by saying that the RG evolution “induces” many-body forces, this should not be interpreted as meaning the initial Hamiltonian has a “true” three-body force. The initial and evolved interactions are equally effective interactions and if the EFT truncation error is preserved in the evolution, there is no physics reason to prefer one over the other. (Indeed, referring to the initial interaction as the “bare” interaction is misleading in the same way.) Each Hamiltonian has different associated many-body components and operators, although the long-range parts are the same, as they are not modified by the evolution. A consequence of the latter is that operators that probe only long distances will not evolve, as seen by the weak cutoff dependence until

<sup>8</sup>The SRG Hamiltonian is denoted equivalently by  $H_\lambda$  or  $H_s$ , where  $\lambda \equiv 1/s^{1/4}$ .

small  $\Lambda$  for matrix elements of the bare quadrupole moment operator in Fig. 16(b).

## 2.6 Cutoff dependence as a tool

The RG equations for  $V_{\text{low } k}$  or SRG interactions start with a Hamiltonian as an initial condition, which together with the corresponding operators fixes the values of observables. In principle there should be no change in observables as the Hamiltonian is evolved. (More precisely, in the usual  $V_{\text{low } k}$  formulation, low-energy observables are unchanged while for the SRG all observables are preserved.) In practice there will be approximations both in the implementation of the RG and then in the subsequent calculations of nuclear structure observables. That is, cutoff dependence arises because of the truncation (or approximation) of “induced” many-body forces (see Section 2.5) or because of many-body approximations. Because observables should be by construction independent of the RG cutoff or flow parameter, we can use changes as a diagnostic of approximations and to estimate theoretical errors.

In more general applications of the RG, it is expected that significant changes in the cutoff are needed to glean useful information. In the examples considered here, however, the range of cutoff variation is a factor of two or in some cases even smaller. However, even small changes in the RG parameter can make dramatic shifts in the physics of nuclear structure observables, such as integrating out the short-range repulsion or short-range tensor forces.

Here are some examples of using RG cutoff dependence as a tool:

- Cutoff dependence at different orders in an EFT expansion. In Figs. 4(b), 5(a), and 5(b), the spread of predictions for EFT interactions with a range of cutoffs indicates whether the results improve as expected. This carries over directly to low-momentum interactions constructed from initial EFT Hamiltonians at different orders.
- Running of ground-state energies with cutoff in few-body systems. The variation in Fig. 35 shows the scale of the (net) omitted many-body forces, which is then an estimate of the error from this approximation. This allows a comparison with expectations from EFT power counting.
- Tjon line and the nature of correlations (see Fig. 24). The cutoff dependence obtained from low-momentum NN interactions  $V_{\text{low } k}$  in Fig. 24(a) explains the empirical (solid) Tjon line [8]. This correlation is driven by large scattering lengths, as demonstrated by the band in Fig. 24(b) obtained in pionless EFT [84].
- Calculations of nuclear matter. The decrease in cutoff dependence with improved approximations (see Fig. 40) helps validate the many-body convergence and establishes a lower bound on the error from short-range many-body interactions.
- Calculations of nuclei. For example, the cutoff variation in helium halo nuclei with NN-only interactions identifies sensitivity to 3N force effects [15,86] (see Fig. 49). We refer to Section 6.1 for more examples of cutoff dependence used as a diagnostic of missing many-body forces.
- Identification of (non-)observables. If a quantity changes more rapidly with the cutoff than any possible error, it is not an observable. An example is the D-state probability of the deuteron, whose cutoff dependence as shown in Fig. 57 demonstrates it is not an observable. In contrast, the independence of the asymptotic D/S-state ratio is evidence it is an observable.
- Cutoff dependence can be used in EFT as a tool to determine power counting (see Ref. [71] and references therein). This entails running a cutoff  $\Lambda$  lower, rescaling in units of  $\Lambda$ , and looking for fixed points of the RG flow; that is, for flows that end in scale independence. The EFT is then expanded around such a fixed point. Examples for the nuclear case are described in Ref. [71].

The common lesson here is that it is advantageous to do calculations for a range of cutoff values.

### 3 Low-momentum technology for two-nucleon interactions

In this section, we give an overview of the equations and techniques used to derive low-momentum NN interactions (with many-body interactions treated in Section 4). We use the equations as a guide to how renormalization group methods decouple low- and high-energy degrees of freedom but refer to the literature for the more technical details.

#### 3.1 Sharp cutoff $V_{\text{low } k}$

Imposing a sharp cutoff  $\Lambda$  in relative momentum is the most direct way to limit the resolution of an NN potential by excluding high-momentum modes. But to incorporate the relevant details from such modes into low-momentum interactions, they must be integrated out rather than simply truncated. The  $V_{\text{low } k}$  approach [5, 58, 87] does this by demanding that the (half-on-shell)  $T$  matrix for an initial potential  $V_{\text{NN}}$  be unchanged in every NN partial wave as  $\Lambda$  is lowered, so that

$$T(k', k; k^2) = V_{\text{NN}}(k', k) + \frac{2}{\pi} \mathcal{P} \int_0^{\Lambda_\infty} \frac{V_{\text{NN}}(k', p) T(p, k; k^2)}{k^2 - p^2} p^2 dp, \quad (8)$$

$$= V_{\text{low } k}^\Lambda(k', k) + \frac{2}{\pi} \mathcal{P} \int_0^\Lambda \frac{V_{\text{low } k}^\Lambda(k', p) T(p, k; k^2)}{k^2 - p^2} p^2 dp, \quad (9)$$

for all  $k, k' < \Lambda$ . Note that this means that  $V_{\text{low } k}$  only has momentum components below the cutoff but the invariance of  $T(k', k; k^2)$  ensures that observables for these momenta (such as phase shifts and the deuteron binding energy) are preserved.

Imposing  $dT(k', k; k^2)/d\Lambda = 0$  on Eq. (9) gives the RG equation [58, 87]<sup>9</sup>

$$\frac{d}{d\Lambda} V_{\text{low } k}^\Lambda(k', k) = \frac{2}{\pi} \frac{V_{\text{low } k}^\Lambda(k', \Lambda) T^\Lambda(\Lambda, k; \Lambda^2)}{1 - (k/\Lambda)^2}. \quad (10)$$

Integrating Eq. (10) with the large cutoff initial condition<sup>10</sup>  $V_{\text{low } k}^{\Lambda_\infty} = V_{\text{NN}}$  is equivalent to first re-summing high-momentum ladders in an energy-dependent effective interaction, which is the solution to the two-body Bloch-Horowitz equation in momentum space with the projector  $Q = \frac{2}{\pi} \int_\Lambda^\infty q^2 dq |q\rangle\langle q|$ , and subsequently trading energy dependence for momentum dependence by using the equations of motion. This two-step procedure is also equivalent to the commonly-used Lee-Suzuki transformation method used to construct energy-independent effective interactions [5, 89–91]. Note, however, that the RG approach differs from Lee-Suzuki as the  $Q$ -space block of the effective Hamiltonian is set to zero. As a result of this equivalence (see Ref. [88]), the  $V_{\text{low } k}$  interactions can be constructed in energy-independent form either using model-space methods (such as Lee-Suzuki or Okubo [92] transformations) or through the RG treatment. In practice, most calculations of  $V_{\text{low } k}$  have used the model-space methods<sup>11</sup> (followed by an Okubo Hermitization [5, 6]) rather than the differential equations of the RG because they are more robust numerically. This is true for both sharp and smooth cutoff versions of  $V_{\text{low } k}$ .

The evolution to lower cutoffs shifts contributions from the sum over intermediate states to the interactions, just as RG equations in quantum field theory shift strength from loop integrals to coupling constants. The change in the interactions include subleading contact interactions to all orders. Because only large momentum modes are decoupled, long-range pion exchanges are preserved. As documented in Section 2.3, different initial  $V_{\text{NN}}$  interactions collapse to the same nearly universal  $V_{\text{low } k}$  at sufficiently small cutoffs ( $\Lambda \sim 2.0 \text{ fm}^{-1}$ ).

<sup>9</sup>The derivation of Eq. (10) is slightly more complicated in the presence of bound states, although the final result remains the same [88].

<sup>10</sup>The cutoff  $\Lambda_\infty$  is chosen large enough so that the initial potential  $V_{\text{NN}}$  is effectively zero for  $k > \Lambda_\infty$ . This can be very large for phenomenological potentials, for example,  $\Lambda_\infty \gtrsim 25 \text{ fm}^{-1}$  for the Argonne  $v_{18}$  potential [18].

<sup>11</sup>See Refs. [93, 94] for a three-dimensional formulation that avoids partial-wave decompositions.

### 3.2 Smooth regulators for $V_{\text{low } k}$

The sharp cutoff RG equation for  $V_{\text{low } k}$  takes a particularly simple form that preserves two-body observables for all momenta up to the cutoff. However, a sharp momentum cutoff leads to cusp-like behavior close to the cutoff in some channels and for the deuteron wave function (see inset in Fig. 25(a)), which becomes increasingly evident as the cutoff is lowered below  $2 \text{ fm}^{-1}$ . In some applications, this leads to slow convergence, for example at the 10–100 keV level in few-body calculations using harmonic-oscillator bases, as shown in Fig. 26(b). One would expect that such calculations for the deuteron and the triton, which are particularly low-energy bound states, should show improvement for cutoffs well below  $2 \text{ fm}^{-1}$ , but instead a degradation was observed in Ref. [10]. This result was attributed to the use of sharp cutoffs, and subsequent studies [6, 11] have shown that these problems are alleviated by using a smooth-cutoff version of  $V_{\text{low } k}$ .

The sharp cutoff  $V_{\text{low } k}$  interactions were originally constructed using model-space methods (such as Lee-Suzuki [5, 58] or Okubo [62] transformations) that rely on the definition of orthogonal projectors  $P$  and  $Q$ , such that  $P + Q = 1$  and  $PQ = QP = 0$ . While smooth cutoffs seem incompatible with methods requiring  $PQ = 0$ , it is not a conceptual problem for the RG approach. Indeed, there is an appreciable literature on smooth-cutoff regulators for applications of the functional or exact RG [95]. The functional RG keeps invariant the full generating functional, which translates into preserving all matrix elements of the fully off-shell inter-nucleon  $T$  matrix. While this straightforwardly leads to RG equations, it also implies an energy-dependent interaction, which is undesirable for practical few- and many-body calculations. This conflict can be resolved by a generalization of the energy-independent RG equation derived in Section 3.1 to smooth cutoffs [6]. It is convenient to first define the partial-wave  $V_{\text{low } k}$  and the corresponding  $T_{\text{low } k}$  matrix in terms of a reduced potential  $v$  and a reduced  $t$  matrix as

$$V_{\text{low } k}(k', k) = f(k') v(k', k) f(k), \quad (11)$$

$$T_{\text{low } k}(k', k; k^2) = f(k') t(k', k; k^2) f(k). \quad (12)$$

where  $f(k)$  is a smooth cutoff function satisfying

$$f(k) \xrightarrow{k \ll \Lambda} 1 \quad \text{and} \quad f(k) \xrightarrow{k \gg \Lambda} 0. \quad (13)$$

Representative examples are exponentials  $f(k) = \exp[-(k^2/\Lambda^2)^{n_{\text{exp}}}]$  and Fermi-Dirac functions  $f(k) = 1/(1 + e^{(k^2 - \Lambda^2)/\epsilon^2})$ . The reduced half-on-shell  $t$  matrix obeys a Lippmann-Schwinger equation with loop integrals smoothly cut off by  $f^2(p)$ ,

$$t(k', k; k^2) = v(k', k) + \frac{2}{\pi} \int_0^\infty p^2 dp \frac{v(k', p) f^2(p) t(p, k; k^2)}{k^2 - p^2}. \quad (14)$$

Analogous to the RG derivation for a sharp cutoff, we impose that the reduced half-on-shell  $t$  matrix is independent of the cutoff,  $dt(k', k; k^2)/d\Lambda = 0$ . This choice preserves the on-shell  $t$  matrix while also maintaining energy independence. The resulting RG equation is

$$\frac{d}{d\Lambda} v(k', k) = \frac{2}{\pi} \int_0^\infty p^2 dp \frac{v(k', p) \frac{d}{d\Lambda} [f^2(p)] t(p, k; k^2)}{p^2 - k^2}, \quad (15)$$

which describes the evolution of the reduced low-momentum interaction with the cutoff. If one takes an energy-independent NN potential as the large-cutoff initial condition and numerically integrates Eq. (15), then the resulting  $v$  preserves the half-on-shell  $T_{\text{NN}}$  matrix for *all* external momenta,  $t(k', k; k^2) = T_{\text{NN}}(k', k; k^2)$ . Therefore,  $V_{\text{low } k}(k', k) = f(k') v(k', k) f(k)$  preserves the low-momentum half-on-shell  $T_{\text{NN}}$  matrix up to factors of the smooth cutoff function. In the limit  $f(p) \rightarrow \theta(\Lambda - p)$ , the RG equation for a sharp cutoff, Eq. (10), is recovered.



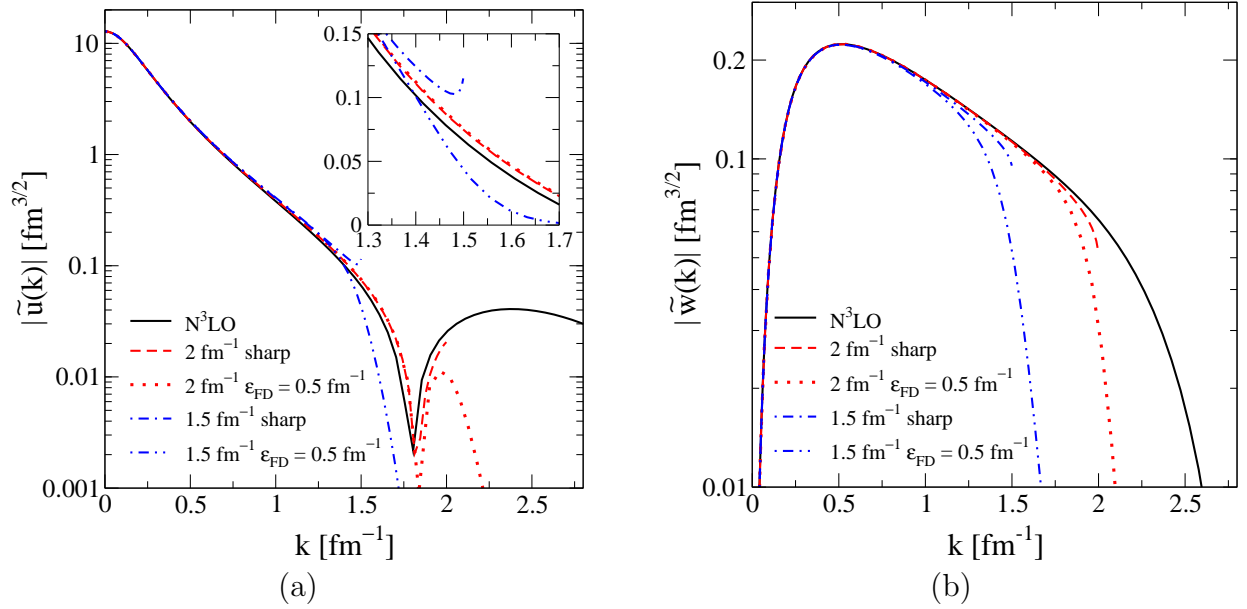


Figure 25: (a) S-state and (b) D-state components of the deuteron wave function in momentum space ( $\tilde{u}(k)$  and  $\tilde{w}(k)$  respectively) for the  $N^3\text{LO}$  potential of Ref. [20] and evolved  $V_{\text{low } k}$  using smooth and sharp cutoffs at  $\Lambda = 2.0 \text{ fm}^{-1}$  and  $1.5 \text{ fm}^{-1}$ .

The solution to Eq. (15) is non-Hermitian. However, one can show [6] that a simple generalization of the Okubo Hermitization transformation to smooth cutoffs is obtained by symmetrizing the smooth-cutoff RG equation, Eq. (15), to obtain

$$\frac{d}{d\Lambda} v(k', k) = \frac{1}{\pi} \int_0^\infty p^2 dp \left[ \frac{v(k', p) \frac{d}{d\Lambda} [f^2(p)] t(p, k; p^2)}{p^2 - k^2} + \frac{t(k', p; p^2) \frac{d}{d\Lambda} [f^2(p)] v(p, k)}{p^2 - k'^2} \right]. \quad (16)$$

Here, the Hermitian low-momentum interaction  $V_{\text{low } k}$  preserves the low-momentum fully-on-shell  $T_{\text{NN}}$  matrix, up to factors of the regulator function  $T_{\text{low } k}(k, k; k^2) = f^2(k) T_{\text{NN}}(k, k; k^2)$ , and the deuteron binding energy. Note that demanding  $dt(k, k; k^2)/d\Lambda$  does not imply a “unique” Hermitian RG equation. In conventional model-space methods, this non-uniqueness corresponds to the choice in the Hermitization procedure (or to residual unitary transformations in the  $P$ -space block). In RG language, this can be viewed as demanding  $dt(k', k; k^2)/d\Lambda = (k^2 - k'^2) \Phi(k', k)$ , where  $\Phi(k', k)$  is any function satisfying  $\lim_{k \rightarrow k'} (k^2 - k'^2) \Phi(k', k) = 0$ . The above RG equation derived from the Okubo transformation corresponds to a particular choice for  $\Phi(k', k)$ .

In practice, the numerical solution of Eq. (16) is slowed by the  $t$  matrix evaluations involved at each step. In addition, the RG equation involves two-dimensional interpolations and principal-value integrals over narrowly peaked functions making it easy to introduce small errors at each step that can accumulate as the cutoff is lowered. Therefore, an alternative 3-step procedure to construct a low-momentum, energy-independent interaction with smooth cutoffs that is better suited for numerical calculations has been formulated (see Ref. [6] for details):

1. Evolve a large-cutoff potential to a lower, smooth cutoff while preserving the *full* off-shell  $T$  matrix modulo factors of the smooth cutoff functions. This generates an energy-dependent low-momentum interaction, and amounts to solving the Bloch-Horowitz equation with a smooth cutoff.
2. Convert the energy dependence to momentum dependence using equations of motion, which results in a non-Hermitian smooth-cutoff interaction that preserves the low-momentum half-on-shell  $T$ -matrix modulo factors of the smooth cutoff functions.

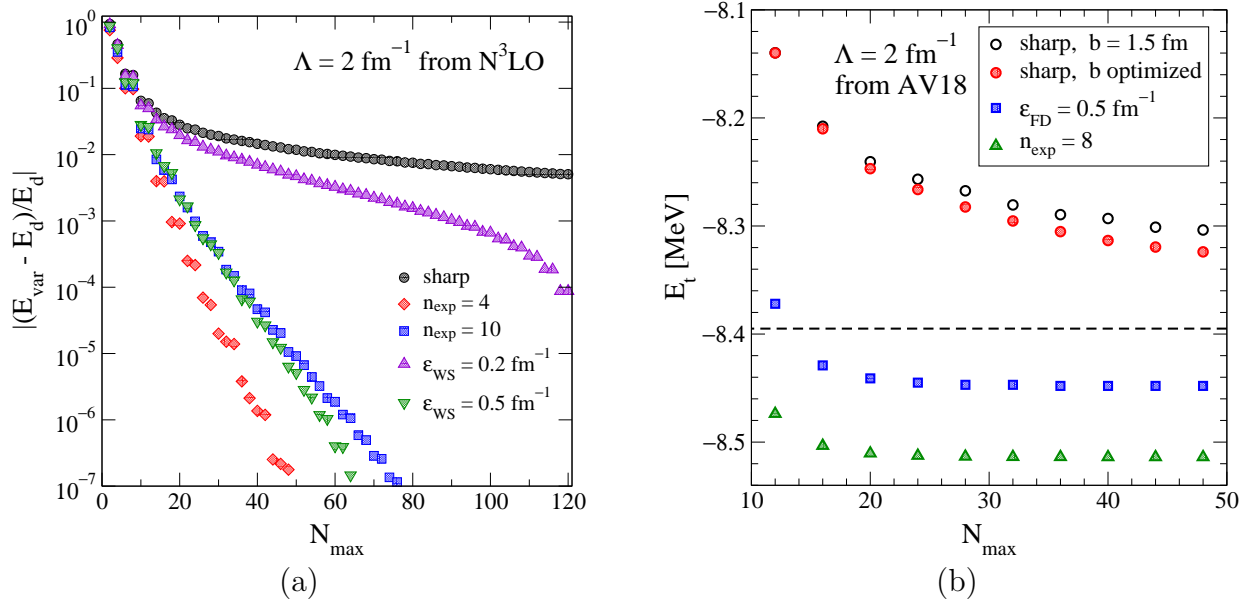


Figure 26: (a) The relative error in the deuteron binding energy  $E_d$  as a function of the size of the oscillator space for sharp cutoff and various smooth regulators. (b) The triton binding energy  $E_t$  calculated from a direct diagonalization in a harmonic-oscillator basis of the low-momentum Hamiltonian evolved from the Argonne  $v_{18}$  potential with cutoff  $\Lambda = 2 \text{ fm}^{-1}$ , as a function of the size of the oscillator space ( $N_{\text{max}} \hbar\omega$  excitations). The open circles are calculated with a sharp cutoff for a fixed oscillator parameter  $b$  while the filled ones correspond to optimizing  $b$  at each  $N_{\text{max}}$ . The dashed line indicates the exact Faddeev result [8], which shows the slow convergence at the 100 keV level of the diagonalization for the sharp cutoff. The squares are for a smooth Fermi-Dirac regulator and the triangles for a smooth exponential regulator, which each solve the convergence problem. For details see Ref. [6].

3. Perform a similarity transformation to Hermitize the low-momentum interaction. The resulting low-momentum interaction is energy-independent and Hermitian, and preserves the low-momentum fully on-shell  $T$ -matrix up to factors of the smooth cutoff functions.

It has been verified numerically that Eq. (16) and the 3-step procedure give very similar results, and both tend towards the sharp cutoff  $V_{\text{low } k}$  (with Okubo Hermitization) calculated using the Lee-Suzuki method in the limit of a sharp cutoff. However, due to its computational advantages the 3-step method is used in most applications, although Eq. (16) has also been used in practical calculations [17, 96, 97].

The momentum space deuteron wave functions for smooth and sharp cutoffs are contrasted in Fig. 25. We follow the notation of Ref. [74], with S- and D-state components denoted in coordinate space by  $u$  and  $w$  respectively, and with tildes in momentum space. The sharp-cutoff wave functions develop cusp-like structures in momentum space below  $2 \text{ fm}^{-1}$  (see inset in Fig. 25(a)), which are removed by the Fermi-Dirac (or any other smooth) regulator. As with the sharp cutoff  $V_{\text{low } k}$ , the smooth-cutoff evolution removes the short-range correlation “wound” in the coordinate-space deuteron wave function at lower cutoffs, and only modifies short-distance physics as indicated by the weak cutoff dependence of long-range operators like the “bare” quadrupole moment in the deuteron, see Fig. 16(b). These features lead to more perturbative behavior in nuclear matter [9] as well as in few-body systems [11, 12].

The primary motivation for smooth cutoffs was to remedy the slow convergence at the 10 keV level in the deuteron and at the 100 keV level in the triton, when calculated in a harmonic-oscillator basis. In Fig. 26(a), the relative error in the binding energy of the deuteron (with respect to the converged result) is shown as a function of the size of the oscillator space ( $N_{\text{max}} \hbar\omega$  excitations) for a range of smooth regulators. The slow convergence is evident for the sharp cutoff, where the error is below the percent

level only for the largest space. The Fermi-Dirac regulator eliminates this problem, with improved convergence by increasing the smoothness parameter  $\epsilon$  from  $0.2 \text{ fm}^{-1}$  to  $0.5 \text{ fm}^{-1}$ . Very similar results are obtained for the exponential regulator, or any other smooth regulator function. The convergence is also greatly improved for the triton. In Fig. 26(b), the triton binding energy is plotted as a function of the size of the oscillator space. For efficiency, convergence for the smallest possible space is desirable, as the computational cost grows rapidly with  $N_{\text{max}}$  and for larger systems. Convergence at the keV level is achieved by all exponential regulators with  $n_{\text{exp}} \geq 4$  ( $n_{\text{exp}} = 8$  is shown) soon after  $N_{\text{max}} = 20$ . The consequence in moving from sharp to increasingly smooth regulators is also seen from the Fermi-Dirac regulators, where  $\epsilon = 0.5 \text{ fm}^{-1}$  yields very satisfactory results.

### 3.3 Similarity renormalization group (SRG)

An alternative path to decoupling high-momentum from low-momentum physics is the similarity renormalization group (SRG), which is based on a continuous sequence of unitary transformations that suppress off-diagonal matrix elements, driving the Hamiltonian towards a band-diagonal form [98–102]. The SRG potentials are automatically energy independent and have the feature that high-energy phase shifts (and other high-energy NN observables), while typically highly model dependent (see Fig. 1), are preserved, unlike the case with  $V_{\text{low } k}$  as usually implemented. Most important, the same transformations renormalize all operators, including many-body operators, and the class of transformations can be tailored for effectiveness in particular problems.

In Ref. [7], the first application of SRG transformations to NN interactions using the flow equation formalism of Wegner [99, 102] was made. The evolution or flow of the Hamiltonian with a parameter  $s$  is a series of unitary transformations,

$$H_s = U_s H U_s^\dagger \equiv T_{\text{rel}} + V_s, \quad (17)$$

where  $T_{\text{rel}}$  is the relative kinetic energy and  $H = T_{\text{rel}} + V$  is the initial Hamiltonian. Equation (17) defines the evolved potential  $V_s$ , with  $T_{\text{rel}}$  taken to be independent of  $s$ . Then  $H_s$  evolves according to

$$\frac{dH_s}{ds} = [\eta_s, H_s], \quad (18)$$

with

$$\eta_s = \frac{dU_s}{ds} U_s^\dagger = -\eta_s^\dagger. \quad (19)$$

Choosing  $\eta_s$  specifies the transformation, which is taken as the commutator of an operator,  $G_s$ , with the Hamiltonian,

$$\eta_s = [G_s, H_s], \quad (20)$$

so that

$$\frac{dH_s}{ds} = [[G_s, H_s], H_s]. \quad (21)$$

Applications to nuclear forces have used  $G_s = T_{\text{rel}}$  [7], but one could also use momentum-diagonal operators such as  $T_{\text{rel}}^2$ , or the running diagonal Hamiltonian  $H_D$ , as advocated by Wegner [99] (see also Ref. [103]). Taking the simplest choice  $G_s = T_{\text{rel}}$ , the flow equation in a partial wave takes the form

$$\frac{dV_s(k, k')}{ds} = -(k^2 - k'^2)^2 V_s(k, k') + \frac{2}{\pi} \int_0^\infty q^2 dq (k^2 + k'^2 - 2q^2) V_s(k, q) V_s(q, k'). \quad (22)$$

For matrix elements far from the diagonal, the first term on the right side of Eq. (22) evidently dominates and exponentially suppresses these elements as  $s$  increases,

$$V_s(k, k') \approx V_{s=0}(k, k') e^{-s(k^2 - k'^2)^2}. \quad (23)$$

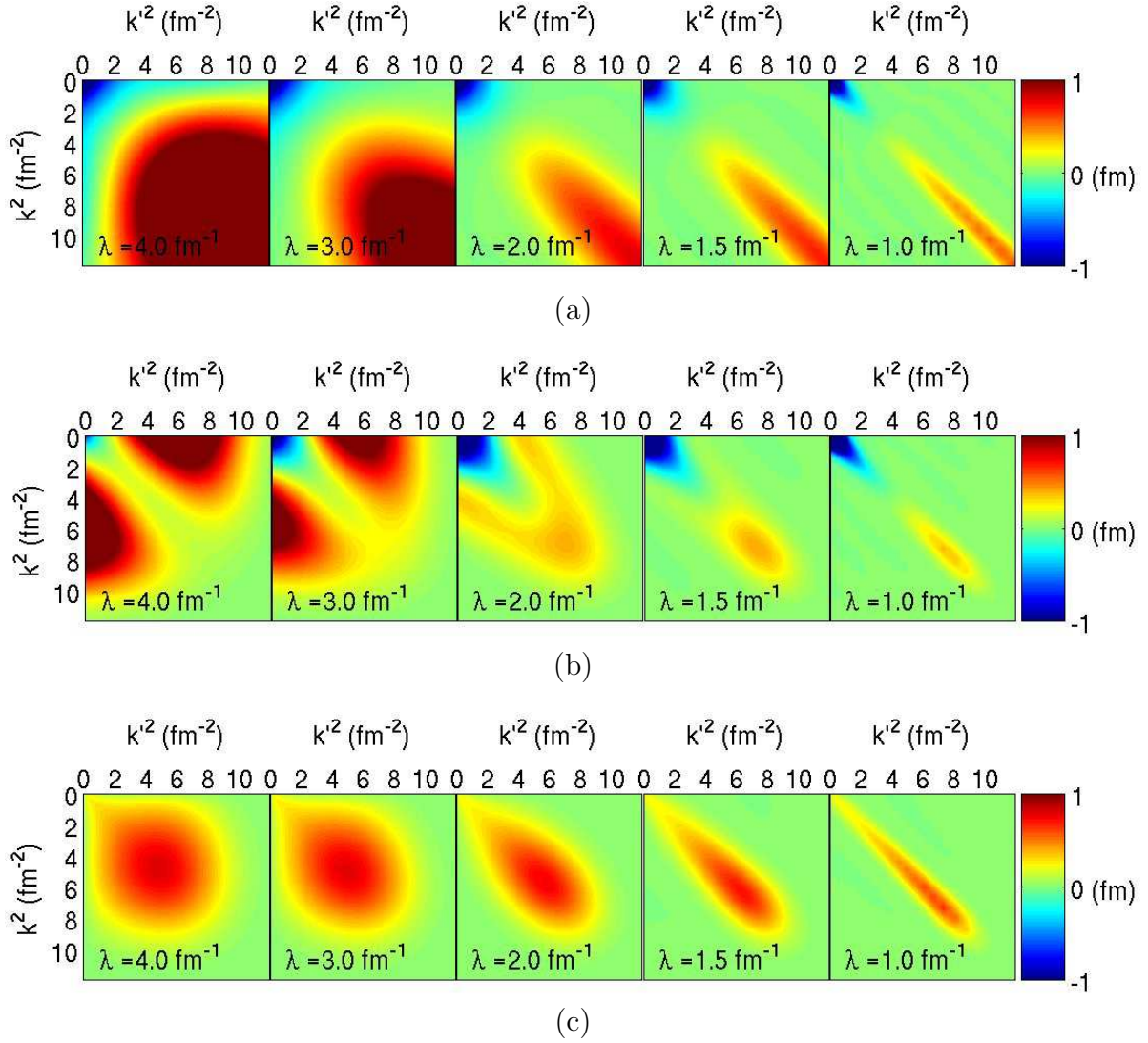


Figure 27: Contour plots of momentum-space matrix elements for the SRG evolution with  $\lambda$  in the (a)  $^1S_0$ , (b) S-wave part of the  $^3S_1$ – $^3D_1$  and (c)  $^1P_1$  channels. The initial potential in (a) is the ( $\Lambda = 600$  MeV)  $N^3$ LO potential [20] and in (b) and (c) the  $N^3$ LO potential with  $\Lambda/\tilde{\Lambda} = 500/600$  MeV [44].

It is convenient to switch to the flow variable  $\lambda \equiv s^{-1/4}$ , which has units of  $\text{fm}^{-1}$ , because Eq. (23) shows that  $\lambda$  is a measure of the resulting diagonal width of  $V_s$  in momentum space.

The evolution of the Hamiltonian according to Eq. (22) as  $s$  increases (or  $\lambda$  decreases) is illustrated in Fig. 27, using two initial chiral EFT potentials. On top is  $^1S_0$  starting from the harder ( $\Lambda = 600$  MeV)  $N^3$ LO potential of Ref. [20], which has significant strength near the high-momentum diagonal, in the middle is the S-wave part of the  $^3S_1$ – $^3D_1$  channel starting from one of the potentials of Ref. [44], which has more far off-diagonal strength initially and comparatively weaker higher-momentum strength on the diagonal, and on bottom is  $^1P_1$  with that same potential. Each of these examples show the characteristic features of the evolution in  $\lambda$ , namely the systematic suppression of off-diagonal strength, as anticipated, with the width of the diagonal scaling as  $\lambda^2$ .

The SRG-evolved interactions share key similarities (universality, increased perturbativeness, weaker correlations, etc.) with the smooth-cutoff  $V_{\text{low } k}$  potentials, even though the decoupling of low and high momenta is achieved in a somewhat different manner. As  $\lambda$  is lowered, different initial potentials flow to similar forms at low momentum (while remaining distinct at higher momentum), with the universal low-momentum parts numerically similar to the  $V_{\text{low } k}$  potentials. These observations are illustrated in

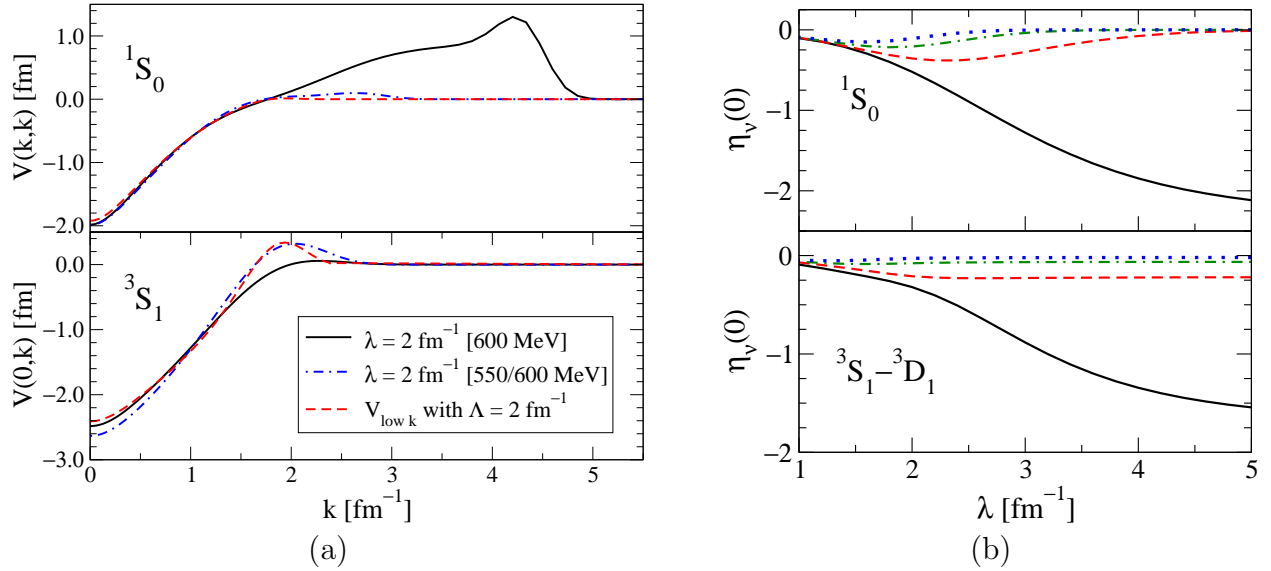


Figure 28: (a) Low-momentum universality for momentum-space matrix elements of the evolved SRG potentials at  $\lambda = 2 \text{ fm}^{-1}$  for  $^1S_0$  (top, diagonal elements) and  $^3S_1$  (bottom, off-diagonal elements). Also shown is the  $V_{\text{low } k}$  potential for a smooth regulator with  $\Lambda = 2 \text{ fm}^{-1}$  and  $n_{\text{exp}} = 4$ . (b) Largest repulsive Weinberg eigenvalues in the  $^1S_0$  and  $^3S_1$ - $^3D_1$  channels as a function of  $\lambda$ , with initial potentials as in Fig. 27. For details see Ref. [7].

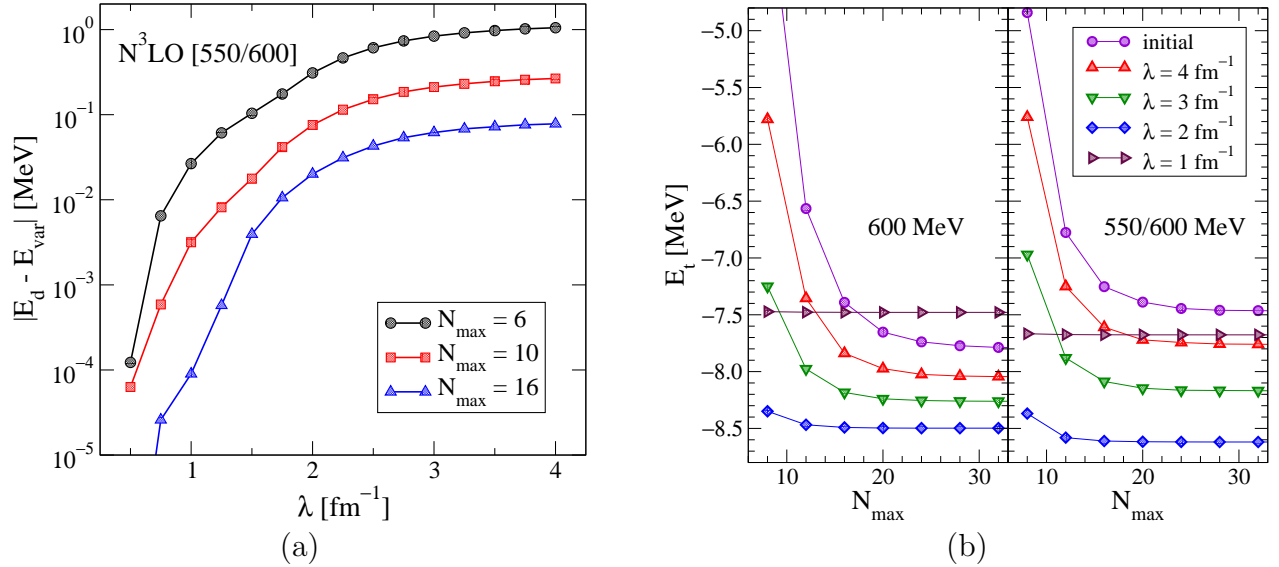


Figure 29: (a) Absolute error versus  $\lambda$  of the deuteron binding energy from a variational calculation in a fixed-size basis of harmonic oscillators ( $N_{\text{max}} \hbar\omega$  excitations). (b) Variational triton binding energy for selected  $\lambda$  with NN interactions only, as a function of  $N_{\text{max}}$ . For details see Ref. [7].

Fig. 28(a) for the diagonal and off-diagonal matrix elements.

Similarly, the nonperturbative features associated with strong short-range repulsion and strong short-range tensor forces are substantially softened as we evolve to lower  $\lambda$ . The largest repulsive Weinberg eigenvalues (see Section 2.4) for  $E = 0$  are shown as a function of  $\lambda$  in Fig. 28(b) for the  $^1S_0$  and  $^3S_1$ - $^3D_1$  channels. In both channels, the large eigenvalues decrease rapidly as  $\lambda$  evolves to  $2 \text{ fm}^{-1}$  and below, as observed with the  $V_{\text{low } k}$  evolution in Section 2.4. The more perturbative potentials at lower  $\lambda$  induce weaker short-range correlations in few- and many-body wave functions, which leads to

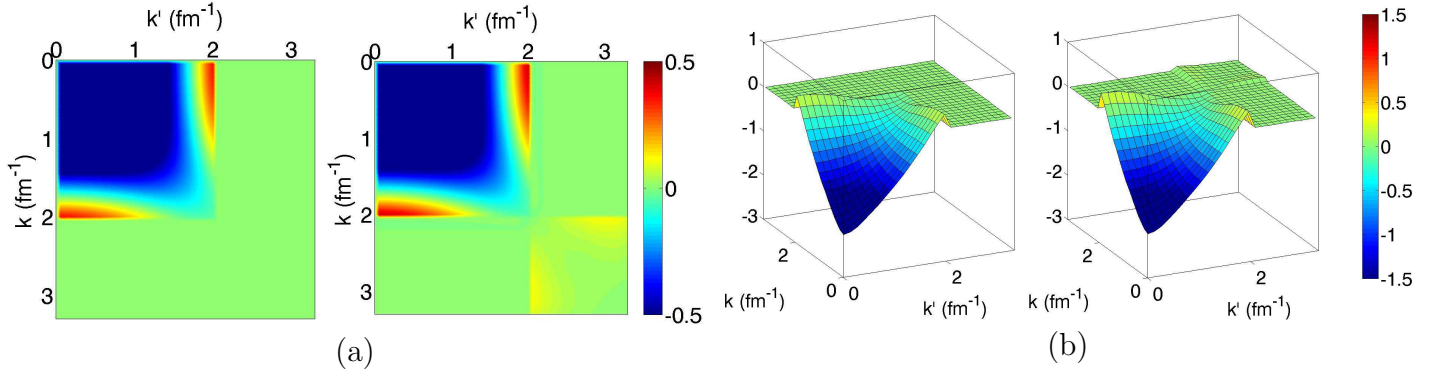


Figure 30: (a) and (b): Comparison of momentum-space  $V_{\text{low } k}$  (left) and SRG block-diagonal (right) potentials with  $\Lambda = 2 \text{ fm}^{-1}$  evolved from the N<sup>3</sup>LO  $^3\text{S}_1$  potential of Ref. [20]. The color and  $z$  axes are in fm. For details see Ref. [104].

greatly improved convergence in variational calculations. This is illustrated in Figs. 29(a) and 29(b) via calculations of the deuteron and triton binding energies by diagonalization in a harmonic-oscillator basis. The improvement in convergence is similar to that found with smoothly-cutoff  $V_{\text{low } k}$  interactions [6].

In Fig. 29(b), the calculations for different  $\lambda$  converge to different values for the triton binding energy. This reflects the contributions of the omitted (and evolving) three-body interactions, and follows a similar pattern to that seen with NN-only  $V_{\text{low } k}$  calculations [6, 8]. The consistent evolution of many-body forces is an important issue for low-momentum interactions. For the SRG, the evolution of 3N forces is readily practical, as discussed in Section 4.2.

### 3.4 $V_{\text{low } k}$ from SRG flow equations

A powerful feature of the SRG is that the generator  $G_s$  can be tailored to decouple high- and low-momentum physics in different ways [104]. Block-diagonal decoupling of the sharp  $V_{\text{low } k}$  form can be generated using SRG flow equations by choosing a block-diagonal flow operator [105, 106],

$$G_s = \begin{pmatrix} PH_sP & 0 \\ 0 & QH_sQ \end{pmatrix}, \quad (24)$$

with projection operators  $P$  and  $Q = 1 - P$ . In a partial-wave momentum representation,  $P$  and  $Q$  are step functions defined by a sharp cutoff  $\Lambda$  on relative momenta. This choice for  $G_s$ , which means that  $\eta_s$  is non-zero only where  $G_s$  is zero, suppresses off-diagonal matrix elements such that the Hamiltonian approaches a block-diagonal form as  $s$  increases. If one considers a measure of the off-diagonal coupling of the Hamiltonian,

$$\text{Tr}[(QH_sP)^\dagger(QH_sP)] = \text{Tr}[PH_sQH_sP] \geq 0, \quad (25)$$

then its derivative is easily evaluated by applying the SRG equation, Eq. (21):

$$\begin{aligned} \frac{d}{ds} \text{Tr}[PH_sQH_sP] &= \text{Tr}[P\eta_sQ(QH_sQH_sP - QH_sPH_sP)] + \text{Tr}[(PH_sPH_sQ - PH_sQH_sQ)Q\eta_sP] \\ &= -2 \text{Tr}[(Q\eta_sP)^\dagger(Q\eta_sP)] \leq 0. \end{aligned} \quad (26)$$

Thus, the off-diagonal  $QH_sP$  block will decrease in general as  $s$  increases [105, 106].

The right panels of Figs. 30(a) and 30(b) result from evolving the N<sup>3</sup>LO potential of Ref. [20] using the block-diagonal  $G_s$  of Eq. (24) with  $\Lambda = 2 \text{ fm}^{-1}$  to  $\lambda = 0.5 \text{ fm}^{-1}$ . The agreement between  $V_{\text{low } k}$  and SRG potentials for momenta below  $\Lambda$  is striking, where a similar degree of universality is found in other channels. Deriving an explicit connection between these approaches is the topic of ongoing research.



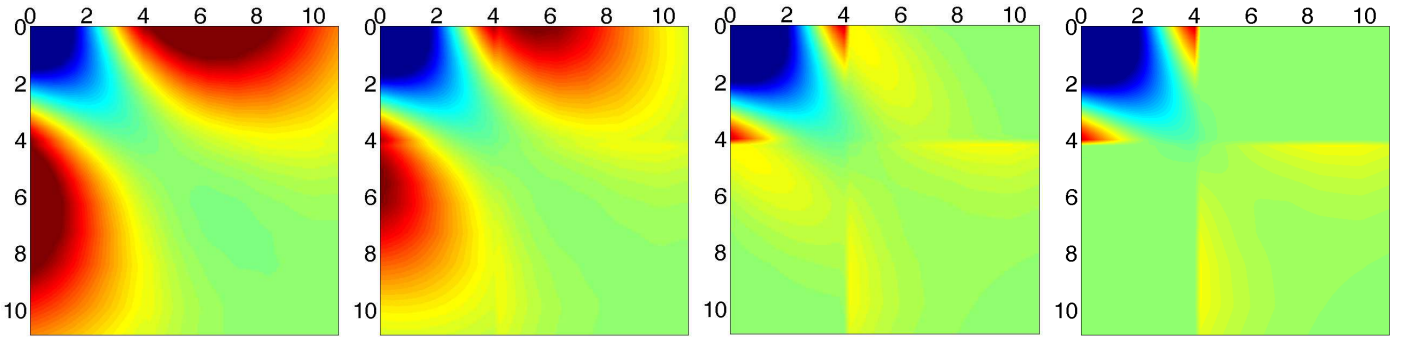


Figure 31: Evolution of the  $^3S_1$  partial wave using the SRG block-diagonal flow equation with  $\Lambda = 2 \text{ fm}^{-1}$  at  $\lambda = 4, 3, 2$ , and  $1 \text{ fm}^{-1}$  [104]. The initial  $N^3\text{LO}$  potential is from Ref. [20]. The axes are in units of  $k^2$  from  $0 - 11 \text{ fm}^{-2}$  and the color scale ranges from  $-0.5$  to  $+0.5 \text{ fm}$  as in Fig. 30(a).

The evolution with  $\lambda$  of the  $^3S_1$  channel is shown in Fig. 31 (for results in the  $^1P_1$  channel see Ref. [104]). The evolution of the “off-diagonal” matrix elements (meaning those outside the  $PH_sP$  and  $QH_sQ$  blocks) can be roughly understood from the dominance of the kinetic energy on the diagonal. Let the indices  $p$  and  $q$  run over indices of the momentum states in the  $P$ - and  $Q$ -spaces, respectively. To good approximation we can replace  $PH_sP$  and  $QH_sQ$  by their eigenvalues  $E_p$  and  $E_q$  in the SRG equations, yielding [105, 106]

$$\frac{d}{ds} h_{pq} \approx \eta_{pq} E_q - E_p \eta_{pq} = -(E_p - E_q) \eta_{pq} \quad \text{and} \quad \eta_{pq} \approx E_p h_{pq} - h_{pq} E_q = (E_p - E_q) h_{pq}. \quad (27)$$

Combining these two results, we have the evolution of any off-diagonal matrix element:

$$\frac{d}{ds} h_{pq} \approx -(E_p - E_q)^2 h_{pq}. \quad (28)$$

For two-nucleon interactions we can replace the eigenvalues by those for the relative kinetic energy, which gives the explicit solution

$$h_{pq}(s) \approx h_{pq}(0) e^{-s(p^2 - q^2)}. \quad (29)$$

Thus the off-diagonal matrix elements go to zero with the energy differences just like with the SRG with  $T_{\text{rel}}$ ; one can see the width of order  $1/\sqrt{s} = \lambda^2$  in the  $k^2$  plot of the evolving potential in Fig. 31 (this is even clearer in other partial waves, see Ref. [104]).

While in principle the evolution to a sharp block-diagonal form means going to  $s = \infty$  ( $\lambda = 0$ ), in practice one must only take  $s$  as large as needed to quantitatively achieve the decoupling implied by Eq. (29). Furthermore, this should hold for more general definitions of  $P$  and  $Q$ . To smooth out the cutoff, one can introduce a smooth regulator  $f_\Lambda$ , which can be taken as an exponential  $f_\Lambda(k) = e^{-(k^2/\Lambda^2)^{n_{\text{exp}}}}$ . For  $V_{\text{low } k}$  interactions, typical values used are  $n_{\text{exp}} = 4, 6$ , and  $8$  (the latter is considerably sharper but still numerically robust). By replacing the generator with

$$G_s = f_\Lambda H_s f_\Lambda + (1 - f_\Lambda) H_s (1 - f_\Lambda), \quad (30)$$

one obtains a smooth block-diagonal potential (for examples, see Ref. [104]).

### 3.5 Related methods

There are various other methods used to transform nuclear Hamiltonians for use in few- and many-body calculations. Although they are not cast in the RG language, many of the same principles and features discussed in Section 2 apply. While space does not permit detailed discussions of each, here we give a brief synopsis and comparison, with pointers to the literature for more information.

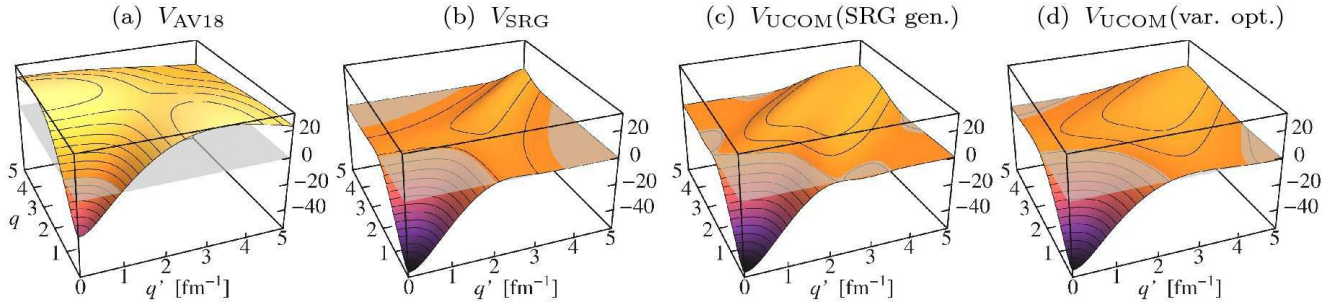


Figure 32: Comparison of momentum-space matrix elements of  $^1S_0$  potentials (in units of  $\text{MeV fm}^3$ ) for (a) Argonne  $v_{18}$ , (b) SRG-evolved with  $\lambda = 2.4 \text{ fm}^{-1}$ , (c) UCOM-transformed using SRG-generated correlators ( $\lambda = 2.25 \text{ fm}^{-1}$ ), and (d) UCOM-transformed using variationally optimized correlators [107]. Reprinted with permission from R. Roth et al. [107], copyright (2008) by the American Physical Society.

**Bloch-Horowitz.** The energy-dependent Bloch-Horowitz (BH) equation is used as an intermediate step in deriving energy-independent sharp and smooth-cutoff  $V_{\text{low } k}$  interactions. The BH method has also been used directly in other approaches, where the energy is determined self-consistently. The harmonic-oscillator-based effective theory [108–111] is one such example. While most detailed applications have been limited to  $A = 2, 3$  because energy-dependent interactions are difficult to handle in other approaches, perturbative expansions and clever resummations may overcome this hurdle.

**UCOM.** Feldmeier, Neff, Roth and collaborators have developed a method using unitary transformations designed to remove short-range “hard core” and tensor correlations [101, 112–114]. The approach is called the Unitary Correlation Operator Method (UCOM). The result is a soft Hamiltonian that shares favorable features of the RG-based interactions. They have also studied parallels (and some distinctions) of UCOM to the SRG approach [107, 115], as shown in Fig. 32. Using a UCOM NN potential, which is phase equivalent to a given initial Hamiltonian, they have investigated ground-state energies and radii of many nuclei (including heavy nuclei such as  $^{208}\text{Pb}$ ) in Hartree-Fock plus many-body perturbation theory. Preliminary results from supplementing the NN potential by a short-range three-body force with fitted strength are encouraging [116]. As originally formulated, the UCOM procedure is difficult to carry out beyond the two-body level. However, the connections to the SRG approach established in [107, 115] may help to transform 3N forces.

**NCSM Lee-Suzuki.** The Lee-Suzuki transformations used in the No-Core-Shell-Model (NCSM) are constructed to decouple low from high energy within a harmonic-oscillator model space [117]. A cluster expansion is used to organize and truncate the many-body components. This approach has been successfully used to describe nuclear spectra, especially in  $p$ -shell nuclei starting from chiral EFT interactions [57, 118]. A detailed overview of this approach including recent developments is given in Ref. [65]. As usually constructed, the Lee-Suzuki approach is not variational and does not always show smooth convergence with respect to the model-space size. Unlike the momentum-space RG evolution, it is not clear if evolving in the harmonic-oscillator basis is problematic for long-range operators, as indicated by the sizable effective three- and higher-body contributions to  $B(E2)$  values [65].

**UMOA.** In the Unitary Model Operator Approach (UMOA), a Hermitian, energy-independent effective interaction is derived by Okubo-type unitary transformations of an initial Hamiltonian (see Ref. [119] and references therein). The transformation is applied twice to make the effective interaction more suitable to larger nuclei. In the first transformation, the short-range repulsion is softened by partitioning the  $P$ - and  $Q$ -space with an energy cutoff on two-body harmonic-oscillator states. In the second transformation, the softened interaction is transformed so that there are no matrix elements between the unperturbed ground state and two-particle–two-hole states for a given closed-shell nucleus. Calculations have been performed for stable nuclei around  $^{16}\text{O}$  [120],  $\Lambda$ -hypernuclei [121] and for ground-state and single-particle energies of  $^{40}\text{Ca}$  and  $^{56}\text{Ni}$  [122].

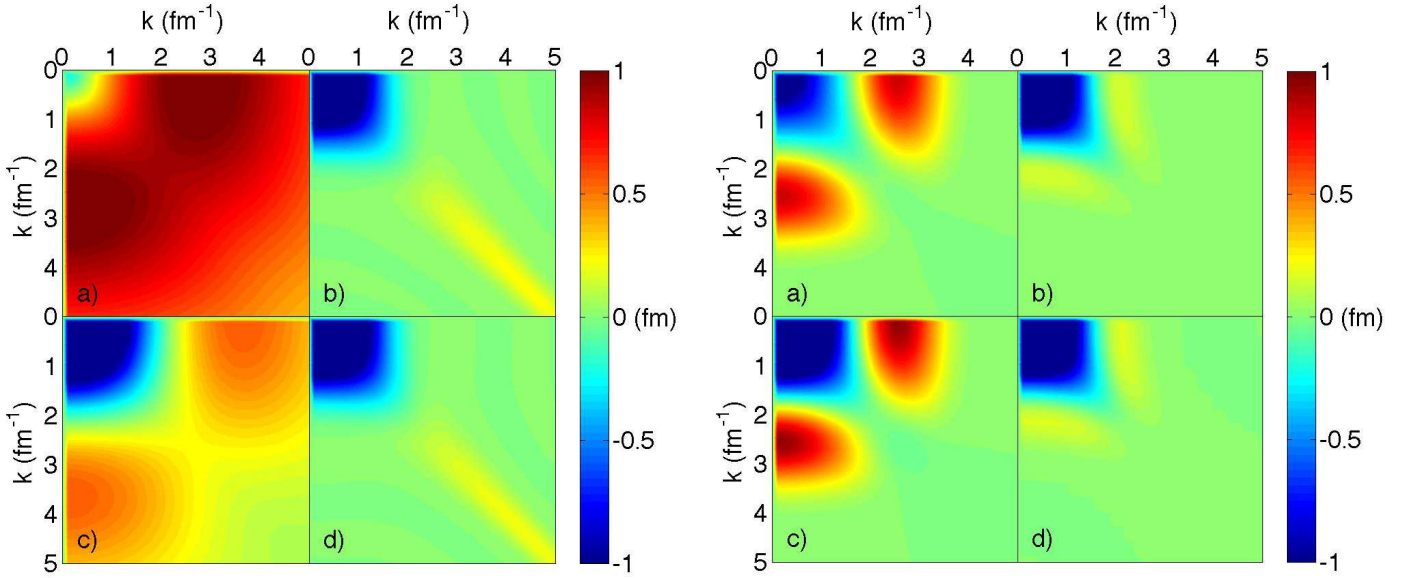


Figure 33:  $G$  matrix at saturation density for the Argonne  $v_{18}$  potential [18] (left panels) and the N<sup>3</sup>LO potential of Ref. [20] (right panels) in the  $^3\text{S}_1$  channel. Each set of four panels are a) initial potential, b) potential evolved by the SRG to  $\lambda = 2 \text{ fm}^{-1}$ , c)  $G$  matrix based on a), and d)  $G$  matrix based on b).

**$G$  matrix.** The  $G$  matrix is the in-medium sum of ladder diagrams to form a two-body effective interaction from a starting NN potential. This formalism has been used in calculations of nuclear matter [123], for effective interactions in nuclei [91], and in self-consistent Green’s function approaches [124]. It has been suggested that  $V_{\text{low } k}$  NN interactions are essentially the same as a  $G$  matrix but there are substantial differences. First,  $V_{\text{low } k}$  at a given cutoff  $\Lambda$  is a free-space interaction, equivalent in practice to any low-energy Hamiltonian (with no “starting energy” dependence). Second, significant coupling between low and high momenta remains in the  $G$  matrix. This is demonstrated in Fig. 33, which shows the Argonne  $v_{18}$  and an N<sup>3</sup>LO potential in the  $^3\text{S}_1$  channel compared to low-momentum interactions (SRG evolved to  $\lambda = 2 \text{ fm}^{-1}$ , similar results are found for  $V_{\text{low } k}$  interactions) and to the  $G$  matrices obtained from each. (The qualitative conclusions do not depend on the particular choice of starting energy.) We observe that the summation into the  $G$  matrix has a relatively small effect on low-momentum interactions, in stark contrast to the Argonne  $v_{18}$  potential case. The resulting low-momentum matrix elements are indeed similar, but it is also apparent that there is substantial off-diagonal strength in the  $G$  matrix in this case. This coupling to high momenta prevents the expansion of nuclear matter properties from being perturbative in the  $G$  matrix, necessitating a non-perturbative scheme such as the hole-line expansion. One might expect the softer N<sup>3</sup>LO  $^3\text{S}_1$  potential to avoid this problem, but we see that the off-diagonal strength, while limited to lower momentum, is actually increased.

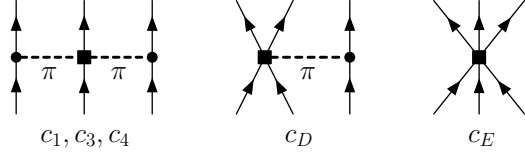
## 4 Many-body interactions and operators

When evolving nuclear interactions to lower resolution, it is inevitable that many-body interactions and operators are induced even if initially absent. This might be cause for alarm if nuclei could be accurately calculated with interactions truncated at the two-body level, as was assumed for part of the history of nuclear structure calculations. However, chiral EFT reveals the natural scale and hierarchy of many-body forces, which dictates their inclusion in modern calculations of nuclei and nucleonic matter. Thus the real concern is whether this hierarchy is maintained as nuclear interactions are evolved. In this section, we review the current status of RG technology to include many-body interactions and operators and the currently known impact on the hierarchy.

## 4.1 Three-nucleon interactions

Three-nucleon interactions are a frontier. They are crucial for binding energies and radii, they play a central role for spin-orbit effects, spin dependencies, for few-body scattering and the evolution of nuclear structure with isospin, and they drive the density dependence of nucleonic matter (see Sections 5 and 6) [73]. Three-nucleon interactions are also required for renormalization [125,126]. The construction of 3N forces based on chiral EFT provides a systematic organization of the physics and an operator basis that can be used to approximate the evolution of low-momentum 3N interactions.

In chiral EFT without explicit  $\Delta$  isobars, 3N forces first enter at N<sup>2</sup>LO (see Fig. 4(a)) and contain a long-range  $2\pi$ -exchange part  $V_c$ , an intermediate-range  $1\pi$ -exchange part  $V_D$  and a short-range contact interaction  $V_E$  [127,128]:



$$(31)$$

The  $2\pi$ -exchange interaction is given by

$$V_c = \frac{1}{2} \left( \frac{g_A}{2f_\pi} \right)^2 \sum_{i \neq j \neq k} \frac{(\boldsymbol{\sigma}_i \cdot \mathbf{q}_i)(\boldsymbol{\sigma}_j \cdot \mathbf{q}_j)}{(q_i^2 + m_\pi^2)(q_j^2 + m_\pi^2)} F_{ijk}^{\alpha\beta} \tau_i^\alpha \tau_j^\beta, \quad (32)$$

where  $\mathbf{q}_i = \mathbf{k}'_i - \mathbf{k}_i$  denotes the difference of initial and final nucleon momenta ( $i, j$  and  $k = 1, 2, 3$ ) and

$$F_{ijk}^{\alpha\beta} = \delta^{\alpha\beta} \left[ -\frac{4c_1 m_\pi^2}{f_\pi^2} + \frac{2c_3}{f_\pi^2} \mathbf{q}_i \cdot \mathbf{q}_j \right] + \sum_\gamma \frac{c_4}{f_\pi^2} \epsilon^{\alpha\beta\gamma} \tau_k^\gamma \boldsymbol{\sigma}_k \cdot (\mathbf{q}_i \times \mathbf{q}_j), \quad (33)$$

while the  $1\pi$ -exchange and contact interactions are given respectively by

$$V_D = -\frac{g_A}{8f_\pi^2} \frac{c_D}{f_\pi^2 \Lambda_\chi} \sum_{i \neq j \neq k} \frac{\boldsymbol{\sigma}_j \cdot \mathbf{q}_j}{q_j^2 + m_\pi^2} (\boldsymbol{\tau}_i \cdot \boldsymbol{\tau}_j) (\boldsymbol{\sigma}_i \cdot \mathbf{q}_j), \quad (34)$$

$$V_E = \frac{c_E}{2f_\pi^4 \Lambda_\chi} \sum_{j \neq k} (\boldsymbol{\tau}_j \cdot \boldsymbol{\tau}_k). \quad (35)$$

Typical values for applying Eqs. (32)–(35) are  $g_A = 1.29$ ,  $f_\pi = 92.4$  MeV,  $m_\pi = 138.04$  MeV and  $\Lambda_\chi = 700$  MeV. In the RG calculations based on chiral EFT interactions discussed here, the 3N force contributions are regulated as in Ref. [16] using

$$f_R(p, q) = \exp \left[ -\frac{(p^2 + 3q^2/4)^2}{\Lambda_{3\text{NF}}^4} \right], \quad (36)$$

with a 3N cutoff  $\Lambda_{3\text{NF}}$  that is allowed to vary independently of the NN cutoff. Here,  $p$  and  $q$  are Jacobi momenta. The exchange terms of the 3N force are included by means of the antisymmetrizer

$$\mathcal{A}_{123} = (1 + P_{12}P_{23} + P_{13}P_{23})(1 - P_{23}) = 1 - P_{12} - P_{13} - P_{23} + P_{12}P_{23} + P_{13}P_{23}, \quad (37)$$

where  $P_{ij}$  is the exchange operator for spin, isospin and momenta of nucleons  $i$  and  $j$ . The regulator  $f_R(p, q)$  is totally symmetric when expressed in the nucleon momenta  $\mathbf{k}_i$ , and thus the direct and exchange terms contain the same regulator.

The low-energy  $c_i$  couplings for the long-range parts relate  $\pi$ N, NN and 3N interactions, which means they can be fitted in different processes. The determination of the  $c_i$  couplings from  $\pi$ N scattering agrees reasonably well with the extraction from NN partial waves [31]. However, there are large uncertainties in the values (and some controversy, see Ref. [129]). More accurate determinations are needed for nuclear

$\Lambda$	${}^3\text{H}$					${}^4\text{He}$					max	${}^4\text{He}$
	$T$	$V_{\text{low } k}$	$V_c$	$V_D$	$V_E$	$T$	$V_{\text{low } k}$	$V_c$	$V_D$	$V_E$	$ V_{3N}/V_{\text{low } k} $	$k_{\text{rms}}$
1.0	21.06	-28.62	0.02	0.11	-1.06	38.11	-62.18	0.10	0.54	-4.87	0.08	0.55
1.3	25.71	-34.14	0.01	1.39	-1.46	50.14	-78.86	0.19	8.08	-7.83	0.10	0.63
1.6	28.45	-37.04	-0.11	0.55	-0.32	57.01	-86.82	-0.14	3.61	-1.94	0.04	0.67
1.9	30.25	-38.66	-0.48	-0.50	0.90	60.84	-89.50	-1.83	-3.48	5.68	0.06	0.70
2.5(a)	33.30	-40.94	-2.22	-0.11	1.49	67.56	-90.97	-11.06	-0.41	6.62	0.12	0.74
2.5(b)	33.51	-41.29	-2.26	-1.42	2.97	68.03	-92.86	-11.22	-8.67	16.45	0.18	0.74
3.0(*)	36.98	-43.91	-4.49	-0.73	3.67	78.77	-99.03	-22.82	-2.63	16.95	0.23	0.80

Table 1: Expectation values of the kinetic energy  $T$ ,  $V_{\text{low } k}$  and the different 3N contributions (long-range  $2\pi$ -exchange part  $V_c$ ,  $1\pi$ -exchange part  $V_D$  and contact interaction  $V_E$ ) for  ${}^3\text{H}$  and  ${}^4\text{He}$ . All energies are in MeV and momenta are in  $\text{fm}^{-1}$ . (a) and (b) denote two possible solutions for  $\Lambda = 2.5 \text{ fm}^{-1}$  and (\*) indicates that the  ${}^4\text{He}$  fit is approximate, for details see Ref. [8]. Also listed is the ratio of maximum 3N to  $V_{\text{low } k}$  contribution and an average relative momentum  $k_{\text{rms}}$  [132].

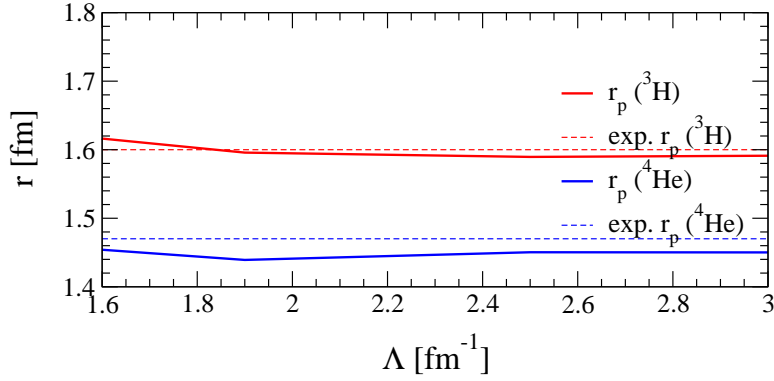


Figure 34: The  ${}^3\text{H}$  and  ${}^4\text{He}$  radii are approximately cutoff independent with low-momentum NN and 3N interactions [73, 133].

structure, where  $c_3$  and  $c_4$  are particularly important (see Fig. 44(b) for an example of the impact of the  $c_i$  uncertainties). The remaining  $c_D$  and  $c_E$  couplings are usually fit to the  ${}^3\text{H}$  binding energy and another observable in  $A \geq 3$ . These leading 3N interactions generally improve the agreement of theory with experiment in nucleon-deuteron scattering [31, 36] and in the spectra of light nuclei [57] (see Figs. 5(a) and 8). The subleading 3N interactions at  $\text{N}^3\text{LO}$  are parameter free and several parts have been calculated to date [130, 131]. The subleading 3N interactions at  $\text{N}^3\text{LO}$  are parameter free and several parts have been calculated to date [130, 131], including two-pion-one-pion-exchange and pion-ring diagrams, spin-orbit forces, and contributions that involve NN contacts [31]. One consequence is that operator structures of the form in Eq. (32) are generated at  $\text{N}^3\text{LO}$ , effectively weakening the values of the  $c_i$  couplings [31].

Instead of explicitly evolving 3N interactions to low momentum, one can take the  $\text{N}^2\text{LO}$  3N forces as a truncated basis and assume that the  $c_i$  couplings are not modified by the RG evolution. This is the strategy adopted in Refs. [8, 9, 16]. In this scheme,  $V_{3N}(\Lambda)$  is constructed by fitting the  $c_D$  and  $c_E$  couplings to the  ${}^3\text{H}$  binding energy and the  ${}^4\text{He}$  binding energy [8] or matter radius [16] for a range of cutoff values. When the  ${}^4\text{He}$  radius is fit, the predicted  ${}^4\text{He}$  binding energies are very reasonable. Fit values for  $c_D$  and  $c_E$  are found to be natural and are tabulated in Refs. [8] (with Argonne  $v_{18}$  [18] as initial NN potential) and [16] (with the  $\text{N}^3\text{LO}$  potential of Ref. [20]). For cutoffs  $\Lambda \lesssim 2.0 \text{ fm}^{-1}$ , there are linear dependencies in the fitting, which are consistent with a perturbative  $V_D$  and  $V_E$  contribution:  $E_{\text{gs}} = E(V_{\text{low } k} + V_c) + c_D \langle D\text{-term} \rangle + c_E \langle E\text{-term} \rangle$  (where  $\langle \dots \rangle$  denotes the matrix elements of the operators). This has been verified explicitly and also for  $V_c$ .

Thus, when evolved to lower cutoffs, low-momentum 3N interactions become perturbative in light nuclei [8, 16] which means  $\langle \Psi^{(3)} | V_{3N} | \Psi^{(3)} \rangle \approx \langle \Psi^{(2)} | V_{3N} | \Psi^{(2)} \rangle$ , where  $|\Psi^{(n)}\rangle$  are exact solutions including up to  $n$ -body forces. It is instructive to look at the expectation values of different contributions to the  $^3\text{H}$  and  $^4\text{He}$  ground-state energies, as listed in Table 1. The expectation values are consistent with chiral EFT power counting estimates, which means that the hierarchy of many-body forces is maintained. Note also that the sign of the  $c_i$  contribution is cutoff dependent. This contribution is repulsive in nuclear and neutron matter for low-momentum interactions (see Sections 5.1 and 5.2), which is counter to the intuition from conventional NN and 3N potentials [53, 134].

As discussed in Section 2.6 (see Fig. 24), neglecting 3N interactions leads to a universal correlation (empirically known as Tjon-line) between the  $^3\text{H}$  and  $^4\text{He}$  binding energies [8, 84]. This is an example of how cutoff variation can provide lower bounds for theoretical uncertainties due to neglected many-body interactions or an incomplete many-body treatment. Another example is shown in Fig. 34, where the radii for  $^3\text{H}$  and  $^4\text{He}$  are shown as a function of  $V_{\text{low } k}$  cutoff  $\Lambda$ . With 3N forces included, there is only a small cutoff dependence that shows the scale of the residual dependence on higher-order shorter-range many-body interactions.

## 4.2 Three-nucleon force evolution

While the use of a chiral EFT basis to approximate low-momentum 3N interactions is convenient and computationally efficient, it has not been verified against explicitly evolved three-body forces. This will be possible using SRG flow equations, which offer a tractable approach to evolving 3N forces (that avoids solving for any  $T$  matrices). The SRG flow equation,

$$\frac{dH_s}{ds} = [[G_s, H_s], H_s], \quad (38)$$

can be applied directly in the three-particle space. The right side involves only the Hamiltonian and the generator  $G_s$ , which can be evaluated in a basis without solving bound state or scattering equations. A potential issue is the role of spectator nucleons; we consider two solutions: first a decoupling of the 3N part in momentum-space representation and then a direct solution in a harmonic-oscillator basis. In both cases, we take  $G_s = T_{\text{rel}}$  and return at the end to other choices.

To show the basic idea in momentum space, we adopt a notation in which  $V_{12}$  means the two-body interaction between particles 1 and 2 while  $V_{123}$  is the irreducible three-body potential. We start with the Hamiltonian including up to three-body interactions (keeping in mind that higher-body interactions will be induced as we evolve in  $s$  but will not contribute to three-body systems):

$$H_s = T_{\text{rel}} + V_{12} + V_{13} + V_{23} + V_{123} \equiv T_{\text{rel}} + V_s. \quad (39)$$

(Note: all of the potentials depend implicitly on  $s$ .) The relative kinetic energy operator  $T_{\text{rel}}$  can be decomposed in three ways:

$$T_{\text{rel}} = T_{12} + T_3 = T_{13} + T_2 = T_{23} + T_1, \quad (40)$$

and  $T_i$  commutes with  $V_{jk}$ ,

$$[T_3, V_{12}] = [T_2, V_{13}] = [T_1, V_{23}] = 0, \quad (41)$$

so the commutators of  $T_{\text{rel}}$  with  $V_{jk}$  become  $[T_{\text{rel}}, V_{12}] = [T_{12}, V_{12}]$  and similarly for  $V_{13}$  and  $V_{23}$ .

Because we define  $T_{\text{rel}}$  to be independent of  $s$ , the SRG flow equation, (38), for the three-body Hamiltonian  $H_s$  simplifies to

$$\frac{dV_s}{ds} = \frac{dV_{12}}{ds} + \frac{dV_{13}}{ds} + \frac{dV_{23}}{ds} + \frac{dV_{123}}{ds} = [[T_{\text{rel}}, V_s], H_s], \quad (42)$$



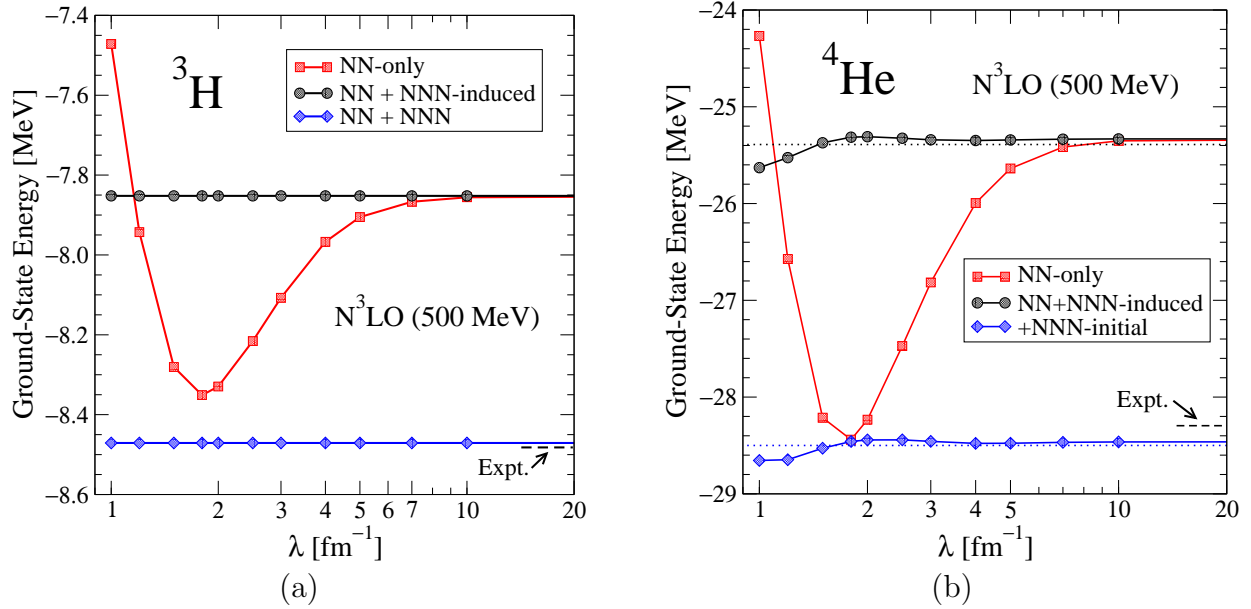


Figure 35: Ground-state energy of (a)  ${}^3\text{H}$  and (b)  ${}^4\text{He}$  as a function of  $\lambda$ . For details see Ref. [85].

with  $V_s$  defined by Eq. (39). The corresponding equations for each of the two-body potentials (which are completely determined by their evolved matrix elements in the two-body systems) are

$$\frac{dV_{12}}{ds} = [[T_{12}, V_{12}], (T_{12} + V_{12})], \quad (43)$$

and similarly for  $V_{13}$  and  $V_{23}$ . After expanding Eq. (42) using Eq. (39) and the different decompositions of  $T_{\text{rel}}$ , it is straightforward to show that the derivatives of two-body potentials on the left side cancel precisely with terms on the right side, leaving

$$\begin{aligned} \frac{dV_{123}}{ds} = & [[T_{12}, V_{12}], (T_3 + V_{13} + V_{23} + V_{123})] + [[T_{13}, V_{13}], (T_2 + V_{12} + V_{23} + V_{123})] \\ & + [[T_{23}, V_{23}], (T_1 + V_{12} + V_{13} + V_{123})] + [[T_{\text{rel}}, V_{123}], H_s]. \end{aligned} \quad (44)$$

The importance of these cancellations is that they eliminate the “dangerous” delta functions, which make setting up the integral equations for the three-body system problematic [135]. We emphasize that the  $s$ -dependence of the two-body potentials on the right side of Eq. (44) is completely determined by solving the two-body problem in Eq. (22). This is in contrast to RG methods that run a cutoff on the total energy of the basis states (as in the Bloch-Horowitz or Lee-Suzuki approaches). Such methods generate “multi-valued” two-body interactions, in the sense that the RG evolution of two-body operators in  $A > 2$  systems depends on the excitation energies of the unlinked spectator particles [109, 136].

Further simplifications of Eq. (44) follow from antisymmetrization and applying the Jacobi identity, but this form is sufficient to make clear that there are no disconnected pieces. The problem is thus reduced to the technical implementation of a momentum-space decomposition analogous to Eq. (22). A diagrammatic approach is introduced in Refs. [137, 138] to handle this decomposition. Work is in progress on evolving 3N forces in momentum space. It has been verified that this formalism leaves eigenvalues invariant for three-particle systems described by simple model Hamiltonians, such as a two-level system of bosons [137].

To summarize, because only the Hamiltonian enters the SRG flow equations, there are no difficulties from having to solve  $T$  matrices (bound state plus scattering wave functions) in all three-body (including breakup) channels, as required by the analogous three-body  $V_{\text{low } k}$  evolution equations. In a momentum



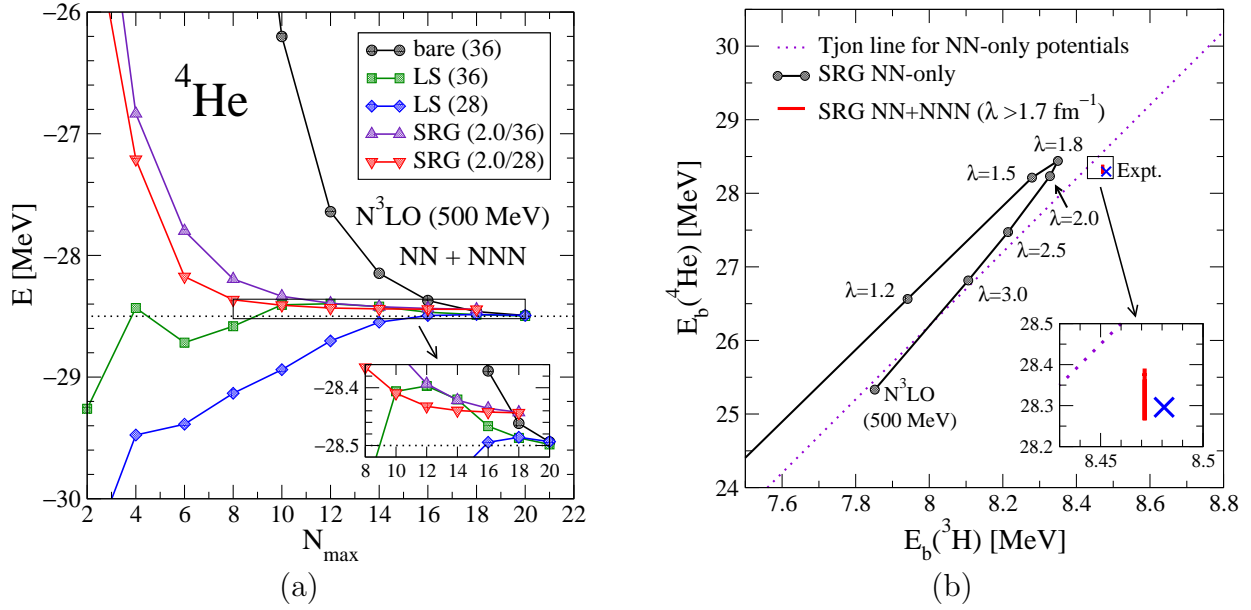


Figure 36: (a) Ground-state energy of  ${}^4\text{He}$  as a function of the basis size  $N_{\text{max}}$  based on the  $\text{N}^3\text{LO}$  potential of Ref. [20] and  $\text{N}^2\text{LO}$  3N forces from Ref. [139]. Unevolved (bare) results are compared to those obtained with a Lee-Suzuki (LS) NCSM transformation and based on SRG-evolved interactions to  $\lambda = 2.0 \text{ fm}^{-1}$  at  $\hbar\Omega = 28$  and  $36 \text{ MeV}$ . (b) Binding energy of  ${}^4\text{He}$  versus  ${}^3\text{H}$ . The Tjon line from phenomenological NN potentials (dotted) is compared with the trajectory of SRG energies when only NN interactions are kept (circles). When 3N interactions (initial and induced) are included, the trajectory lies close to experiment (cross) for  $\lambda \geq 1.8 \text{ fm}^{-1}$  (see inset). For details see Ref. [85].

basis the presence of spectator nucleons requires solving separate equations for each set of  $\langle V_\lambda^{(n)} \rangle$  matrix elements. But while it is natural to solve Eq. (38) in momentum space, it is an operator equation so one can use any convenient representation. A convenient choice is to evolve in a discrete basis, where spectators are handled without a decomposition. This results in coupled first-order differential equations for the matrix elements of the flowing Hamiltonian  $H_s$  where the right side of Eq. (38) is evaluated using simple matrix multiplications.

Such calculations have been recently performed in the Jacobi coordinate harmonic-oscillator basis of the No-Core Shell Model (NCSM) [65]. This is a translationally invariant, antisymmetric basis for each  $A$ , with a complete set of states up to a maximum excitation of  $N_{\text{max}}\hbar\Omega$  above the minimum energy configuration, where  $\Omega$  is the harmonic oscillator parameter. The 3N evolution used builds directly on Ref. [138], which presents a one-dimensional implementation of the approach along with a general analysis of the evolving many-body hierarchy.

One starts by evolving  $H_\lambda$  in the  $A = 2$  subsystem, which completely fixes the two-body matrix elements  $\langle V_\lambda^{(2)} \rangle$ . Next, by evolving  $H_\lambda$  in the  $A = 3$  subsystem, the combined two-plus-three-body matrix elements are determined. The three-body matrix elements are isolated by subtracting the evolved  $\langle V_\lambda^{(2)} \rangle$  elements in the  $A = 3$  basis [138]. Having obtained the separate NN and 3N matrix elements, they can be applied unchanged to any nucleus. The inclusion of 3N forces in the initial Hamiltonian is straightforward. If applied to  $A \geq 4$  systems, four-body (and higher) forces will not be included and so the SRG transformation will be only approximately unitary. This allows one to study whether the decreasing hierarchy of many-body forces is maintained and whether the induced four-body contribution is unnaturally large.

Results from Ref. [65] for the SRG evolution are shown in Fig. 35. The initial NN interaction is the ( $\Lambda = 500 \text{ MeV}$ )  $\text{N}^3\text{LO}$  potential of Ref. [20] while the initial 3N interaction is the  $\text{N}^2\text{LO}$  3N force

(discussed in Section 4.1) in the local form of Ref. [140] with  $c_D$  and  $c_E$  couplings fit to the average of the  ${}^3\text{H}$  and  ${}^3\text{He}$  binding energies and to triton beta decay according to Ref. [139]. Similar results are expected starting from other initial potentials because of the low-momentum universality. NCSM calculations with these initial interactions and the parameter set in Table I of Ref. [139] yield energies of  $-8.473(4)$  MeV for  ${}^3\text{H}$  and  $-28.50(2)$  MeV for  ${}^4\text{He}$  compared with  $-8.482$  MeV and  $-28.296$  MeV from experiment, respectively. So there is a 20 keV uncertainty in the calculation of  ${}^4\text{He}$  from incomplete convergence and a 200 keV discrepancy with experiment. The latter is consistent with the omission of three- and four-body interactions at  $\text{N}^3\text{LO}$ . These provide a scale for assessing whether induced four-body contributions are important compared to other uncertainties. Figure 35 shows the SRG evolution as a function of  $\lambda$  of the  ${}^3\text{H}$  and  ${}^4\text{He}$  ground-state energies. When the induced three-body part is included, the  ${}^3\text{H}$  ground-state energy is completely independent of  $\lambda$ . For  ${}^4\text{He}$ , the deviation from  $\lambda$  independence due to induced four-body forces is less than about 50 keV for  $\lambda \geq 1.5 \text{ fm}^{-1}$ .

As seen in Fig. 36(a), the NCSM calculations with SRG-evolved interactions are variational and converge smoothly and rapidly from above with or without an initial three-body force. This shows the dramatic improvement in convergence rate compared to the initial chiral EFT interactions (circles), although the latter are relatively soft. Thus, once evolved, a much smaller  $N_{\text{max}}$  basis is adequate for a desired accuracy and extrapolating in  $N_{\text{max}}$  is also feasible (in contrast to the Lee-Suzuki NCSM results). The impact of evolving 3N forces is illustrated in Fig. 36(b), where the binding energy of  ${}^4\text{He}$  is plotted against the binding energy of  ${}^3\text{H}$ . The experimental values define a point in this plane. The SRG NN-only results follow a trajectory that is analogous to the Tjon line (see Fig. 24). In contrast, the short SRG trajectory including 3N interactions highlights the small variations from omitted short-range three- and four-body forces.<sup>12</sup>

These results demonstrate that the SRG is a practical method to evolve 3N (and higher-body) forces in a harmonic-oscillator basis. Calculations of  $A \leq 4$  nuclei including 3N forces show the same favorable convergence properties observed with low-momentum NN interactions, with a net induced four-body contribution in  $A = 4$  that is smaller than the truncation errors of the initial chiral interactions. However, because of the stronger density dependence of four-nucleon forces, it will be important to monitor the size of the induced four-body contributions for heavier nuclei and nuclear matter. The SRG evolution is an alternative to the Lee-Suzuki NCSM transformation and the SRG-evolved harmonic-oscillator matrix elements can also be used with other many-body methods. The success of the block-diagonal SRG (see Section 3.4) in evolving a  $V_{\text{low } k}$  two-body interaction using flow equations motivates an extension to three- and higher-body forces (and operators). Work on this is in progress.

### 4.3 In-medium SRG

The SRG methods described so far carry out the evolution to low momentum at zero density in free space. A convenient feature of the free-space evolution is that it does not have to be repeated for each different nucleus or nuclear matter density; the evolved NN interaction is completely determined by solving the two-body SRG equation in free space, the evolved 3N interaction is completely determined by solving the three-body SRG equation in free space, and so on.

An interesting alternative is to perform the SRG evolution directly in the  $A$ -body system of interest. In contrast to the free-space SRG, the in-medium evolution must be repeated for each nucleus or density. As with all RG methods, evolving to low momentum generates many-body interactions that must be truncated for practical calculations. However, unlike the free-space evolution, the in-medium SRG has the appealing feature that one can approximately evolve 3, ...,  $A$ -body operators using only two-body machinery. The key to this simplification is the use of normal-ordering with respect to a finite-density reference state. That is, starting from the second-quantized Hamiltonian with two- and three-body

---

<sup>12</sup>Note that the trajectory for NN plus 3N-induced results would be a similarly small line at the  $\text{N}^3\text{LO}$  NN-only point.

interactions,

$$H = \sum_{12} T_{12} a_1^\dagger a_2 + \frac{1}{(2!)^2} \sum_{1234} \langle 12|V|34 \rangle a_1^\dagger a_2^\dagger a_4 a_3 + \frac{1}{(3!)^2} \sum_{123456} \langle 123|V^{(3)}|456 \rangle a_1^\dagger a_2^\dagger a_3^\dagger a_6 a_5 a_4, \quad (45)$$

all operators are normal-ordered with respect to a finite-density Fermi vacuum  $|\Phi\rangle$  (for example, the Hartree-Fock ground state or the non-interacting Fermi sea in nuclear matter), as opposed to the zero-particle vacuum. Wick's theorem can then be used to *exactly* write  $H$  as

$$H = E_0 + \sum_{12} f_{12} \{a_1^\dagger a_2\} + \frac{1}{(2!)^2} \sum_{1234} \langle 12|\Gamma|34 \rangle \{a_1^\dagger a_2^\dagger a_4 a_3\} + \frac{1}{(3!)^2} \sum_{123456} \langle 123|\Gamma^{(3)}|456 \rangle \{a_1^\dagger a_2^\dagger a_3^\dagger a_6 a_5 a_4\}, \quad (46)$$

where the zero-, one-, and two-body normal-ordered terms are given by

$$E_0 = \langle \Phi|H|\Phi \rangle = \sum_1 T_{11} n_1 + \frac{1}{2} \sum_{12} \langle 12|V|12 \rangle n_1 n_2 + \frac{1}{3!} \sum_{123} \langle 123|V^{(3)}|123 \rangle n_1 n_2 n_3, \quad (47)$$

$$f_{12} = T_{12} + \sum_i \langle 1i|V|2i \rangle n_i + \frac{1}{2} \sum_{ij} \langle 1ij|W|2ij \rangle n_i n_j, \quad (48)$$

$$\langle 12|\Gamma|34 \rangle = \langle 12|V|34 \rangle + \sum_i \langle 12i|V^{(3)}|34i \rangle n_i, \quad (49)$$

where  $n_i = \theta(\varepsilon_F - \varepsilon_i)$  denotes the sharp occupation numbers in the reference state, with Fermi level or Fermi energy  $\varepsilon_F$ . By construction, the normal-ordered strings of creation and annihilation operators obey  $\langle \Phi|\{a_1^\dagger \cdots a_n\}|\Phi \rangle = 0$ . It is evident from Eqs. (47)–(49) that the coefficients of the normal-ordered zero-, one-, and two-body terms include contributions from the three-body interaction  $V^{(3)}$  through sums over the occupied single-particle states in the reference state  $|\Phi\rangle$ . Therefore, truncating the in-medium SRG equations to two-body *normal-ordered* operators will (approximately) evolve induced three- and higher-body interactions through the density-dependent coefficients of the zero-, one-, and two-body operators in Eq. (46).

The in-medium SRG flow equations at the normal-ordered two-body level are obtained by evaluating  $dH/ds = [\eta, H]$  with the normal-ordered Hamiltonian  $H = E_0 + f + \Gamma$  and the SRG generator  $\eta = \eta^{1b} + \eta^{2b}$  (with one- and two-body terms) and neglecting three- and higher-body normal-ordered terms. For infinite matter, a natural generator choice is  $\eta = [f, \Gamma]$  in analogy with the free-space SRG. In this case, the explicit form of the SRG equations simplifies because  $\eta^{1b} = 0$  and  $f_{ij} = f_i \delta_{ij}$ . This leads to

$$\frac{dE_0}{ds} = \frac{1}{2} \sum_{1234} (f_{12} - f_{34}) |\Gamma_{1234}|^2 n_1 n_2 \bar{n}_3 \bar{n}_4, \quad (50)$$

$$\frac{df_1}{ds} = \sum_{234} (f_{41} - f_{23}) |\Gamma_{4123}|^2 (\bar{n}_2 \bar{n}_3 n_4 + n_2 n_3 \bar{n}_4), \quad (51)$$

$$\begin{aligned} \frac{d\Gamma_{1234}}{ds} = & -(f_{12} - f_{34})^2 \Gamma_{1234} + \frac{1}{2} \sum_{ab} (f_{12} + f_{34} - 2f_{ab}) \Gamma_{12ab} \Gamma_{ab34} (1 - n_a - n_b) + \sum_{ab} (n_a - n_b) \\ & \times \left\{ \Gamma_{a1b3} \Gamma_{b2a4} [(f_{a1} - f_{b3}) - (f_{b2} - f_{a4})] - \Gamma_{a2b3} \Gamma_{b1a4} [(f_{a2} - f_{b3}) - (f_{b1} - f_{a4})] \right\}, \end{aligned} \quad (52)$$

where the single-particle indices refer to momentum states and include spin and isospin labels. While the in-medium SRG equations are of second order in the interactions, the flow equations build up non-perturbative physics via the successive interference between the particle-particle and the two particle-hole channels in the SRG equation for  $\Gamma$ , Eq. (52), and between the two-particle-one-hole and two-hole-one-particle channels for  $f$ , Eq. (51). In terms of diagrams, one can imagine iterating the SRG

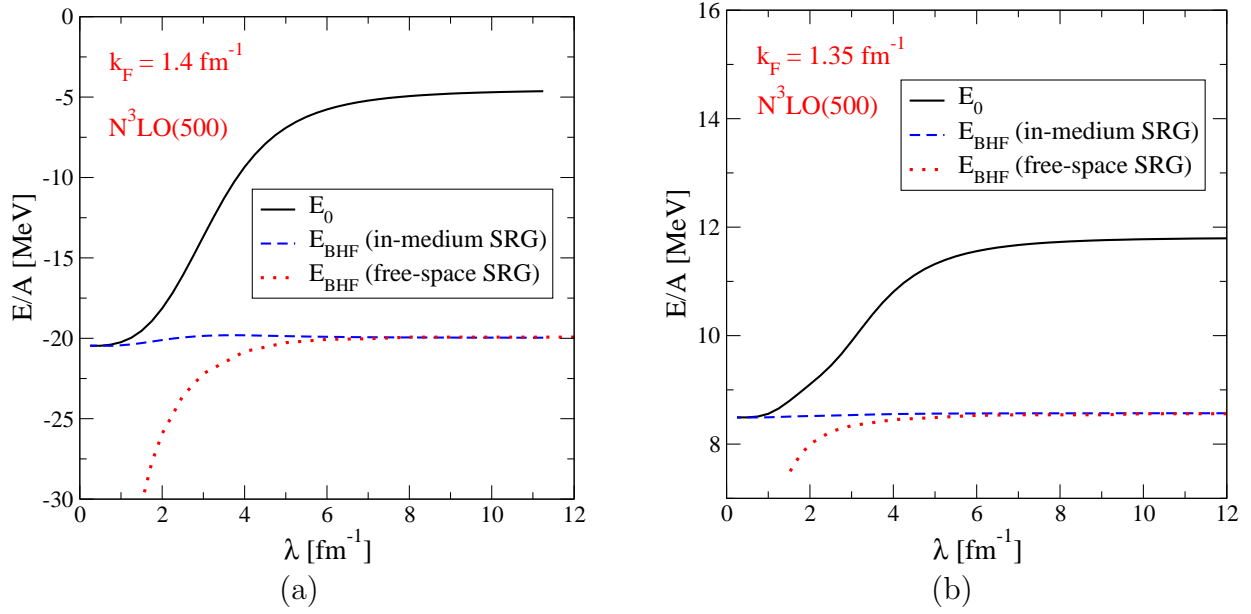


Figure 37: In-medium SRG evolution of the energy per particle of (a) symmetric nuclear matter at a Fermi momentum  $k_F = 1.4 \text{ fm}^{-1}$  and (b) neutron matter at  $k_F = 1.35 \text{ fm}^{-1}$  [141]. The solid line denotes the  $E_0$  flow of the Hartree-Fock energy. The dashed line is the energy calculated in the ladder or Brueckner-Hartree-Fock approximation (BHF) using interactions evolved with the in-medium SRG at the two-body level, and the dotted line is the same many-body calculation based on NN-only SRG interactions evolved in free space. The initial NN interaction is the  $N^3\text{LO}$  potential of Ref. [20].

equations in increments of  $\delta s$ . At each additional increment  $\delta s$ , the interactions from the previous step are inserted back into the right side of the SRG equations. Iterating this procedure, one sees that the SRG accumulates complicated particle-particle and particle-hole correlations to all orders.

With this choice of generator  $\eta = [f, \Gamma]$ , the Hamiltonian is driven towards the diagonal. This means that Hartree-Fock becomes increasingly dominant with the off-diagonal  $\Gamma$  matrix elements being driven to zero. As with the free-space SRG, it is convenient for momentum-space evolution to switch to the flow variable  $\lambda \equiv s^{-1/4}$ , which is a measure of the resulting band-diagonal width of  $\Gamma$ . In the limit  $\lambda \rightarrow 0$ , Hartree-Fock becomes exact for the evolved Hamiltonian; the zero-body term,  $E_0$ , approaches the interacting ground-state energy,  $f$  approaches fully dressed single-particle energies, and the remaining diagonal matrix elements of  $\Gamma$  approach a generalization of the quasiparticle interaction in Landau's theory of Fermi liquids [102]. An approximate<sup>13</sup> solution of the  $E_0$  flow equation for symmetric nuclear matter and neutron matter as a function of  $\lambda$  is shown in Fig. 37 for two different Fermi momenta  $k_F$  (corresponding to different densities) [141]. As expected, the in-medium SRG drives the Hamiltonian to a form where Hartree-Fock becomes exact in the limit  $\lambda \rightarrow 0$ . In contrast to the ladder approximation based on NN-only SRG interactions evolved in free space, the same many-body calculation using interactions evolved with the in-medium SRG at the two-body level gives energies that are approximately independent of  $\lambda$ . This indicates that truncations based on normal-ordering efficiently include the dominant induced many-body interactions via the density-dependent zero-, one-, and two-body normal-ordered terms.

In a similar manner, the in-medium SRG can be used as an ab initio method for finite nuclei. Figure 38 illustrates this with calculations of the ground-state energy of  $^4\text{He}$  [142]. As the flow parameter  $s$  increases, Fig. 38(a) shows that the  $E_0$  flow and including second-order (in  $\Gamma$ ) many-body perturbation

<sup>13</sup>The particle-hole contributions to the SRG flow equation for  $\Gamma$ , given by the last sum and the second line of Eq. (52), are neglected in the infinite matter calculations. No such approximation is made for the  $^4\text{He}$  results presented in Fig. 38.

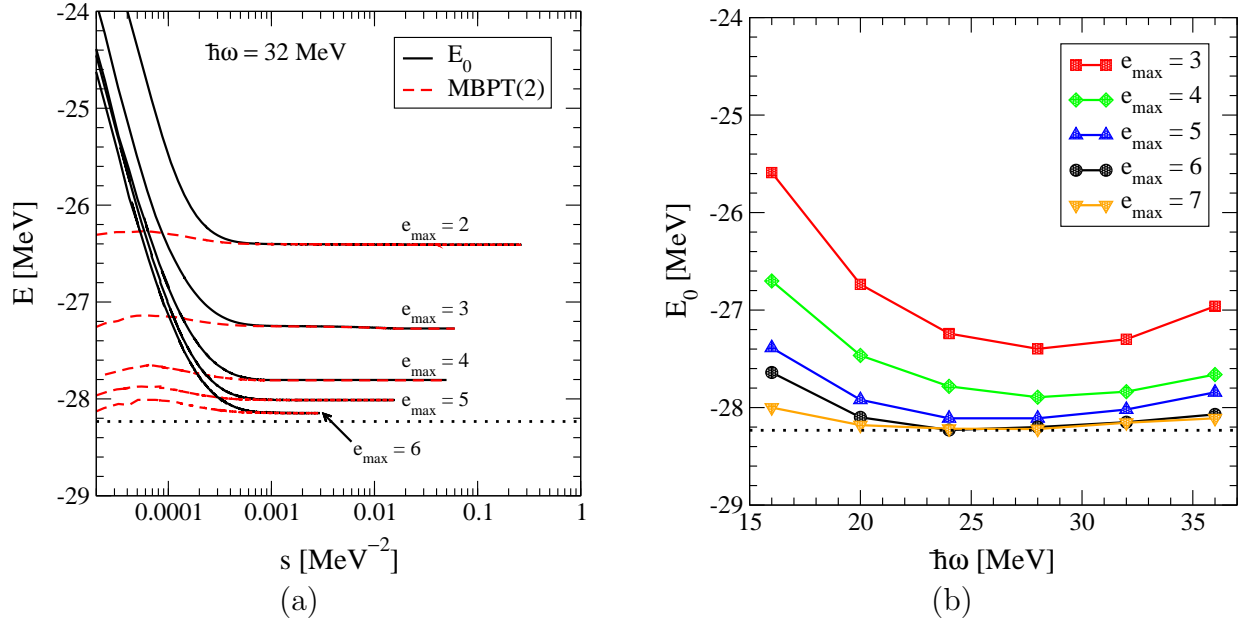


Figure 38: Ground-state energy of  $^4\text{He}$  based on the in-medium SRG starting from a free-space SRG potential ( $\lambda = 2.0 \text{ fm}^{-1}$  from the  $\text{N}^3\text{LO}$  potential of Ref. [20]) [142]. (a)  $E_0$  flow (solid line) and including second-order many-body perturbation theory (MBPT) contributions (dashed line) as a function of flow parameter  $s$ . (b) Convergence behavior as a function of harmonic oscillator parameter  $\hbar\omega$  with increasing single-particle  $e_{\text{max}} \equiv \max(2n + l)$ . The horizontal dotted line denotes the ground-state energy obtained from an exact diagonalization [85].

theory contributions approach each other, as was the case for the infinite matter results in Fig. 37. In addition, the convergence behavior with increasing harmonic-oscillator spaces in Fig. 38(b) is very promising. Based on these preliminary calculations, the in-medium SRG truncated at the normal-ordered two-body level appears to give accuracies comparable to coupled-cluster calculations truncated at the singles and doubles (CCSD) level. Future applications to  $^{16}\text{O}$  and  $^{40}\text{Ca}$  will help clarify if this similarity to CCSD is systematic, although such a connection was suggested by White in his work on similar methods in quantum chemistry [143]. Finally, we note that the in-medium SRG is a promising method for non-perturbative calculations of valence shell-model effective interactions and operators.

#### 4.4 Effective operators

As discussed in Section 2.5, *all* operators in a low-energy effective theory will evolve under a change of resolution. Given an initial operator that is consistent with the initial Hamiltonian (and which will also have many-body components), it is important to consistently evolve the operators along with the Hamiltonian. When this evolution is via unitary transformations, the operator evolution is well defined and in principle straightforward to implement.

For  $V_{\text{low } k}$  interactions, the use of Lee-Suzuki transformations provides a convenient formalism to evolve consistent two-body operators [68]. In the notation of Ref. [144, 145], the evolution of an operator  $O$  from a momentum cutoff  $\Lambda_0$  to lower resolution  $\Lambda$  is given by

$$O(\Lambda) = \frac{1}{\sqrt{P + \omega^\dagger \omega}} (P + \omega^\dagger) O(\Lambda_0) (P + \omega) \frac{1}{\sqrt{P + \omega^\dagger \omega}}, \quad (53)$$

where the operator  $\omega = Q\omega P$  generates the Lee-Suzuki transformation, the projection operator  $P$  projects onto relative momenta  $k < \Lambda$ , and  $Q = 1 - P$  projects onto  $\Lambda < k < \Lambda_0$ . While this approach

is straightforward to implement at the two-body level (and has been tested), the generalization to higher-body components is not simple.

For the SRG approach, the evolution with  $s$  of any other operator  $O$  is given by the same unitary transformation that evolves the Hamiltonian,  $O_s = U(s)OU^\dagger(s)$ , which means that  $O_s$  evolves as

$$\frac{dO_s}{ds} = [\eta(s), O_s] = [[T, V_s], O_s]. \quad (54)$$

Just as with the Hamiltonian  $H_s$ , this evolution will induce many-body operators even if the initial operator is purely two-body. If we restrict ourselves to two-body operators in relative momentum space, one has

$$\frac{dO_s(k, k')}{ds} = \frac{2}{\pi} \int_0^\infty q^2 dq \left[ (k^2 - q^2) V_s(k, q) O_s(q, k') + (k'^2 - q^2) O_s(k, q) V_s(q, k') \right]. \quad (55)$$

To evolve a particular  $O_s$  simultaneously with  $V_s$ , we can simply include the discretized version of Eq. (55) as additional coupled first-order differential equations.

An alternative, more direct, approach is to construct the unitary transformation at each  $s$  explicitly, and then use it to transform operators. Let  $|\psi_\alpha(s)\rangle$  be an eigenstate of  $H_s$  with eigenvalue  $E_\alpha$  (which is independent of  $s$ ). Then  $U(s)$  is given by

$$U(s) = \sum_\alpha |\psi_\alpha(s)\rangle \langle \psi_\alpha(0)|. \quad (56)$$

In a discretized partial-wave momentum-space basis with momenta  $\{k_i\}$ , we can solve for the eigenvectors of  $H = H_{s=0}$  and  $H_s$ , then construct the matrix elements of  $U(s)$  [which we denote  $U_s(k_i, k_j)$ ] by summing over the product of momentum-space wave functions:

$$U_s(k_i, k_j) = \sum_\alpha \langle k_i | \psi_\alpha(s) \rangle \langle \psi_\alpha(0) | k_j \rangle. \quad (57)$$

In practice this is an efficient way to construct the unitary transformation and subsequently to evolve any operator in a few-body space. For example, in the harmonic-oscillator basis used for evolving 3N interactions (see Section 4.2), one can simply apply Eq. (56) in this basis. Proof-of-principle tests for operators in a one-dimensional model show that this works as expected [146].

As an example in the two-body system, we consider the momentum distribution in the deuteron [68]. The momentum distribution at relative momentum  $\mathbf{q}$  is the expectation value of  $a_{\mathbf{q}}^\dagger a_{\mathbf{q}}$  (summed over spin substates  $M_S$ ) and is proportional to the sum of the squares of the normalized S- and D-state parts of the deuteron wave function,  $u(q)^2 + w(q)^2$ . It is not an observable (see, for example, Ref. [147]) but is useful to illustrate some points. Because the SRG proceeds via unitary transformations, by construction no information is lost in the evolution. But even more, we can show explicitly that by evolving to a low-momentum interaction, we decouple the low- and high-momentum physics in a low-energy state.

In Fig. 39(a), we plot deuteron matrix elements of  $a_{\mathbf{q}}^\dagger a_{\mathbf{q}}$  for the Argonne  $v_{18}$  [18] and CD-Bonn [19] potentials, as well as for two SRG and a smooth-cutoff  $V_{\text{low } k}$  interaction evolved from Argonne  $v_{18}$ . We emphasize again that matrix elements of this operator are not measurable, so one should not ask which of these is the “correct” momentum distribution in the deuteron; it is a potential- and scale-dependent quantity. It is evident that the  $V_s$  distributions have substantial momentum components only for  $k$  below  $\lambda$ , and that the  $V_{\text{low } k}$  distribution is very similar to the corresponding  $V_s$  distribution. Nevertheless, if we use the SRG- or RG-evolved operator with these deuteron wave functions, we precisely reproduce the momentum distribution from the original potential at *all momenta* and for *all*  $\lambda$ .

This result by itself is guaranteed by construction. The more interesting issue is where the strength of the matrix element comes from. For example, for the bare operator and the Argonne  $v_{18}$  potential,

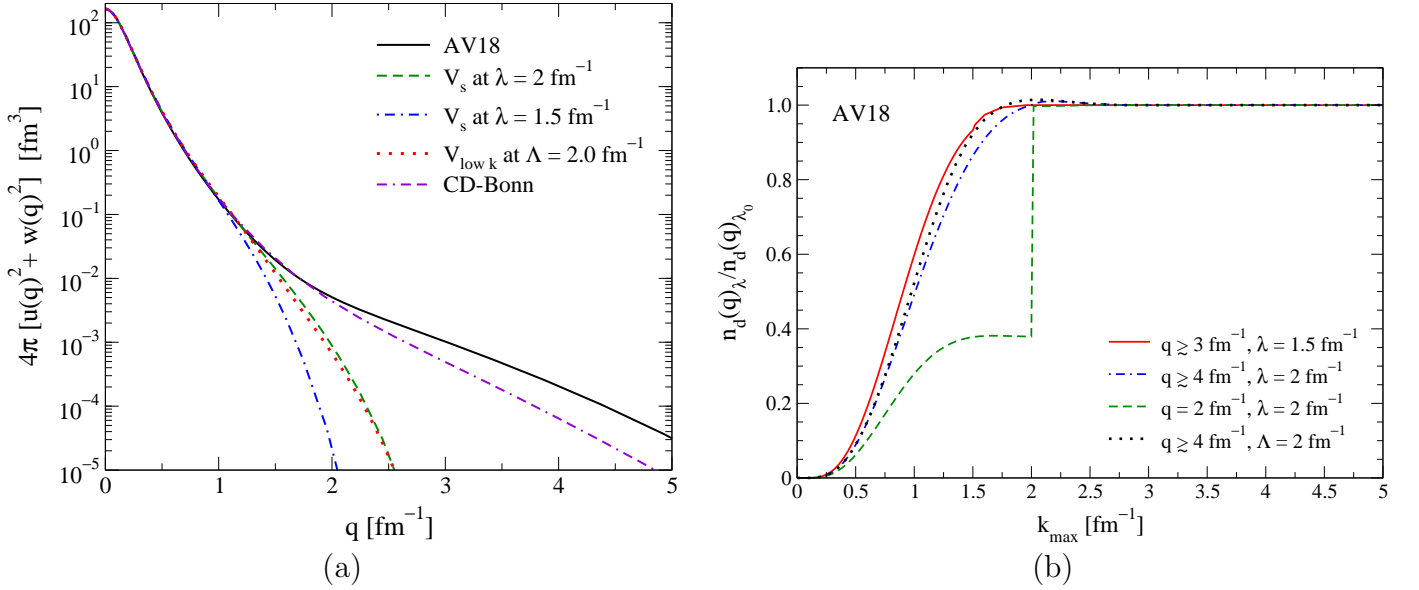


Figure 39: (a) Deuteron momentum distribution  $\langle a_{\mathbf{q}}^\dagger a_{\mathbf{q}} \rangle_d = 4\pi[u(q)^2 + w(q)^2]$  using the Argonne  $v_{18}$  [18], CD-Bonn [19] and SRG potentials evolved from Argonne  $v_{18}$  to  $\lambda = 1.5 \text{ fm}^{-1}$  and  $2 \text{ fm}^{-1}$  (but not evolving the operator), and a smooth-cutoff  $V_{\text{low } k}$  interaction with  $\Lambda = 2 \text{ fm}^{-1}$  and  $n_{\text{exp}} = 2$ . (b) Ratio of the deuteron momentum distribution at various momenta  $q$  evolved from the Argonne  $v_{18}$  potential via the SRG to  $\lambda = 1.5 \text{ fm}^{-1}$  and  $2 \text{ fm}^{-1}$ , to the corresponding initial momentum distribution, as a function of the maximum momentum  $k_{\text{max}}$  in the deuteron wave functions in the numerator. Note that the unevolved Argonne  $v_{18}$  result is simply a step function at  $q$ . For comparison, we also show the result for a smooth-cutoff  $V_{\text{low } k}$  interaction with  $\Lambda = 2 \text{ fm}^{-1}$  and  $n_{\text{exp}} = 2$ . For details see Ref. [68].

the momentum distribution at  $q = 4 \text{ fm}^{-1}$  comes entirely from deuteron wave function components at that momentum. But when  $\lambda = 2 \text{ fm}^{-1}$ , it is clear from Fig. 39(a) that the deuteron does not have appreciable momentum components above  $2.5 \text{ fm}^{-1}$  (even though  $V_s$  has matrix elements near the diagonal [7]) because of decoupling. One might imagine that the operator becomes pathological to compensate. In fact, it is also softened.

In Fig. 39(b), we take the ratio of the evolved operator evaluated with the evolved wave function at  $q$  to the corresponding initial quantity, but include in the numerator only momenta up to  $k_{\text{max}}$ . The numerator is thus:

$$\int_0^{k_{\text{max}}} d\mathbf{k} \int_0^{k_{\text{max}}} d\mathbf{k}' \psi_d^\dagger(\mathbf{k}; \lambda) U_\lambda(\mathbf{k}, \mathbf{q}) U_\lambda^\dagger(\mathbf{q}, \mathbf{k}') \psi_d(\mathbf{k}'; \lambda). \quad (58)$$

We observe that for all  $q$ , the ratio approaches unity for large enough  $k_{\text{max}}$ , as dictated by the unitary transformation. For  $\lambda = 1.5 \text{ fm}^{-1}$  or  $2 \text{ fm}^{-1}$ , larger values of  $q$  ( $q \gtrsim 3 \text{ fm}^{-1}$  or  $q \gtrsim 4 \text{ fm}^{-1}$ , respectively) give results approximately independent of  $q$ , with a smooth approach to unity by  $k_{\text{max}} \approx 1.3\lambda$ . This is consistent with the operator  $U_\lambda(\mathbf{k}, \mathbf{q})$  factorizing into  $K_\lambda(\mathbf{k}) Q_\lambda(\mathbf{q})$  for  $k < \lambda$  and  $q \gg \lambda$ , and thus the  $q$  dependence cancels in the ratio [68]. It remains to be seen whether this factorization is a general feature that can be understood using operator product expansion ideas [56, 146]. The immediate point is that the flow of the operator strength weighted by  $\psi_d$  is toward lower momenta (softened). Furthermore, there is no sign of fine-tuning in the evolved operator, because even a rough variational Ansatz for the wave function is accurate. More work on operators is needed, but thus far these observations seem to be general [146].



## 5 Applications to infinite matter

The physics of nucleonic matter ranges over exciting extremes: from universal properties at low densities [34,148] that can be probed in experiments with ultracold atoms [149]; to understanding nuclear densities in known and new exotic nuclei [67,150]; to dense matter in neutron stars and supernovae [151,152]. At very low densities, the details of pion exchanges are not resolved and pionless EFT is well suited for capturing large scattering-length physics with systematic improvements from including effective range and higher-order terms [30,32]. For very dilute neutron matter, there are no length scales associated with the interaction, because the scattering length is large  $k_F a_s \gg 1$ . As a result, only the density sets the scale and the properties of neutron matter are universal [33].<sup>14</sup> With increasing density the effective range correction weakens the interactions of nucleons with higher momenta. This simplifies the many-body problem and has been used to predict the energy of neutron matter with controlled uncertainties for densities  $\rho \sim \rho_0/10$  [34] (with saturation density  $\rho_0 = 0.16 \text{ fm}^{-3}$ ).

For nuclear densities, Pauli blocking suppresses the nonperturbative physics due to weakly and nearly bound states and the large scattering lengths are dissolved [9,154,155]. The difficulties in the theory of nuclear matter arise from the strong short-range repulsion and strong short-range tensor forces in phenomenological or chiral EFT potentials. The resulting coupling between low and high momenta is still present in the  $G$  matrix, as discussed in Section 3.5. This renders the Bethe-Brueckner-Goldstone expansion nonperturbative [156]. As detailed in Sects. 2.1 and 2.4, the RG evolution softens these short-range parts, which makes the many-body calculation more controlled. In this section, we review the application of low-momentum interactions to infinite matter with  $\rho \sim \rho_0$  and highlight the possibility of perturbative approaches [9,16,17]. The findings can provide a starting point to develop a new power counting for nuclear matter. We focus on calculations including 3N forces and so only mention the work of Refs. [157–163].

### 5.1 Nuclear matter

Over the last fifty years, an accurate prediction of nuclear matter starting from nuclear forces has been a theoretical milestone on the way to finite nuclei, but has proved to be an elusive target. Despite the long-term emphasis on the infinite uniform system, most advances in microscopic nuclear structure theory over the last decade have been through expanding the reach of few-body calculations. This has unambiguously established the quantitative role of 3N forces for light nuclei ( $A \leq 12$ ) [22–24,57,60,61]. However, until recently few-body fits have not sufficiently constrained 3N force contributions at higher density such that nuclear matter calculations are predictive. Nuclear matter saturation is very delicate, with the binding energy resulting from cancellations of much larger potential and kinetic energy contributions. When a quantitative reproduction of empirical saturation properties has been obtained, it was imposed by hand through adjusting phenomenological short-range three-body forces (see, for example, Refs. [53,164]).

Progress for controlled nuclear matter calculations has long been hindered by the difficulty of the nuclear many-body problem when conventional nuclear potentials are used. Recent calculations overcome these hurdles by combining systematic starting Hamiltonians based on chiral EFT [20,44] with RG methods [5,6] to soften the short-range repulsion and short-range tensor components of the initial chiral interactions [12]. The RG evolution to low momenta leads to contributions in the particle-particle channel that are well converged at second order in the potential, suggesting that perturbative approaches can be used in place of the Bethe-Brueckner-Goldstone hole-line expansion [9,16]. The Weinberg eigenvalue analysis discussed in Section 2.4 provides quantitative backing to these observations [7,12].

---

<sup>14</sup>In this regime, nuclear matter exists as a mixture of nucleons and nuclei that collapses to clusters at low temperatures [153].

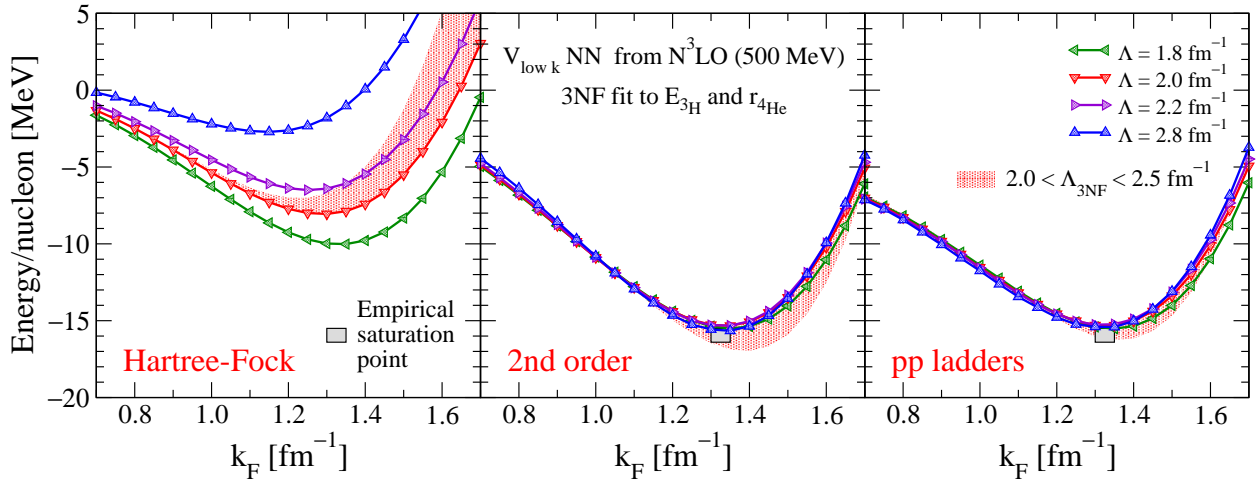


Figure 40: Nuclear matter energy per particle as a function of Fermi momentum  $k_F$  at the Hartree-Fock level (left) and including second-order (middle) and particle-particle-ladder contributions (right), based on evolved  $N^3\text{LO}$  NN potentials and 3N forces fit to  $E_{3\text{H}}$  and  $r_{4\text{He}}$  [16]. Theoretical uncertainties are estimated by the NN (lines) and 3N (band) cutoff variations.

The key nuclear matter results are summarized in Fig. 40, which shows the energy per particle of symmetric nuclear matter as a function of Fermi momentum  $k_F$ , or the density  $\rho = 2k_F^3/(3\pi^2)$ . A grey square representing the empirical saturation point reflects the ranges of nuclear matter saturation properties predicted by phenomenological Skyrme energy functionals that most accurately reproduce properties of finite nuclei. Nuclear matter is calculated in three approximations: Hartree-Fock (left) and including approximate second-order (middle) and summing particle-particle-ladder contributions (right). These are the first results for nuclear matter based on chiral NN and 3N interactions. The technical details are given in Refs. [9, 16] and work is in progress to improve the 3N treatment.

The calculations of Fig. 40 start from the  $N^3\text{LO}$  NN potential ( $\Lambda = 500\text{ MeV}$ ) of Ref. [20]. This NN potential is RG-evolved to smooth-cutoff low-momentum interactions  $V_{\text{low } k}$  using the techniques of Section 3.2. Based on the universality of  $V_{\text{low } k}$  discussed in Section 2.3, we do not expect large differences starting from different  $N^3\text{LO}$  potentials. The  $N^2\text{LO}$  3N forces of Section 4.1 are taken as a truncated basis for low-momentum 3N interactions,<sup>15</sup> where the  $c_D$  and  $c_E$  couplings have been fit for various cutoffs to the  $^3\text{H}$  binding energy and the  $^4\text{He}$  matter radius [16]. (In the future, it will be possible to include consistently evolved three-body forces starting from chiral EFT using the recent advances in extending the SRG methods beyond the NN level [85, 137, 138].) The 3N force fits to the  $^4\text{He}$  radius improve the cutoff independence significantly compared to fitting to  $A = 3, 4$  energies only (see Fig. 6 in Ref. [9]). The calculations of Fig. 40 use the same 3N regulator of Ref. [127, 128], but with a 3N cutoff  $\Lambda_{3\text{NF}}$  that is allowed to vary independently of the NN cutoff. The shaded regions in Fig. 40 show the range of results for  $2.0\text{ fm}^{-1} < \Lambda_{3\text{NF}} < 2.5\text{ fm}^{-1}$  at fixed  $\Lambda = 2.0\text{ fm}^{-1}$ . These predictions are particularly sensitive to uncertainties in the  $c_i$  coefficients (also for neutron matter, see Section 5.2), which raises the possibility of using nuclear matter to constrain some of the  $c_i$  couplings.

The Hartree-Fock results show that nuclear matter is bound even at this simplest level. A calculation without approximations should be independent of the cutoffs, so the spread in Fig. 40 sets the scale for omitted many-body contributions. The second-order results show a dramatic narrowing of this spread, with predicted saturation consistent with the empirical range. The narrowing happens across the full density range. This is strong evidence that these encouraging results are not fortuitous, but that cutoff independence has been reached at the level of 1–2 MeV per particle. The controlled theoretical

<sup>15</sup>This assumes that the  $c_i$  coefficients of the long-range  $2\pi$ -exchange part of 3N forces are not modified by the RG evolution.

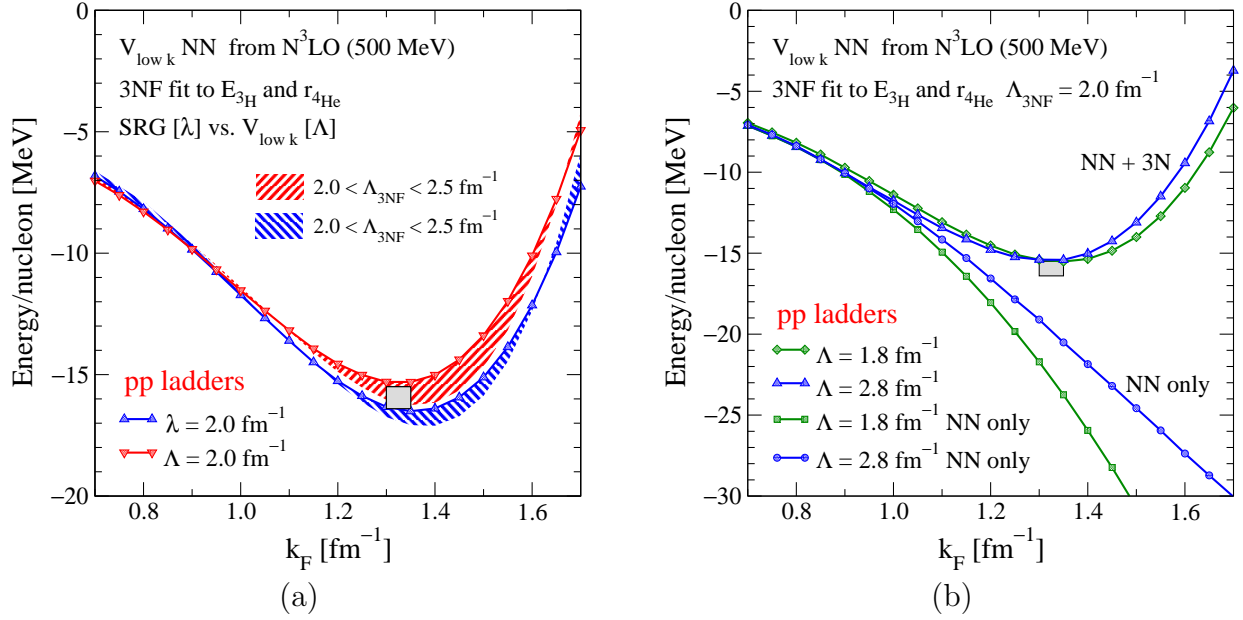


Figure 41: (a) Nuclear matter energy of Fig. 40 at the particle-particle-ladders level compared to SRG-evolved chiral NN interactions. (b) Nuclear matter energy of Fig. 40 at the particle-particle-ladders level compared to NN-only results for two representative NN cutoffs and a fixed 3N cutoff.

uncertainties come as a result of the combination of chiral EFT and RG methods. For all cases, the compressibility  $K = 190\text{--}240$  MeV is in the empirical range. To our knowledge, these are the first nuclear forces fit only to  $A \leq 4$  nuclei that predict realistic saturation properties. Similar nuclear matter energies are found in Fig. 41(a) when the SRG is used to evolve the NN potential. This helps support the general nature of the 3N force fit. On the other hand, the difference of 2 MeV per particle at saturation and above enlarges the theoretical uncertainty.

The decreases in cutoff dependence in Fig. 40 with more complete approximations is necessary but not sufficient to conclude that the calculations are under control. Indeed, approximations that are independent of the cutoff will shift the answer but not widen the error band from cutoff variation. The theoretical errors arise from truncations in the initial chiral EFT Hamiltonian, the many-body approximations, and the approximation of 3N forces. The latter is particularly uncertain here because it involves long-range contributions that are independent of the cutoff. Many-body corrections to the current approximations include higher-order terms in the hole-line expansion and particle-hole corrections. An approach such as coupled cluster theory that can perform a high-level resummation will be necessary for a robust validation.

The evolution of the cutoff  $\Lambda$  to smaller values is accompanied by a shift of physics. In particular, effects due to iterated tensor interactions, which peak in the relative momentum range  $k \sim 4$  fm $^{-1}$  (and thus lead to saturation at too high density), are replaced by three-body contributions. We emphasize that the relative importance of contributions to observables from the tensor force or from 3N forces are scale or resolution dependent. Renormalizing the potential to lower momenta redistributes these contributions and makes the many-body approach tractable. The role of 3N forces for saturation is demonstrated in Fig. 41(b). The two pairs of curves show the differences between the nuclear matter results for NN-only and NN plus 3N interactions. It is evident that saturation is driven by 3N forces [9, 16]. Even for  $\Lambda = 2.8$  fm $^{-1}$ , which is similar to the lower cutoffs in chiral EFT potentials, saturation is at too high density without 3N forces. While 3N forces drive saturation for low-momentum interactions, the 3N contributions are not unnaturally large. This is demonstrated in Fig. 42 by the ratio of  $\langle V_{3\text{N}} \rangle / \langle V_{\text{low } k} \rangle$  for the triton, alpha particle, and nuclear matter at various densities.

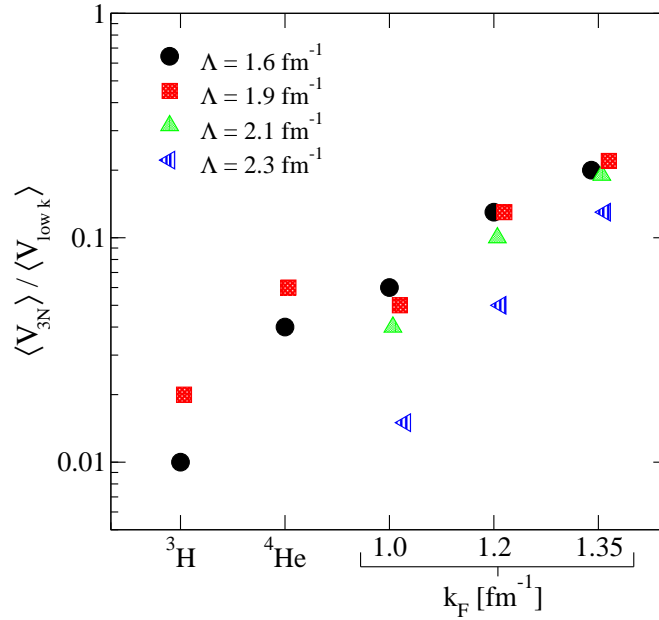


Figure 42: Ratio of  $V_{3N}$  to  $V_{\text{low } k}$  expectation values. For nuclear matter, the expectation values are obtained by the Feynman-Hellman method and  $\langle V_{3N} \rangle$  corresponds to the total 3N contribution at second order from Ref. [9], whereas the values shown for  ${}^3\text{H}$  and  ${}^4\text{He}$  are the largest 3N contributions from Ref. [8] (because of cancellations in the light nuclei).

In Fig. 40 the particle-particle-ladder sum is little changed from second order except at the lowest densities shown, where the presence of two-body bound and nearly bound states necessitate a nonperturbative summation. The rapid convergence for  $\rho \sim \rho_0$  may justify in part the application of chiral EFT to nuclear matter in perturbation theory [165–168], but a detailed study is needed, in particular regarding the cutoff dependence and the contributions from contact interactions and 3N forces beyond  $\Delta$  excitations.

While nuclear matter has lost its status to light nuclei as the first step to nuclear structure, it is still key as a step to heavier nuclei. The low-momentum results, while not conclusive, open the door to ab initio density functional theory based on expanding about nuclear matter [67, 169]. This is discussed further in Section 6.4.

## 5.2 Neutron matter

Neutron matter provides a different perspective from symmetric nuclear matter, because only the long-range  $2\pi$ -exchange  $c_1$  and  $c_3$  terms of  $\text{N}^2\text{LO}$  3N forces contribute [17, 170]. Density-dependent two-body interactions  $\bar{V}_{3N}$  based on these terms for general momentum and spin configurations and including all exchange diagrams were derived in Ref. [17] by summing the third particle over occupied states in the Fermi sea. This corresponds to the normal-ordered two-body part of 3N forces. Effective interactions of this type have been studied in the past using 3N potential models and approximate treatments (see, for example, Refs. [171, 172]) and recently in the framework of in-medium chiral perturbation theory [173]. The partial-wave matrix elements in Fig. 43 show that the resulting  $\bar{V}_{3N}$  is dominated in neutron matter by a repulsive central part. The density dependence of the two-body matrix elements depends on the partial wave. In the  ${}^1\text{S}_0$  channel this dependence can be approximately parameterized by a power of the Fermi momentum. In the spin-triplet channels this is more complex due to the different momentum and density dependences of the various operator structures in  $\bar{V}_{3N}$ . In addition to the density dependence, in general  $\bar{V}_{3N}$  depends on the two-body center-of-mass momentum, but this dependence is weak and the  $P = 0$  approximation for  $\bar{V}_{3N}$  leads to energies that agree very well with the exact result at the

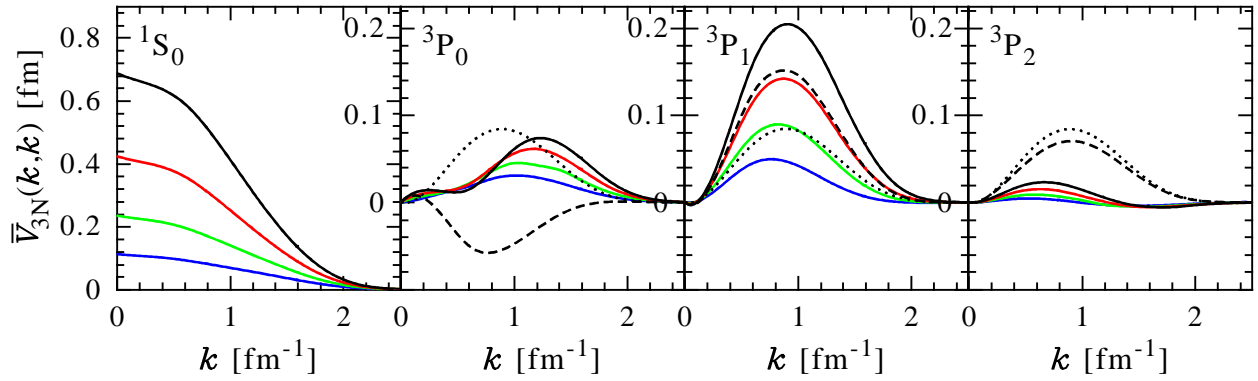


Figure 43: Diagonal momentum-space matrix elements of the density-dependent two-body interaction  $\bar{V}_{3N}$  for  $P = 0$  in the  $^1S_0$  and the spin-triplet  $P$ -wave channels. Results with  $\Lambda_{3NF} = 2.0 \text{ fm}^{-1}$  are shown versus relative momentum  $k$  for different Fermi momenta  $k_F = 1.0, 1.2, 1.4$  and  $1.6 \text{ fm}^{-1}$  (increasing in strength). For the  $P$ -wave channels and  $k_F = 1.6 \text{ fm}^{-1}$ , the dotted lines represent the central parts (degenerate in  $J$ ) of  $\bar{V}_{3N}$ , whereas the dashed lines include the central plus tensor interactions. For details see Ref. [17].

Hartree-Fock level [17].

Using  $\bar{V}_{3N}$  simplifies the neutron matter calculation based on a loop expansion around the Hartree-Fock energy [17]. Figure 44 shows the energy of neutron matter as a function of the density  $\rho = k_F^3/(3\pi^2)$  at second-order. These are the first results for neutron matter based on chiral EFT interactions and including  $N^2\text{LO}$  3N forces. As discussed for nuclear matter, the RG evolution of  $N^3\text{LO}$  NN potentials to low momenta renders the many-body calculation more controlled. The results of Ref. [17] suggest that neutron matter is perturbative at nuclear densities. This is based on small second-order contributions, self-energy corrections being negligible, and a generally weak cutoff dependence in Fig. 44(a). For low-momentum interactions,  $N^2\text{LO}$  3N forces provide a repulsive contribution to the energy due to the repulsive central part in  $\bar{V}_{3N}$ .

Figure 44(b) shows that the theoretical uncertainties of the neutron matter energy are dominated by the uncertainties in the  $c_i$  coefficients, in particular the  $c_3$  part. The  $c_1$  and  $c_3$  variation leads to an energy uncertainty of  $\pm 1.5 \text{ MeV}$  per particle at saturation density. This is larger than the uncertainties probed by cutoff variations, which are due to the many-body approximations or from neglected short-range many-body interactions. We note that other recent neutron matter calculations lie within the  $c_i$  uncertainty band of Fig. 44(b). The spread in the energy band implies microscopic constraints for the symmetry energy and its density dependence [17]. The resulting range for the symmetry energy  $a_4 = (31.6\text{--}34.7) \text{ MeV}$  (where the error is dominated by the uncertainty of  $c_3$ ) is very useful given the scale of the empirical range  $a_4 = (25\text{--}35) \text{ MeV}$  [174]. Other results for neutron matter with low-momentum interactions include studies of the equation of state at finite temperature [170] and of quasiparticle interactions and Fermi liquid parameters using a particle-hole RG approach [175–178].

### 5.3 Pairing

Superfluidity plays a central role in strongly-interacting many-body systems. Pairing in infinite matter impacts the cooling of isolated neutron stars [179–181] and of the neutron star crust following X-ray bursts in accreting neutron stars [182–184]. In addition, studies of superfluidity are used to constrain and improve calculations of pairing in nuclei (see, for example, Ref. [97]). This section provides a brief review of pairing in infinite matter based on low-momentum interactions.

Figure 45(a) shows superfluid pairing gaps in neutron matter, obtained by solving the BCS gap equation with a free spectrum. At low densities (in the crust of neutron stars), neutrons form a  $^1S_0$

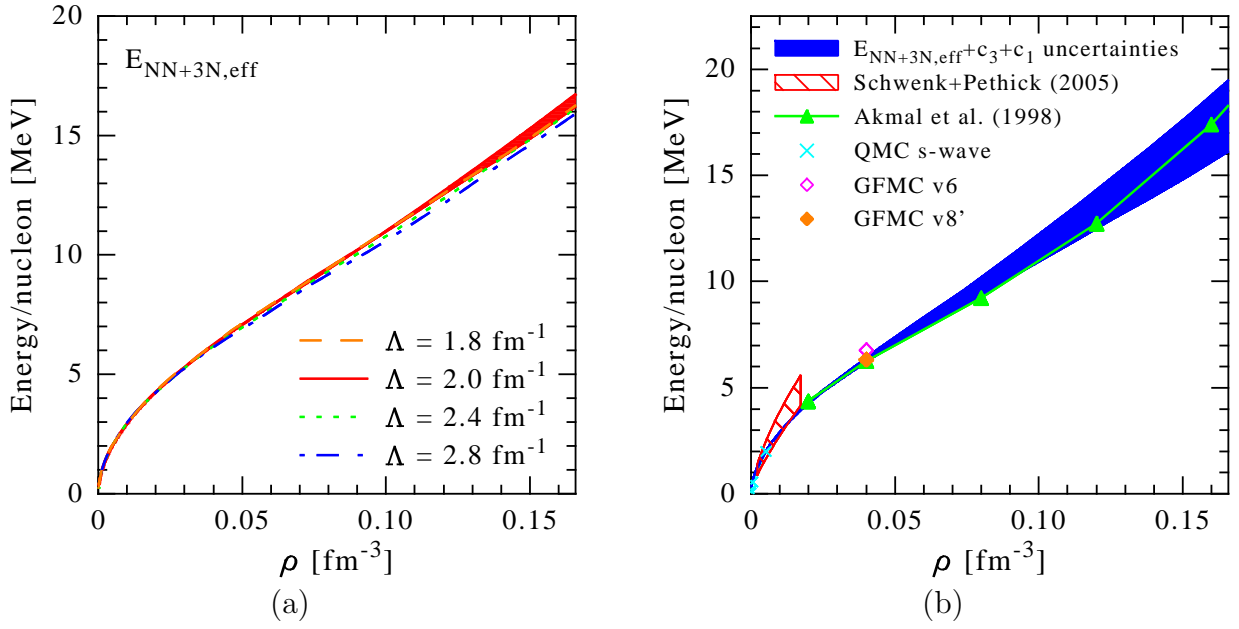


Figure 44: (a) Energy per particle of neutron matter as a function of density  $\rho$  at second order. The results are based on evolved  $N^3\text{LO}$  NN potentials and  $N^2\text{LO}$  3N forces. Theoretical uncertainties are estimated by varying the NN cutoff (lines) and the 3N cutoff (band for fixed  $\Lambda = 2.0 \text{ fm}^{-1}$ ). (b) Theoretical uncertainties of the second-order energy due to the uncertainties in the  $c_1$  and  $c_3$  coefficients of 3N forces. The resulting band is compared to other neutron matter results, for details see Ref. [17].

superfluid. At higher densities, the S-wave interaction is repulsive and neutrons pair in the  $^3\text{P}_2$  channel (with a small coupling to  $^3\text{F}_2$  due to the tensor force). Figure 45(a) demonstrates that the  $^1\text{S}_0$  BCS gap is practically independent of nuclear interactions, and therefore strongly constrained by NN phase shifts [96]. This includes a very weak cutoff dependence for low-momentum interactions  $V_{\text{low } k}$  with sharp or sufficiently narrow smooth regulators with  $\Lambda > 1.6 \text{ fm}^{-1}$ . The inclusion of  $N^2\text{LO}$  3N forces leads to a reduction of the  $^1\text{S}_0$  BCS gap for Fermi momenta  $k_F > 0.6 \text{ fm}^{-1}$  [17]. This reduction becomes significant for densities where the gap is decreasing and agrees qualitatively with results based on 3N potential models (see, for example, Ref. [185]). Two-nucleon interactions are well constrained by scattering data for relative momenta  $k \lesssim 2 \text{ fm}^{-1}$  [5]. The model dependencies at higher momenta show up prominently in Fig. 45(a) in the  $^3\text{P}_2$ – $^3\text{F}_2$  gaps for Fermi momenta  $k_F > 2 \text{ fm}^{-1}$  [186].

For pairing in nuclei, calculations with  $V_{\text{low } k}$  as pairing interaction provide a good starting description of neutron-neutron and proton-proton gaps [79, 80, 97, 188], as discussed in Section 6.4. This is very promising and also consistent with comparisons of the  $^1\text{S}_0$  BCS gaps in neutron matter with results based on the empirical Gogny interaction [189, 190]. In nuclei, however, partial waves beyond the standard  $^1\text{S}_0$  channel can contribute to the pairing interaction and play an interesting role for the  $T = 1, J = 0$  pair formation (because paired nucleons are not in back-to-back-momentum configurations) [191].

Understanding many-body effects beyond the BCS level constitutes an important open problem. For recent progress and a survey of results, see for instance Ref. [192]. Here we review approaches to this problem using the RG. At low densities, induced interactions due to particle-hole screening and vertex corrections are significant even in the perturbative  $k_F a$  limit [193, 194] and lead to a reduction of the S-wave gap by a factor  $(4e)^{-1/3} \approx 0.45$ ,

$$\frac{\Delta}{\varepsilon_F} = \frac{8}{e^2} \exp \left\{ \left( \text{diagram 1} + \text{diagram 2} + \text{diagram 3} + \dots \right)^{-1} \right\} = (4e)^{-1/3} \frac{8}{e^2} \exp \left\{ \frac{\pi}{2k_F a} + \mathcal{O}(k_F a) \right\}. \quad (59)$$



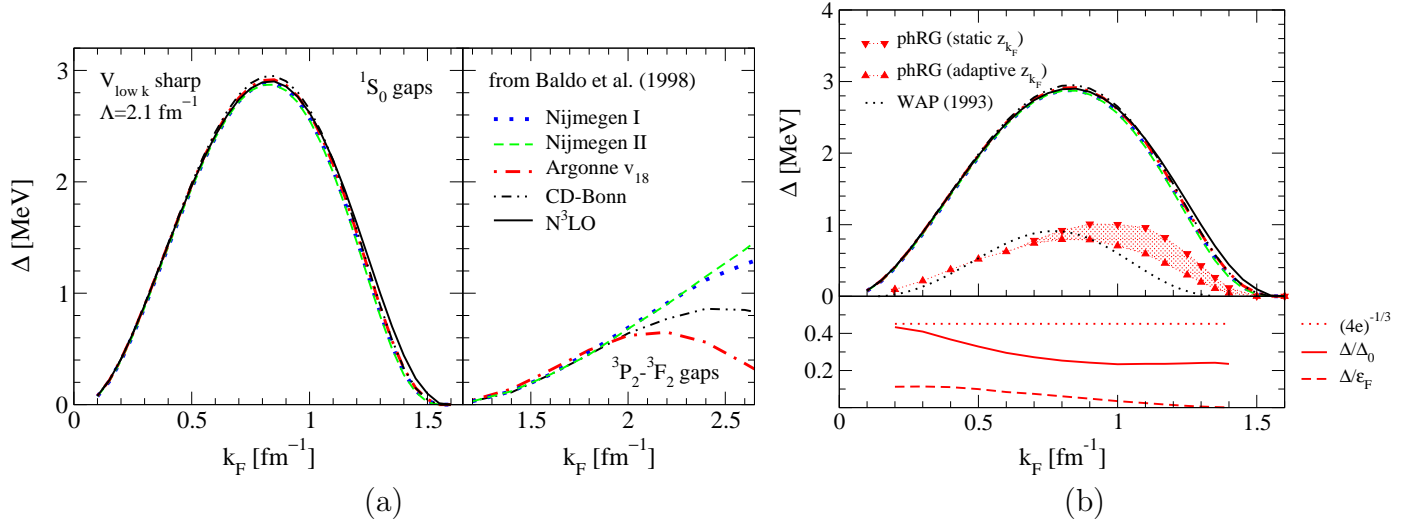


Figure 45: (a) The  $^1S_0$  (left panel) and  $^3P_2$ - $^3F_2$  (right panel) superfluid pairing gaps  $\Delta$  at the Fermi surface as a function of Fermi momentum  $k_F$  in neutron matter. The gaps are obtained from charge-dependent NN interactions at the BCS level. For details see Refs. [96,186]. (b) Top panel: Comparison of the  $^1S_0$  BCS gap to the results including polarization effects through the phRG, for details see Ref. [176], and to the results of Wambach *et al.* [187]. Lower panel: Comparison of the full superfluid gap  $\Delta$  to the BCS gap  $\Delta_0$  and to the Fermi energy  $\epsilon_F$ .

This reduction is due to spin fluctuations, which are repulsive for spin-singlet pairing and overwhelm attractive density fluctuations.<sup>16</sup>

Following Shankar [197], Ref. [176] developed a nonperturbative RG approach for neutron matter, where induced interactions are generated by integrating out modes away from the Fermi surface. Starting from  $V_{\text{low } k}$ , the solution to the RG equations in the particle-hole channels (“phRG”) includes contributions from successive particle-hole momentum shells. The phRG builds up many-body effects similar to the two-body parquet equations, and efficiently includes induced interactions to low-lying states in the vicinity of the Fermi surface beyond a perturbative calculation. The phRG results [176] for the  $^1S_0$  gap are shown in Fig. 45(b), where induced interactions lead to a factor 3–4 reduction to a maximal gap  $\Delta \approx 0.8$  MeV. For the lower densities, the phRG is consistent with the dilute result<sup>17</sup>  $\Delta/\Delta_0 = (4e)^{-1/3}$ , and at the larger densities the dotted band indicates the uncertainty due to an approximate self-energy treatment.

Non-central spin-orbit and tensor interactions are crucial for  $^3P_2$ - $^3F_2$  superfluidity. Without a spin-orbit interaction, neutrons would form a  $^3P_0$  superfluid instead. The first perturbative calculation of non-central induced interactions shows that  $^3P_2$  gaps below 10 keV are possible (while second-order contributions to the pairing interaction are not substantial  $|V_{\text{ind}}/V_{\text{low } k}| < 0.5$ ) [177]. This arises from a repulsive induced spin-orbit interaction due to the mixing with the stronger spin-spin interaction. As a result, neutron P-wave superfluidity (in the interior of neutron stars) may be reduced considerably below earlier estimates. This implies that low-mass neutron stars cool slowly [179–181]. Smaller values for the  $^3P_2$  gap compared to Fig. 45(b) are also required for consistency with observations in a minimal cooling scenario [198].

<sup>16</sup>In finite systems, the spin and density response differs. In nuclei with cores, the low-lying response is due to surface vibrations. Consequently, induced interactions may be attractive, because the spin response is weaker [195,196].

<sup>17</sup>For  $k_F \approx 0.4$  fm $^{-1}$ , neutron matter is close to the universal regime, but theoretically simpler due to an appreciable effective range  $k_F r_e \approx 1$  [34].



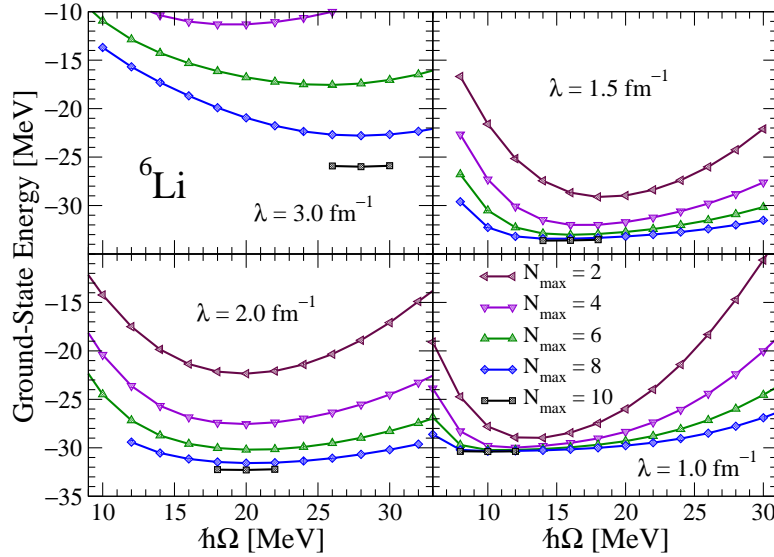


Figure 46: Ground-state energy of  ${}^6\text{Li}$  versus oscillator parameter  $\hbar\Omega$  for different SRG-evolved interactions with  $\lambda = 3.0, 2.0, 1.5$  and  $1.0 \text{ fm}^{-1}$ . The initial interaction is the  $\text{N}^3\text{LO}$  NN-only potential of Ref. [20]. The NCSM results clearly show improved convergence with the maximum number of oscillator quanta  $N_{\text{max}}$  for lower cutoffs. Since 3N interactions are neglected, the different NN calculations converge to different ground-state energies. For details see Ref. [14].

## 6 Applications to finite nuclei

The advantages of low-momentum interactions discussed in Section 5 for infinite matter calculations also apply to finite nuclei. At lower resolution, perturbative methods generally become more effective, finite-basis expansions converge more rapidly, and short-range correlations are substantially weakened. Furthermore, the freedom to vary the cutoff with the RG provides a useful tool to diagnose truncation errors and assess the quality of many-body approximations. In this section, we review applications of low-momentum interactions to finite nuclei, including ab initio calculations of light and medium-mass nuclei, shell model calculations, scattering and reactions, and energy-density functional approaches.

### 6.1 Ab initio calculations

The no-core shell model (NCSM) is a versatile method to calculate ground-state energies and spectra of light nuclei [65]. In Ref. [14], the NCSM was used to study the convergence of nuclei up to  ${}^7\text{Li}$  using RG-evolved chiral NN interactions. Because no additional Lee-Suzuki transformations are required, the energy calculations satisfy the variational principle for a given low-momentum Hamiltonian. As shown in Fig. 46, the convergence of ground-state energies improves rapidly for SRG potentials with decreasing  $\lambda$ , with similar convergence improvements for  $V_{\text{low } k}$  interactions.

When the RG equations are truncated at the two-body level, the evolution is only approximately unitary and converged energies for  $A \geq 3$  vary with  $\lambda$  or  $\Lambda$ . This approximation is systematic, however, and for useful cutoff ranges, the energy variation shown in Fig. 47 is comparable to natural-size truncation errors in chiral EFT, with no unnaturally large contributions from omitted three-body forces for these light nuclei. Further evidence that the evolution preserves the hierarchy of the underlying chiral EFT is shown in Figs. 35 and 36.

Extensions of ab initio methods to heavier and neutron-rich nuclei are a frontier of nuclear theory. Coupled-cluster (CC) theory is the prime method for systems with up to 100 electrons in quantum chemistry [200] and a powerful method for nuclei for which a closed-shell reference state provides a good starting point [86, 201]. For  ${}^3\text{H}$  and  ${}^4\text{He}$ , CC results agree with the corresponding Faddeev and

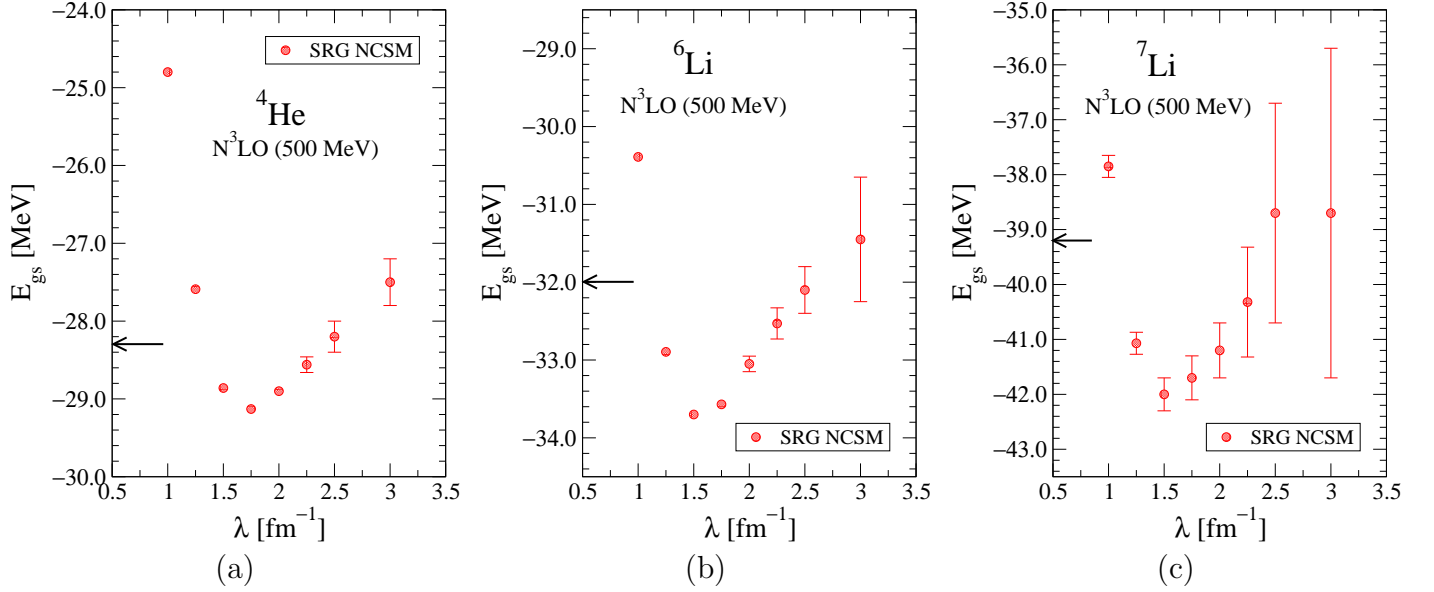


Figure 47: Ground-state energies of (a)  $^4\text{He}$ , (b)  $^6\text{Li}$ , and (c)  $^7\text{Li}$  as a function of  $\lambda$  for SRG interactions evolved from the  $\text{N}^3\text{LO}$  NN-only potential of Ref. [20]. Error bars for larger  $\lambda$  values are from extrapolations in  $N_{\text{max}}$ . The arrow marks the experimental energy. The characteristic increase in  $E_{\text{gs}}$  at small  $\lambda$  signals the modification of the long-range attractive interaction [138]. For details see Ref. [14].

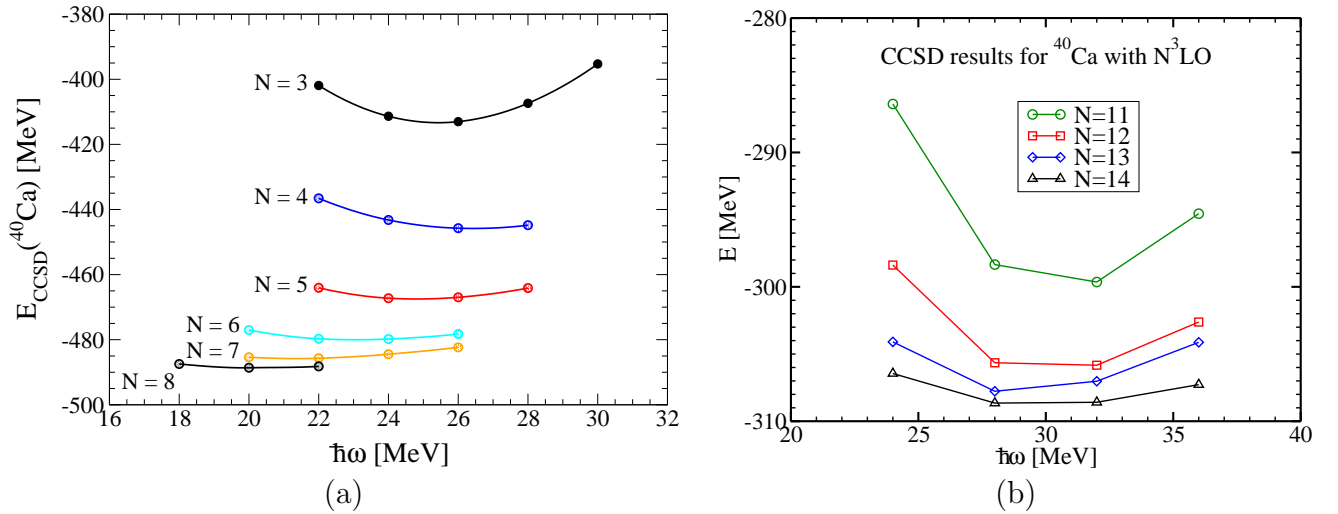


Figure 48: CCSD ground-state energy of  $^{40}\text{Ca}$  as function of the oscillator frequency with increasing basis size  $N$ , based on (a) an RG-evolved low-momentum NN interaction [13] and (b) a  $\text{N}^3\text{LO}$  NN potential [199]. The difference highlights the importance of 3N interactions for ground-state energies.

Faddeev-Yakubovsky energies [13]. Combined with rapid convergence for low-momentum interactions, CC theory has pushed the limits of accurate calculations to medium-mass nuclei and set new benchmarks for  $^{16}\text{O}$  and  $^{40}\text{Ca}$  [13]. Using an angular-momentum-coupled scheme, it is possible to extend CC theory to very large spaces (15 major shells on a single processor) and to obtain near-converged ground-state energies for spherical nuclei,  $^{40}\text{Ca}$ ,  $^{48}\text{Ca}$ , and  $^{48}\text{Ni}$ , based on a  $\text{N}^3\text{LO}$  NN potential [199]. The CC developments for medium-mass nuclei are shown in Fig. 48, where the critical importance of 3N forces for ground-state energies is evident.

Recently, a combination of nuclear and atomic physics techniques led to the first precision mea-

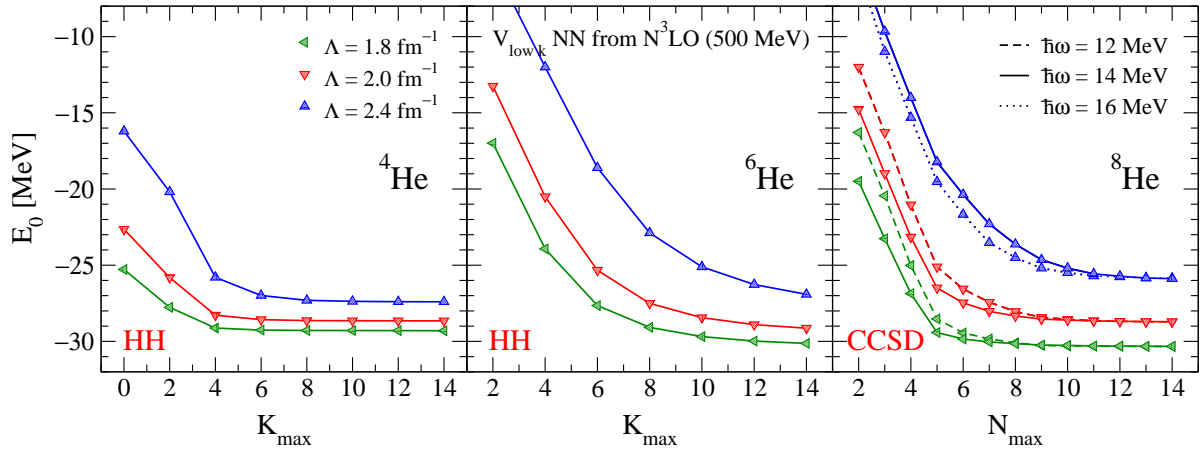


Figure 49: Convergence as a function of the basis size for the HH  ${}^4\text{He}$  and  ${}^6\text{He}$  ground-state energies and for the CCSD ground-state energy of  ${}^8\text{He}$  based on chiral low-momentum NN interactions  $V_{\text{low } k}$  for a range of cutoffs  $\Lambda = 1.8, 2.0$  and  $2.4 \text{ fm}^{-1}$ . For details see Ref. [15].

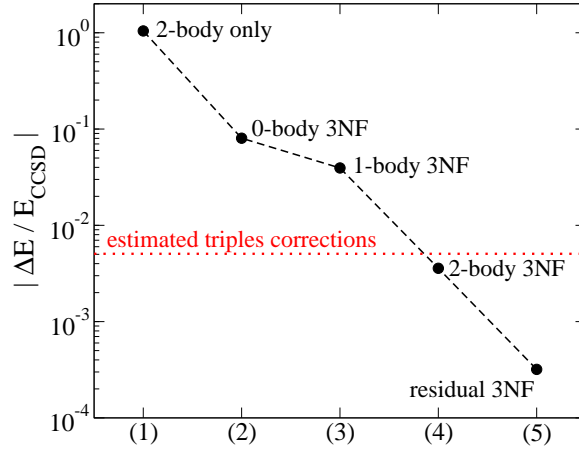


Figure 50: Relative contributions  $|\Delta E/E|$  to the binding energy of  ${}^4\text{He}$  at the CCSD level from  $V_{\text{low } k}$  as well as normal-ordered zero-, one-, two-body and residual three-body parts of 3N forces [202].

measurements of masses and charge radii of the helium halo nuclei,  ${}^6\text{He}$  [203, 204] and  ${}^8\text{He}$  [205, 206], with two or four weakly-bound neutrons forming an extended halo around the  ${}^4\text{He}$  core. In Fig. 49, results are shown for the ground-state energies of helium nuclei based on chiral low-momentum NN interactions [15]. This combines the RG evolution with the exact hyperspherical-harmonics (HH) expansions for  ${}^6\text{He}$  and CC theory for  ${}^8\text{He}$  (see also Ref. [86]), which have the correct asymptotic behavior of the wave function. The cutoff variation in Fig. 49 highlights the importance of 3N interactions. For all studied cutoffs, the NN-only results underbind  ${}^8\text{He}$  [15, 86]. Therefore, the helium isotopes probe 3N effects beyond the overall repulsion observed in infinite nuclear and neutron matter.

Finally, in Fig. 50 the first CC results with 3N forces show that low-momentum 3N interactions are accurately treated as normal-ordered zero-, one-, and two-body terms, and that residual 3N forces can be neglected [202]. This is very promising for developing tractable approximations to handle many-body interactions (see Section 4.3), and supports the idea that phenomenological adjustments in shell model interactions (“monopole shifts”) are due to 3N contributions [207]. These monopole shifts are enhanced in neutron-rich nuclei and have a pivotal impact on shell closures and the location of the neutron drip line, as discussed in Section 6.3.

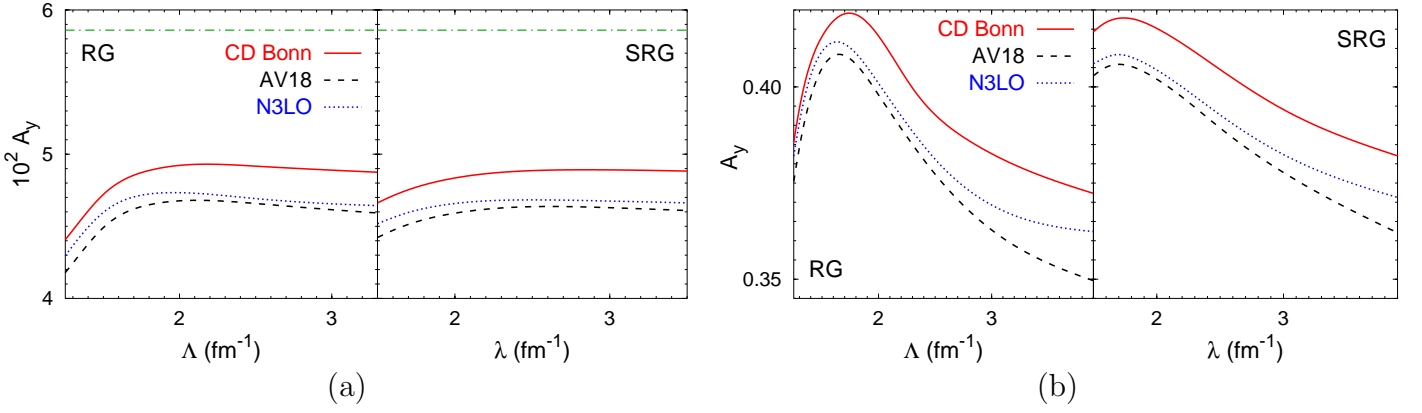


Figure 51: (a) Neutron analyzing power  $A_y$  for neutron-deuteron scattering at  $E_n = 3$  MeV and  $\theta_{\text{cm}} = 104^\circ$  as a function of RG cutoff  $\Lambda$  (left panel) and SRG parameter  $\lambda$  (right panel). The horizontal line at  $10^2 A_y = 5.86$  is the experimental value from Ref. [208]. (b) Maximum of the neutron analyzing power  $A_y$  for neutron- $^3\text{H}$  scattering at  $E_n = 3.5$  MeV as function of RG cutoff  $\Lambda$  (left panel) and SRG parameter  $\lambda$  (right panel). For details see Ref. [209].

## 6.2 Scattering and reactions

In order to probe the sensitivity of 3N and 4N scattering observables to short-range physics, Ref. [209] used low-momentum NN interactions evolved with the RG or SRG to study the variation with the cutoff  $\Lambda$  or  $\lambda$ . The cutoff dependence due to truncating the RG equations at the two-body level provides a measure of the sensitivity to neglected short-range 3N (and higher-body) forces. Comparing the results shown in Fig. 51 one notices that the cutoff dependence of 3N scattering observables is much weaker than the one observed for 4N observables. This weak cutoff dependence in Fig. 51(a) implies that short-range 3N forces are not likely to solve the long-standing discrepancies of the nucleon-deuteron  $A_y$  in elastic scattering with data. This is indeed what has been found when short-range or the leading long-range 3N interactions are included. Nucleon-deuteron  $A_y$  in elastic scattering and the space star differential cross section for breakup barely change by adding a  $2\pi$ -exchange 3N force [210–212], an effective 3N force due to the explicit  $\Delta$ -isobar excitation [213–216], or  $\text{N}^2\text{LO}$  3N forces [128]. In contrast, the maximum of the neutron analyzing power  $A_y$  for neutron- $^3\text{H}$  scattering seems to be more sensitive to short-range many-body forces as demonstrated by the more pronounced dependence on the cutoff in Fig. 51(b). This is consistent with previous findings [217] obtained with various NN potentials.

Neutrinos play a crucial role for the physics of stellar collapse, supernova explosions and neutron stars [218, 219]. The first calculations [220, 221] of neutrino processes based on chiral EFT and RG-evolved interactions have focused on neutrino reactions involving two nucleons: neutrino-pair bremsstrahlung and absorption,  $NN \leftrightarrow NN\nu\bar{\nu}$ , which are key for muon and tau neutrino production in supernovae, and neutrino inelastic scattering,  $\nu NN \leftarrow \nu NN$ . These processes are determined by the spin relaxation rate  $1/\tau_\sigma$  using a unified approach to neutrino interactions in nucleon matter [220]. In supernova simulations, the standard rates for bremsstrahlung are based on the one-pion exchange approximation to NN interactions [222]. Calculations based on chiral EFT and RG-evolved interactions show that shorter-range non-central forces reduce the spin relaxation rate and therefore the rate for bremsstrahlung significantly [220, 221]. In addition, the spin relaxation rate sets the scale for energy transfer in inelastic scattering, which is presently not included in simulations. The spin relaxation rates of Ref. [221] lead to a mean-square energy transfer that is comparable to the incoming neutrino energy, indicating that NN collisions may be important for energy transfer in supernovae.

Quaglioni and Navratil have recently developed an ab initio approach to nuclear reactions based on merging the No-Core Shell Model (NCSM) with the Resonating Group Method (RGM), where the

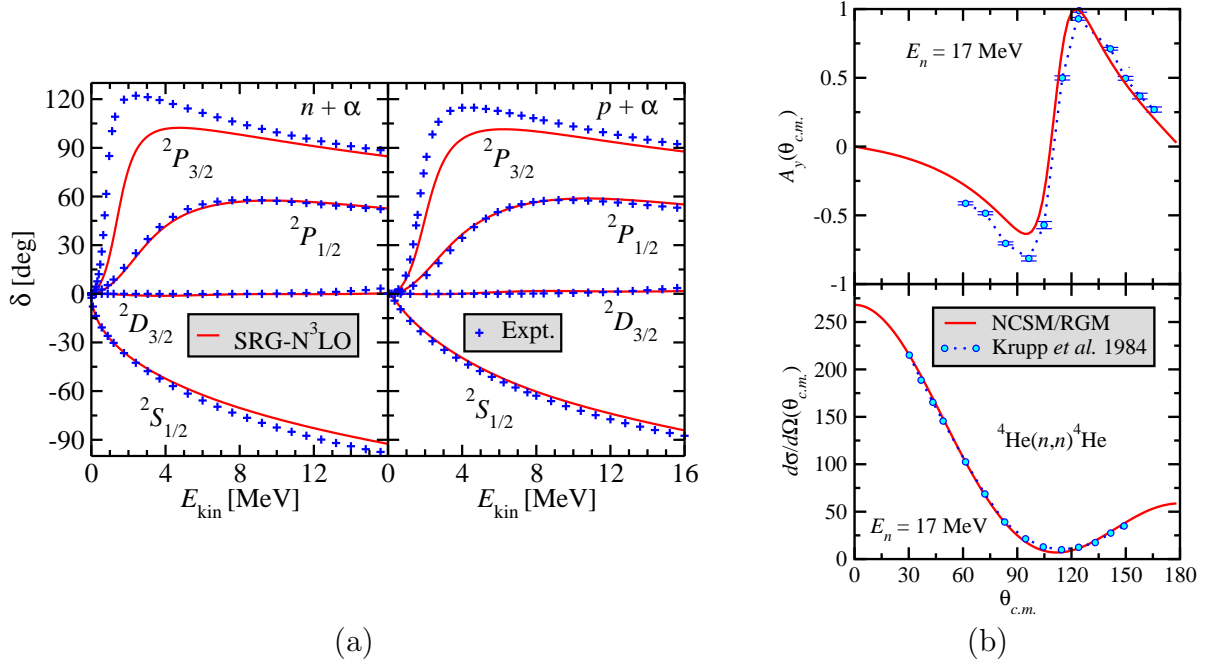


Figure 52: (a) No-Core Shell Model (NCSM) and Resonating Group Method (RGM) applied with an SRG-evolved N<sup>3</sup>LO potential (NN-only,  $\lambda = 2.02 \text{ fm}^{-1}$ ) to calculate nucleon-alpha elastic scattering phase shifts at  $E_n = 17 \text{ MeV}$  [223]. (b) Comparisons are made to the differential cross section (bottom panel) and the analyzing power (top panel) from Karlsruhe polarized-neutron experiments [223].

many-body Hilbert space is spanned by cluster wave functions describing a system of two or more clusters in relative motion [224, 225]. Figure 52 shows nucleon-alpha elastic scattering at  $E_n = 17 \text{ MeV}$  using an SRG-evolved N<sup>3</sup>LO potential [223]. As with the ground-state NCSM calculations, the use of low-momentum interactions in the NCSM/RGM description of nucleon-nucleus scattering results in faster convergence with respect to the basis size. This is a very promising start.

### 6.3 Shell-model approaches

Shell-model applications were one of the main motivations for developing low-momentum interactions [226, 227]. The practical benefit of low-momentum interactions in shell model applications is shown in Fig 53, where we compare S-wave relative harmonic-oscillator matrix elements for a low-momentum cutoff  $\Lambda = 2.0 \text{ fm}^{-1}$  and a  $1.0 \text{ GeV}$  cutoff  $\Lambda = 5.0 \text{ fm}^{-1}$ . We find that for lower cutoffs the matrix elements decrease quite rapidly and become small for  $|n - n'| \sim 5 - 10$ . This is not the case for interactions with high-momentum components, which require basis states up to  $\sim 50$  shells for convergence.

In conventional approaches to shell-model effective interactions, the strong short-range repulsion is tamed by performing a ladder resummation of the NN potential to obtain a  $G$  matrix [91]. However, the  $G$  matrix resummation introduces an inconvenient starting-energy dependence and requires further approximations in practice. Furthermore, as discussed in Section 3.5,  $G$  matrices do not decouple low- and high-energy states. As shown in Fig. 54, low-lying spectra of  $^{18}\text{O}$  and  $^{134}\text{Te}$  based on low-momentum NN interactions are of comparable quality to using  $G$  matrix resummations that are difficult to generalize to 3N forces and involve starting-energy dependences. In addition, as a consequence of decoupling, perturbative valence shell-model calculations starting from low-momentum interactions are under better control than the corresponding  $G$  matrix calculations. We refer to Ref. [66] for a review on low-momentum interactions in perturbative calculations of valence shell-model effective interactions.

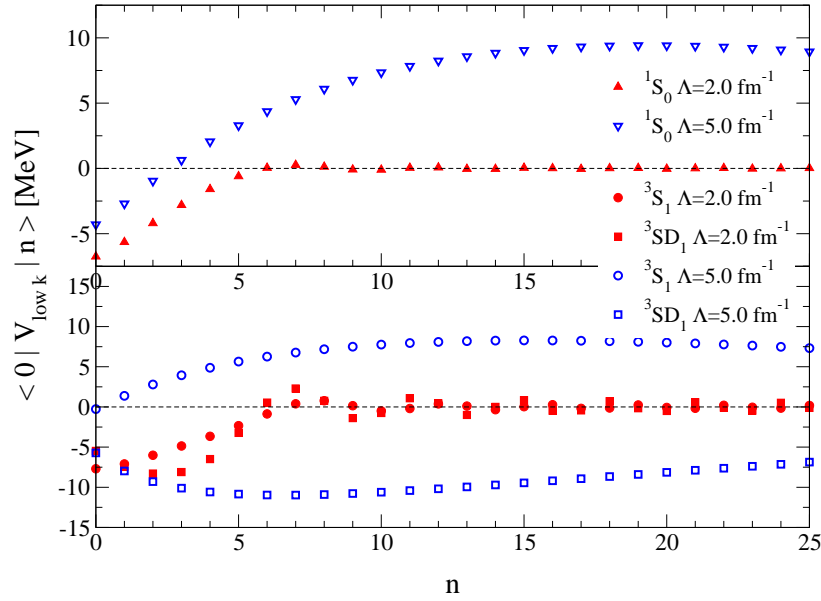


Figure 53: Relative harmonic-oscillator matrix elements  $\langle n' = 0 l' | V_{\text{low } k}^{SJ} | n l \rangle$  versus radial quantum number  $n$  for a low-momentum cutoff  $\Lambda = 2.0 \text{ fm}^{-1}$  and a  $1.0 \text{ GeV}$  cutoff  $\Lambda = 5.0 \text{ fm}^{-1}$ . Results are shown for S-wave matrix elements. In both cases,  $V_{\text{low } k}$  is evolved from the Argonne  $v_{18}$  potential and the harmonic oscillator parameter is  $\hbar\omega = 14 \text{ MeV}$  [132].

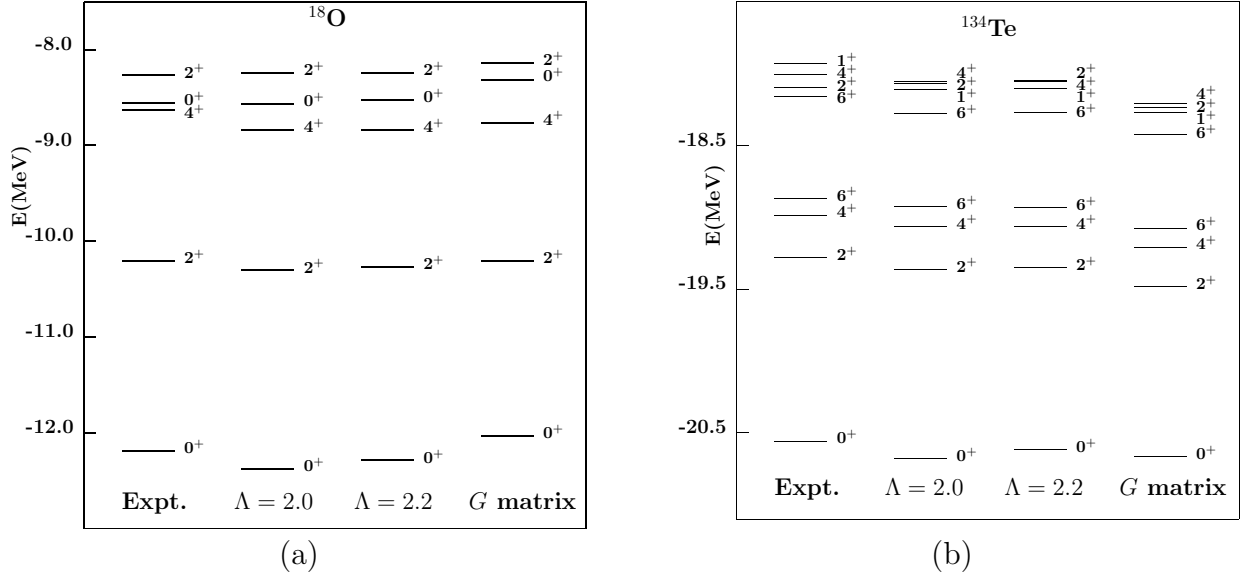


Figure 54: Low-lying spectra using shell-model effective Hamiltonians derived from  $V_{\text{low } k}$  and  $G$  matrix interactions starting from the CD-Bonn potential [19] for (a)  $^{18}\text{O}$  and (b)  $^{134}\text{Te}$  [66].

Moreover, there are promising applications of low-momentum interactions in the Gamow shell model to handle continuum states [228–230].

The neutron drip-line, which is the limit of neutron-rich nuclei, evolves regularly from light to medium-mass nuclei except for a striking anomaly in the oxygen isotopes. This anomaly is not reproduced in theories derived from two-nucleon forces. In Ref. [231], the first microscopic explanation of the oxygen anomaly based on low-momentum 3N forces was presented. As shown in Fig. 55, the inclusion of 3N interactions at  $N^2\text{LO}$  or due to  $\Delta$  excitations leads to repulsive contributions to the interactions among valence neutrons that change the location of the neutron drip-line from  $^{28}\text{O}$  to the experimentally



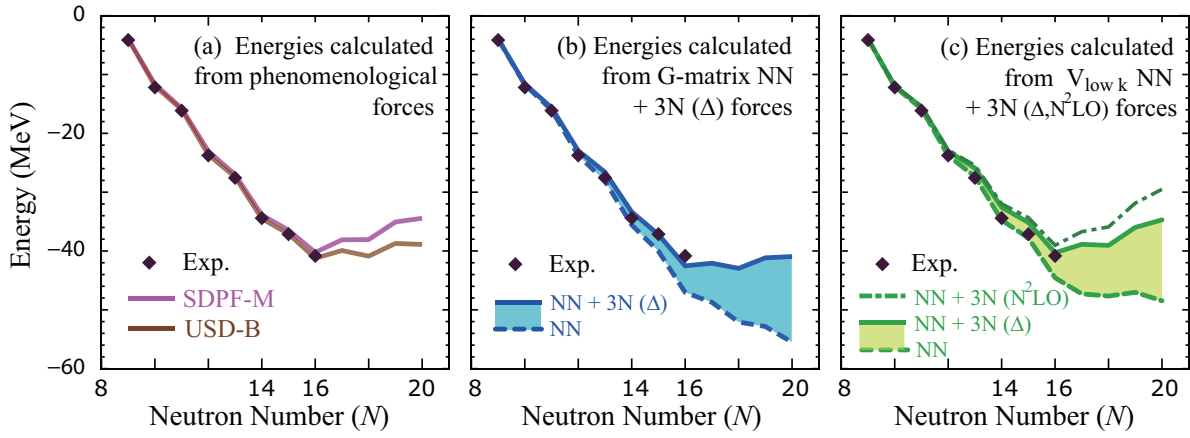


Figure 55: Ground-state energies of neutron-rich oxygen isotopes measured from the energy of  $^{16}\text{O}$ . The experimental energies of the bound oxygen isotopes  $^{16-24}\text{O}$  are included for comparison. The left panel (a) shows the energies obtained from the phenomenological forces SDPF-M [232, 233] and USD-B [234]. The middle panel (b) gives the energies obtained from a  $G$  matrix and including Fujita-Miyazawa 3N forces due to  $\Delta$  excitations [231]. The right panel (c) presents the energies calculated from  $V_{\text{low } k}$  and including chiral EFT 3N interactions at  $N^2\text{LO}$  as well as only due to  $\Delta$  excitations [231]. The changes due to 3N forces based on  $\Delta$  excitations are highlighted by the shaded areas.

observed  $^{24}\text{O}$ . This 3N mechanism is robust and general, and therefore expected to impact predictions of the most neutron-rich nuclei and the synthesis of heavy elements in neutron-rich environments.

## 6.4 Density functional theory

While most advances in microscopic nuclear structure theory over the last decade have been through expanding the reach of few-body calculations, infinite nuclear matter is still a key step to heavier nuclei. In particular, the promising results using low-momentum interactions open the door to ab initio density functional theory (DFT) both directly (through orbital-based methods) and based on expanding about nuclear matter [169]. This is analogous to the application of DFT in quantum chemistry and condensed matter starting with the uniform electron gas in local-density approximations and adding constrained derivative corrections. Phenomenological energy functionals (such as Skyrme) for nuclei have impressive successes but lack a (quantitative) microscopic foundation based on nuclear forces and seem to have reached the limits of improvement with the current form of functionals [235, 236]. Furthermore, without theoretical understanding of errors, extrapolations to the limits of nuclear binding are uncontrolled.

A recent review [67] describes various theoretical paths to ab initio (meaning microscopic) DFT. One formal constructive framework for Kohn-Sham DFT is based on effective actions of composite operators using the inversion method [237–242]. This is an organization of the many-body problem that is based on calculating the response of a finite system to external, static sources rather than seeking the many-body wave function. Other paths include many-body perturbation theory or RG methods applied to effective actions [67, 243, 244]. Either way necessitates a tractable expansion that is controllable in the presence of inhomogeneous sources or single-particle potentials. This is problematic for conventional nuclear forces, for which the single-particle potential needs to be tuned to enhance the convergence of the hole-line expansion [123, 156], but is ideally suited for low-momentum interactions.

The nuclear matter results of Fig. 40 and Ref. [9, 16] imply that exchange correlations are tractable, and this motivates the derivation of an ab initio density functional based on low-momentum interactions, for example, using a density matrix expansion [169] (see also Ref. [33, 245]). This is one of the goals of the SciDAC universal nuclear energy density functional project (UNEDF) [48]. Future work can use



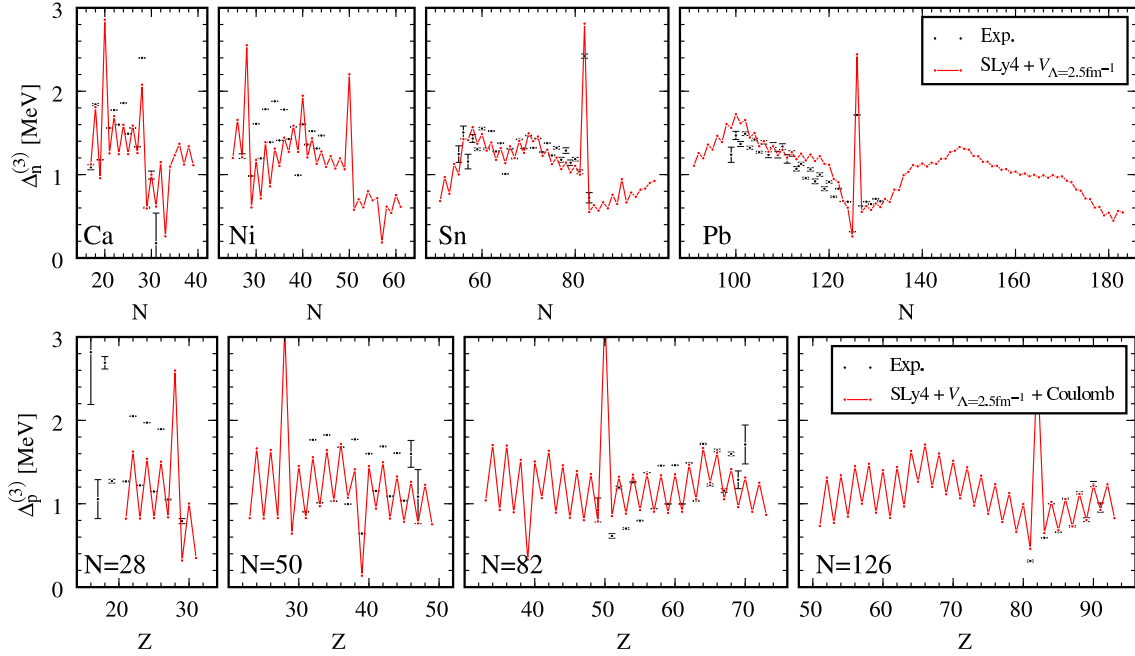


Figure 56: Neutron/proton pairing gaps (upper/lower panel) obtained from calculated and experimental odd-even mass differences along isotopic/isotonic chains. The calculated gaps use the  $^1S_0$  part of  $V_{\text{low } k}$  as pairing interaction in density functional calculations (plus Coulomb for proton gaps) [188, 246].

EFT and RG to identify new terms in the functional, to quantify theoretical errors for extrapolations, and to benchmark with ab initio methods (such as with coupled-cluster theory for medium-mass nuclei).

The theoretical errors of nuclear matter calculations based on low-momentum interactions, while impressively small on the scale of the potential energy per particle, are far too large to be quantitatively competitive with existing energy functionals. However, there is the possibility of fine tuning to heavy nuclei, of using EFT/RG to guide next-generation functional forms, and of benchmarking with ab initio methods for low-momentum interactions. Work in these directions is in progress (see for example Ref. [67]). Overall, these results are very promising for a unified description of all nuclei and nuclear matter but much work is left to be done.

Recent results using existing energy density functionals in the particle-hole channel (to build a reasonable self-consistent single-particle basis) combined with low-momentum interactions  $V_{\text{low } k}$  in the pairing channel suggest that an ab initio DFT treatment of pairing is feasible [79, 80, 97, 188, 191]. Figure 56 shows that the resulting neutron-neutron and proton-proton pairing gaps in semi-magic nuclei are remarkably consistent experiment [188, 246]. Systematic investigations of theoretical corrections, including 3N forces, are underway.

## 7 Summary and outlook

As illustrated in the preceding sections, the use of low-momentum interactions has positively impacted few- and many-body calculations for nuclear structure and reactions in all regions of the nuclear chart. The advantages of softened potentials are unequivocal and recent work on evolving 3N forces addresses some of the most pressing concerns about the RG approach. There remain, however, some misunderstandings and misconceptions about the application and implications for nuclear problems of the RG and related methods and how they connect to EFT. In addition, there is much work in progress with associated open questions and as yet unrealized opportunities. Here we reiterate many of our main points by clarifying some of the misconceptions and surveying the on-going research.

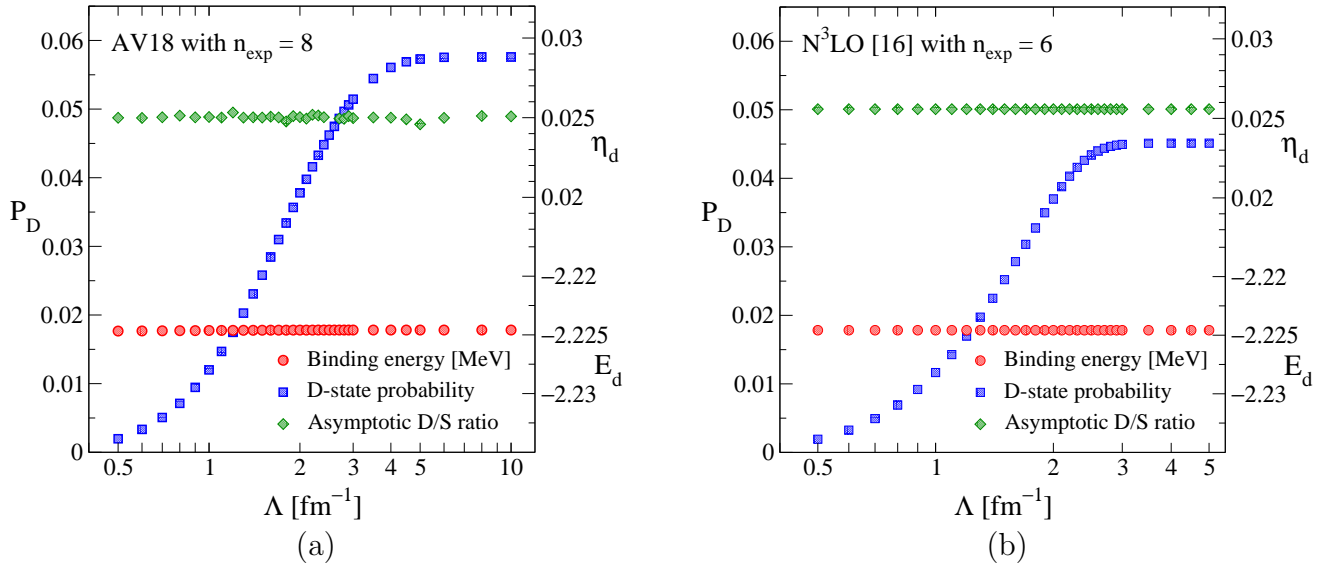


Figure 57: D-state probability  $P_D$  (left axis), binding energy  $E_d$  (lower right axis), and asymptotic D/S-state ratio  $\eta_d$  (upper right axis) of the deuteron as a function of the cutoff [6], starting from (a) the Argonne  $v_{18}$  [18] and (b) the N<sup>3</sup>LO NN potential of Ref. [20] using different smooth  $V_{\text{low } k}$  regulators. Similar results are found with SRG evolution.

## 7.1 Misconceptions and clarifications

In the following we address some of the misleading statements or common misconceptions associated with low-momentum interactions that we have encountered in the literature as well as informally.

- *The nuclear potential is an observable.* Even if not stated explicitly, this is possibly an implicit belief inherited from experience (in both classical and quantum contexts) with the Coulomb potential, and the idea that the potential measures the energy of two particles at fixed separation. This intuition breaks down, of course, for finite-mass composite particles unless at large separations. Because the short-range part of the potential can be modified with a unitary transformation without altering experimental predictions, it is not an observable by any meaningful definition.
- *Both two-nucleon phase shifts and lattice QCD calculations show that the NN interaction has a strongly repulsive core.* We reiterate that a short-range quantum mechanical potential is not a measurable quantity. Fitting the change in sign of S-wave phase shifts from attractive to repulsive with a local potential leads to a repulsive core, but there are an infinity of phase-equivalent potentials without this feature. Similarly, the non-local interaction obtained from lattice simulations and converted to phase-equivalent local form for comparison to phenomenology [28] is based on a non-unique choice of nucleon interpolating field [247, 248].
- *Low-momentum interactions change observable properties such as the D-state probability.* As long as the corresponding operators are evolved together with the Hamiltonian, observables will remain unchanged. While it is true that the D-state probability of the deuteron is reduced as interactions are evolved toward lower cutoffs, this is not an observable [249, 250]. Figure 57 illustrates some observable and non-observable properties of the deuteron. Up to numerical errors, the measurable binding energy and the asymptotic D/S-state ratio are independent of the low-momentum resolution, while the unobservable D-state probability changes dramatically as the short-range part of the tensor force is integrated out.

- *Details of strong-interaction dynamics at high energy are important for low-energy nuclear structure and reactions.* More precisely, it has been claimed that a good (or at least reasonable) description of phase shifts above some energy (such as  $E_{\text{lab}} = 350 \text{ MeV}$ ) is required for a Hamiltonian to be useful for nuclear structure. While it would seem natural that low- and high-energy physics are decoupled, this does not happen automatically and the misconception is often driven by experience with conventional NN potentials with strong short-range repulsion. The repulsion causes even bound states with very low energies (such as the deuteron) to have important contributions to the binding energy and other observables from high-momentum components (well above  $2 \text{ fm}^{-1}$ , see Fig. 12) of the deuteron wave function.<sup>18</sup> For example, Ref. [251] presents cross sections for electron scattering from the deuteron calculated using as input a spectral function that is the momentum distribution times a delta function in energy. After noting the effect of excluding high momenta on the cross section, the conclusion is that “the data confirm the existence of high-momentum components in the deuteron wave function”. Beyond the fact that the short-range parts of wave functions are not observables, these conclusions reinforce the intuition that there is information in quantitatively reproducing high-energy phase shifts that is lost when evolving to low-momentum interactions. However, due to decoupling for the RG-evolved interactions, it is completely irrelevant if phase shifts are zero above some energy.
- *Short-range correlations are important for low-energy properties of nuclei.* Various electron scattering and proton scattering experiments purport to show the existence of short-range correlations in nuclei. These results are then interpreted as implying that such correlations are an important feature of the structure of medium to heavy nuclei (see, for example, Refs. [252, 253]). As shown for the deuteron in Figs. 3(b) and 16(a), the short-range part of a wave function is not an observable and is radically changed by short-range unitary transformations that preserve all observables. Therefore any statement about short-range correlations necessarily relies on the (model-dependent) short-distance details of the Hamiltonian, which in turn depend on the resolution. As has been illustrated in this review, eliminating these correlations by evolving to low resolution greatly enhances the convergence of few- and many-body calculations.
- *The low-momentum RG technology fails for observables that are sensitive to high-momentum components.* In principle, calculated observables [254, 255] from experiments such as  $(e, e'pN)$  are unchanged after RG evolution whether or not they involve high momentum, because the associated operators (which are generally not simple at high momentum) will transform to ensure this invariance. In practice there are many open questions, such as whether consistent operator evolution is difficult to approximate accurately or if factorization approximations might be more valid with low-momentum interactions.
- *Low-momentum interactions are not systematic.* If one starts from a chiral EFT interaction determined to a given order in the power counting, the truncation error of the initial chiral EFT is exactly preserved when many-body interactions are evolved as well. If many-body interactions are truncated, the error remains of the same natural size for cutoffs used in practical calculations. Therefore, low-momentum interactions preserve the systematic nature of the initial EFT and EFT improvements are immediately folded into the RG evolution. In addition, the control of the EFT truncation errors is not lost when two-body forces are evolved exactly but the three-body forces are fit using chiral 3N interactions as a truncated basis. On the other hand, if one starts from phenomenological potentials, then it is correct that the low-momentum Hamiltonian is not systematically improvable because the starting point is not either.

---

<sup>18</sup>We emphasize that the need for high-momentum components in these particular calculations *does not* imply that the high-energy description is correct.

- *Low-momentum interactions are only useful as long as calculations with “bare” chiral EFT interactions are not possible for all nuclei.* We reiterate that there is nothing superior about a “bare” interaction as long as the RG-evolved interactions reproduce observables with a comparable truncation error. Further, converged calculations with different cutoffs are very desirable to quantify theoretical uncertainties. Finally, the certainty that three-body (and possibly four-body) forces will be needed for precision calculations implies that softer interactions will continue to be necessary to push to larger nuclei and to reactions even with the anticipated gains in computing power. (Note that normal-ordering simplifications for many-body forces are more effective for low-momentum Hamiltonians.)
- *There is only one  $V_{\text{low } k}$  or SRG potential.* In fact there are infinitely many different low-momentum interactions, corresponding to different initial potentials (often called “bare” interactions) and different choices for the evolution (cutoff value and renormalization scheme, such as sharp, smooth and SRG). The same holds for chiral EFT interactions, which depend on the regulator and cutoff values, as well as on the level of truncation. There is an analogous misconception that there is only one N<sup>3</sup>LO NN potential, based perhaps on the dominant use of the  $\Lambda = 500$  MeV potential of Ref. [20]. Note that the full advantages of low-momentum potentials are only realized if more than one cutoff is used.
- *The RG evolution of nuclear forces to lower momentum improves the physics.* To our knowledge, this is not a statement that has actually been made by a  $V_{\text{low } k}$  or SRG proponent, but one which is often thought to be implied. However, if the initial Hamiltonian provides a poor representation of nature at low energies, it will not be improved by the RG evolution described here. The correct statement is that an exact RG evolution to lower momentum *preserves* the observable physics, while making it (generally) easier to calculate. If we could easily calculate all many-body systems of interest exactly with an initial Hamiltonian, then there would be no need for the RG evolution. (Unless changing the resolution was useful for other reasons, such as enhancing physical insight.)
- *Evolved low-momentum interactions are strongly non-local.* This is misleading because it omits that the non-locality generated by RG evolution to lower resolution increases with the momentum transfer  $q$ .<sup>19</sup> The local long-range (low  $q$ ) part of low-momentum interactions (given by one-pion exchange) is therefore *not* modified by the evolution. Given the composite nature of nucleons, non-locality at short range (high  $q$ ) is natural.
- *Low-momentum interactions should reproduce the initial NN-only results for  $A > 2$ .* The RG evolution to lower resolution shifts interaction strength from two-body to few-body contributions, so it is *guaranteed* that NN-only calculations will disagree for  $A > 2$ . A related misconception is: *Low-momentum interactions are approximations to “bare” potentials.* Because induced few-body contributions will be truncated at some level, there will be differences from the “bare” result. But any “bare” interaction is also a truncated low-energy effective theory, so there should be no preference over low-momentum interactions with different but still natural few-body contributions.
- *Soft interactions are not realistic Hamiltonians because they overbind nuclei compared to experiment.* This statement tends to follow observations that nuclei calculated with NN-only low-momentum interactions are increasingly overbound with increasing  $A$ . But this is only true if 3N forces (or the uncertainties from neglecting 3N forces) are omitted, which is not justified. The test in the end is whether soft Hamiltonians including many-body forces reproduce observables.

---

<sup>19</sup>This contrasts with a Perey-Buck-type factorized non-local potential [256] such as  $V(\mathbf{r}, \mathbf{r}') = V_{\text{local}}[(\mathbf{r} + \mathbf{r}')/2](\pi^{1/2}\beta)^{-3} \exp[(\mathbf{r} - \mathbf{r}')^2/\beta^2]$ , for which the non-locality is independent of the momentum transfer.

- *Many-body forces will explode after integrating out strong short-range repulsion.* The calculations reviewed in the preceding sections demonstrate explicitly that this is not the case (for example, low-momentum 3N interactions are perturbative in light nuclei). Many-body contributions are natural in size and the decreasing hierarchy is preserved. A related misconception is: *To include 3N forces with low-momentum interactions, it is important to distinguish between “real” (or “genuine”) and “induced” three-body forces.* The initial and evolved 3N forces are both “effective” interactions. Because the EFT truncation error is preserved in the evolution, there is no physics reason to prefer one over the other. Each Hamiltonian has different associated many-body interactions and operators, although the long-range parts are the same as they are not modified by the RG evolution.
- *Weren’t soft potentials ruled out for nuclear physics long ago?* Soft potentials were explored in the mid-sixties and early seventies to improve convergence in nuclear matter and nuclei. In particular, separable potentials such as the Tabakin potential were considered, as well as unitary transformations of local, repulsive-core potentials [47, 59]. These NN-only soft potentials were abandoned primarily because they did not saturate nuclear matter in the empirical range, but at too-high densities and with overbinding. In contrast, with low-momentum interactions saturation is driven by the (natural-sized) 3N forces fit to three- and four-body properties.
- *Nuclear matter saturation with low-momentum interactions is largely due to the (long-range) two-pion-exchange part of 3N forces. But for conventional NN potentials, two-pion-exchange 3N forces are attractive for all nuclei and nuclear matter [53, 134].* The distinction is because decoupling in low-momentum interactions means that 3N contributions are from the low-momentum (long-range) parts of 3N forces, whereas in calculations with conventional potentials, two-pion-exchange 3N forces are also sensitive to the (model-dependent) short-range parts of wave functions. This leads to a net attraction for hard potentials [172]. Due to the importance of 3N forces for nuclei, a quantitative understanding of this change is an important open problem.
- *$V_{\text{low } k}$  is just like a  $G$  matrix.* The  $G$  matrix approach leads to a softened version of an initial NN potential and one can see strong similarities between a  $G$  matrix and  $V_{\text{low } k}$  for matrix elements connecting low-energy states (explicit comparisons are shown in Figs. 33 and 53). But the  $G$  matrix is an in-medium interaction that depends on the nucleus or the density and on a “starting energy”, while low-momentum interactions are (generally) evolved in free space. Most important is that the decoupling between low and high momenta that is the hallmark of low-momentum interactions is *not* achieved by the  $G$  matrix construction. The off-diagonal contributions, evident in Fig. 33, make  $V_{\text{low } k}$  qualitatively different from a  $G$  matrix. A consequence is that while the  $G$  matrix is a softened effective interaction, the off-diagonal parts will be significant in higher-order diagrams. This is why a perturbative expansion in the  $G$  matrix fails and something like the hole-line expansion is needed (with a similar  $G$  matrix resummation at the three-body level).

## 7.2 Open problems and opportunities

We finish with a survey of work in progress to extend the results described in this review together with open problems that may lead to new opportunities. This is, of course, not a comprehensive list, as there will be other efforts of which we are unaware and because new ideas constantly arise. But we hope this will give a reasonable vision of what to expect in the next few years.

Chiral EFT power counting of the hierarchy of many-body forces implies that 3N forces must be included in almost any precision calculation of nuclear properties; this is evident already from

microscopic calculations of light nuclei.<sup>20</sup> Ongoing work includes the effects of 3N forces in one of three ways: matching to a truncated chiral EFT basis (Section 4.1), explicit evolution with RG flow equations (Section 4.2), or through normal-ordering and the in-medium SRG (Section 4.3).

The recent evolution of 3N forces with SRG flow equations in a harmonic-oscillator basis will allow important tests of the matching approach and whether the low-momentum universality observed at the NN level (the collapse of different initial potentials) extends to three-body forces. These studies can also provide useful insights to more general EFT questions regarding the consistency of fits to NN and 3N interactions and the power counting of three-body forces. In addition, the SRG can be extended to evolve 3N forces in momentum space (with the kinetic energy generator) and to generate consistent 3N interactions for  $V_{\text{low } k}$  using the SRG block diagonalization. We note that the formal equivalence between the block-diagonal SRG and  $V_{\text{low } k}$  is not yet established. Likewise, the very similar results in few- and many-body calculations using smooth cutoff  $V_{\text{low } k}$  and band-diagonal SRG (NN-only) interactions is not yet understood.

The availability of low-momentum 3N interactions opens the door to many new results in ab initio calculations of finite nuclei using NCSM, hyperspherical harmonics, and coupled-cluster methods. An important open problem is to determine the range of resolutions for which the RG evolution can be used to soften nuclear Hamiltonians while preserving the hierarchy of many-body interactions. The study of residual cutoff dependencies in calculations of finite nuclei and infinite matter will help answer this question and provide critical tests of the RG approach. Work on the consistent evolution of operators will lead to new opportunities for exploring electroweak processes in nuclei and for assessing theoretical uncertainties of key nuclear matrix elements.

In addition, an important direction for future work is to develop and test tractable approximations to handle many-body forces. The first applications of low-momentum 3N interactions to the shell model are very exciting and open many opportunities for exotic nuclei. The development of the in-medium SRG is promising to include many-body interactions through normal-ordering and to provide a non-perturbative approach to valence shell-model effective interactions and operators. The applications to reactions are another frontier. The NCSM/RGM combination has shown promise with low-momentum NN interactions (both  $V_{\text{low } k}$  and SRG) and the extension to include 3N forces is an additional challenge. Revisiting the nucleon-nucleus optical potential with low-momentum interactions is also inviting, given the improved status of Hartree-Fock as a starting point.

Calculations with evolved cutoff-dependent 3N forces open the door to study 4N interactions. Precision spectroscopy and low-energy reaction theory will require some control and assessment of the size of 4N forces. We note that the density dependence of 4N forces is not known for *any* low-energy nuclear Hamiltonian. Various approximations for evolving 4N interactions are suggested by analyzing the diagrammatic form of the SRG [137].

While the SRG is currently formulated in terms of coupled differential equations, experience with RG evolution for  $V_{\text{low } k}$  suggest that an integral form may be more robust numerically. A possible starting point is the formalism developed in Ref. [257]. There are also many open questions concerning the relationship of the RG techniques discussed here to the wide range of RG technology applied to condensed matter and high-energy problems. For example, what are transformations that convert energy to momentum dependencies? And is there a path integral formulation of the SRG?

The low-momentum RG technology that has been developed can also be usefully applied directly to EFT. Even though the widely available chiral EFT potentials have cutoffs as low as 500 MeV, these are not sharp cutoffs and significant high momentum strength is still present. As shown in Ref. [6], an exponential regulator with  $n_{\text{exp}} \approx 8$  leads to weaker distortions than the conventional value of  $n_{\text{exp}} = 3$  used in the  $N^3\text{LO}$  NN potentials [20, 44]. At still lower cutoffs, an SRG-type regulator may have

---

<sup>20</sup>Calculations with low-momentum NN interactions are useful to establish convergence properties and to use the cutoff dependence to learn about the omitted forces, or in certain applications where 3N contributions are small, such as low-density neutron matter.

additional advantages. Experience with lower momentum regulators could be merged with expertise on fitting EFT low-energy constants to optimize the EFT at lower (softer) cutoffs for testing power counting as well as for applications to few- and many-body methods. This will help resolve questions about the utility of  $V_{\text{low } k}$  interactions compared to unevolved chiral EFT with lower cutoffs and possibly facilitate the use of error plots for the EFT [56].

For infinite matter, a power counting is needed for low-momentum interactions that specifies controlled many-body truncations at finite density. The Bethe-Brueckner-Goldstone expansion, which involves a summation of particle-particle ladders into the  $G$  matrix, shows (for potentials with strong short-range repulsion) that a perturbative expansion in terms of the  $G$  matrix does not work and so further summations are required. (The summation in this case is organized by the hole-line expansion.) Indications are that both summations are unnecessary with low-momentum interactions, but a quantitative power counting (for example, using the momentum dependence of the interactions together with phase-space constraints) needs to be demonstrated. This will involve understanding the evolution of particle-hole physics and what are the non-perturbative aspects of low-momentum interactions for nuclear structure.

Finally, there are also opportunities for applications beyond ordinary nuclei. These include low-momentum interactions between baryons that carry strangeness for descriptions of hypernuclei (see, for example, Refs. [121, 258–260]). Renormalization group methods are already applied widely in condensed matter physics, but the special experience from nuclei may be of advantage. The application to microscopic inter-atomic potentials is an example that may prove fruitful.

In closing, we reiterate that methods to derive low-momentum interactions not based (at least explicitly) on RG evolution are being pursued with promising results and prospects. The future interplay of the different approaches will be fruitful. When low-momentum interactions are coupled with the advances of many-body methods, the steady improvements in computational algorithms and power, and the on-going developments in chiral EFT and lattice QCD, the dream of microscopic calculations connecting QCD to the full range of nuclei and their reactions is within reach.

## Acknowledgments

We thank E. Anderson, S. Bacca, S. Baroni, J. Drut, T. Duguet, K. Hebeler, J. Holt, E. Jurgenson, R. Perry, L. Platter and K. Wendt for useful comments on this review. This work was supported in part by the National Science Foundation under Grant Nos. PHY-0653312, PHY-0758125, and PHY-0456903, the UNEDF SciDAC Collaboration under DOE Grant DE-FC02-07ER41457, the Natural Sciences and Engineering Research Council of Canada (NSERC), and by the Helmholtz Alliance Program of the Helmholtz Association, contract HA216/EMMI “Extremes of Density and Temperature: Cosmic Matter in the Laboratory”. TRIUMF receives federal funding via a contribution agreement through the National Research Council of Canada.

## References

- [1] National Research Council, Nuclear Physics: The Core of Matter, The Fuel of Stars (The National Academies Press, Washington, DC, 1999).
- [2] NuPECC Long Range Plan 2004: Perspectives for Nuclear Physics Research in Europe in the Coming Decade and Beyond (2004).
- [3] DOE/NSF Nuclear Science Advisory Committee, The Frontiers of Nuclear Science: A Long-Range Plan (2007).



- [4] National Research Council, Scientific Opportunities with a Rare-Isotope Facility in the United States (The National Academies Press, Washington, DC, 2007).
- [5] S.K. Bogner, T.T.S. Kuo and A. Schwenk, Phys. Rept. 386 (2003) 1.
- [6] S.K. Bogner et al., Nucl. Phys. A 784 (2007) 79.
- [7] S.K. Bogner, R.J. Furnstahl and R.J. Perry, Phys. Rev. C 75 (2007) 061001.
- [8] A. Nogga, S.K. Bogner and A. Schwenk, Phys. Rev. C 70 (2004) 061002.
- [9] S.K. Bogner et al., Nucl. Phys. A 763 (2005) 59.
- [10] S.K. Bogner and R.J. Furnstahl, Phys. Lett. B 632 (2006) 501.
- [11] S.K. Bogner and R.J. Furnstahl, Phys. Lett. B 639 (2006) 237.
- [12] S.K. Bogner et al., Nucl. Phys. A 773 (2006) 203.
- [13] G. Hagen et al., Phys. Rev. C 76 (2007) 044305.
- [14] S.K. Bogner et al., Nucl. Phys. A 801 (2008) 21.
- [15] S. Bacca et al., Eur. Phys. J. A 42 (2009) 553.
- [16] S.K. Bogner et al., arXiv:0903.3366.
- [17] K. Hebeler and A. Schwenk, arXiv:0911.0483.
- [18] R.B. Wiringa, V.G.J. Stoks and R. Schiavilla, Phys. Rev. C 51 (1995) 38.
- [19] R. Machleidt, Phys. Rev. C 63 (2001) 024001.
- [20] D.R. Entem and R. Machleidt, Phys. Rev. C 68 (2003) 041001.
- [21] S. Aoki, T. Hatsuda and N. Ishii, Comput. Sci. Dis. 1 (2008) 015009.
- [22] S.C. Pieper and R.B. Wiringa, Ann. Rev. Nucl. Part. Sci. 51 (2001) 53.
- [23] S.C. Pieper, R.B. Wiringa and J. Carlson, Phys. Rev. C 70 (2004) 054325.
- [24] S.C. Pieper, Nucl. Phys. A 751 (2005) 516.
- [25] N. Ishii, S. Aoki and T. Hatsuda, Phys. Rev. Lett. 99 (2007) 022001.
- [26] T. Hatsuda et al., Mod. Phys. Lett. A 23 (2008) 2265.
- [27] N. Ishii, S. Aoki and T. Hatsuda, PoS LATTICE2008 (2008) 155.
- [28] S. Aoki, T. Hatsuda and N. Ishii, arXiv:0909.5585.
- [29] G.P. Lepage, “What is Renormalization?”, Lectures given at TASI’89 Summer School: From Actions to Answers, Boulder, CO, June, 1999, nucl-th/0506330.
- [30] P.F. Bedaque and U. van Kolck, Ann. Rev. Nucl. Part. Sci. 52 (2002) 339.
- [31] E. Epelbaum, H.W. Hammer and U.G. Meissner, Rev. Mod. Phys. 81 (2009) 1773.

- [32] E. Braaten and H.W. Hammer, Phys. Rept. 428 (2006) 259.
- [33] R.J. Furnstahl, G. Rupak and T. Schafer, Ann. Rev. Nucl. Part. Sci. 58 (2008) 1.
- [34] A. Schwenk and C.J. Pethick, Phys. Rev. Lett. 95 (2005) 160401.
- [35] L. Platter, Few Body Syst. 46 (2009) 139.
- [36] E. Epelbaum, Prog. Part. Nucl. Phys. 57 (2006) 654.
- [37] R. Machleidt, “Nuclear Forces from Chiral Effective Field Theory”, Lectures given at Workshop on Physics and Astrophysics of Hadrons and Hadronic Matter, Shantiniketan, India, November, 2006, arXiv:0704.0807.
- [38] S.R. Beane, K. Orginos and M.J. Savage, Int. J. Mod. Phys. E 17 (2008) 1157.
- [39] A. Nogga, R.G.E. Timmermans and U. van Kolck, Phys. Rev. C 72 (2005) 054006.
- [40] M. Pavon Valderrama and E. Ruiz Arriola, Phys. Rev. C 74 (2006) 054001.
- [41] M. Pavon Valderrama, arXiv:0912.0699.
- [42] S.R. Beane et al., “From Hadrons to Nuclei: Crossing the Border”, At the Frontier of Particle Physics, Ed. M. Shifman, Vol. 1, p. 133, World Scientific, 2001, arXiv:nucl-th/0008064.
- [43] J. Haidenbauer et al., Lect. Notes Phys. 724 (2007) 113.
- [44] E. Epelbaum, W. Glockle and U.G. Meissner, Nucl. Phys. A 747 (2005) 362.
- [45] D. Rozpedzik et al., Acta Phys. Polon. B 37 (2006) 2889.
- [46] E. Epelbaum and U.G. Meissner, arXiv:0907.1778.
- [47] F. Coester et al., Phys. Rev. C 1 (1970) 769.
- [48] G.F. Bertsch, D.J. Dean and W. Nazarewicz, SciDAC Review 6 (2007) 42.
- [49] H.A. Bethe, Ann. Rev. Nucl. Part. Sci. 21 (1971) 93.
- [50] A.D. Jackson, Ann. Rev. Nucl. Part. Sci. 33 (1983) 105.
- [51] R. Machleidt, Adv. Nucl. Phys. 19 (1989) 189.
- [52] H. Muther and A. Polls, Prog. Part. Nucl. Phys. 45 (2000) 243.
- [53] A. Akmal, V.R. Pandharipande and D.G. Ravenhall, Phys. Rev. C 58 (1998) 1804.
- [54] S.R. Beane et al., Nucl. Phys. A 700 (2002) 377.
- [55] S. Fleming, T. Mehen and I.W. Stewart, Nucl. Phys. A 677 (2000) 313.
- [56] G.P. Lepage, “How to Renormalize the Schrödinger Equation”, Lectures given at 9th Jorge Andre Swieca Summer School: Particles and Fields, Sao Paulo, Brazil, February, 1997, nucl-th/9706029.
- [57] P. Navratil et al., Phys. Rev. Lett. 99 (2007) 042501.
- [58] S.K. Bogner et al., Phys. Lett. B 576 (2003) 265.

- [59] M.I. Haftel and F. Tabakin, Phys. Rev. C 3 (1971) 921.
- [60] A. Nogga, H. Kamada and W. Glöckle, Phys. Rev. Lett. 85 (2000) 944.
- [61] P. Navratil and W.E. Ormand, Phys. Rev. C 68 (2003) 034305.
- [62] E. Epelbaum et al., Nucl. Phys. A 645 (1999) 413.
- [63] P. Deligne et al., editors, Lectures on Quantum Field Theory, Vol. 1 (Amer. Math. Soc. Providence, RI, 2000).
- [64] A.H. Guth, K. Huang and R.L. Jaffe, editors, Asymptotic Realms of Physics (MIT Press, Cambridge, MA, 1983).
- [65] P. Navratil et al., J. Phys. G 36 (2009) 083101.
- [66] L. Coraggio et al., Prog. Part. Nucl. Phys. 62 (2009) 135.
- [67] J.E. Drut, R.J. Furnstahl and L. Platter, Prog. Part. Nucl. Phys. 64 (2010) 120.
- [68] S.K. Bogner et al., Phys. Lett. B 649 (2007) 488.
- [69] E.D. Jurgenson et al., Phys. Rev. C 78 (2008) 014003.
- [70] M.C. Birse, Phys. Rev. C 74 (2006) 014003.
- [71] M.C. Birse, arXiv:0909.4641.
- [72] L. Coraggio et al., Phys. Rev. C 75 (2007) 024311.
- [73] A. Schwenk and J.D. Holt, AIP Conf. Proc. 1011 (2008) 159.
- [74] E. Epelbaum, W. Glöckle and U.G. Meissner, Nucl. Phys. A 671 (2000) 295.
- [75] S. Weinberg, Phys. Rev. 131 (1963) 440.
- [76] G.E. Brown, Unified Theory of Nuclear Models and Forces (North-Holland, Amsterdam, 1971).
- [77] S. Ramanan, S.K. Bogner and R.J. Furnstahl, Nucl. Phys. A 797 (2007) 81.
- [78] J.R. Shepard and J.A. McNeil, arXiv:0909.0974.
- [79] T. Duguet and T. Lesinski, Eur. Phys. J. ST 156 (2008) 207.
- [80] T. Lesinski et al., Eur. Phys. J. A 40 (2009) 121.
- [81] B.M. Axilrod and E. Teller, J. Chem. Phys. 11 (1943) 299.
- [82] G.D. Mahan and K.R. Subbaswamy, Local Density Theory of Polarizability (Plenum Press, New York, 1990).
- [83] R.J. Bell and I.J. Zucker, Long-Range Forces, Rare Gas Solids, Vol. 1, edited by M.L. Klein and J.A. Venables, pp. 122–175, Academic Press, London, 1976.
- [84] L. Platter, H.W. Hammer and U.G. Meissner, Phys. Lett. B 607 (2005) 254.
- [85] E.D. Jurgenson, P. Navratil and R.J. Furnstahl, Phys. Rev. Lett. 103 (2009) 082501.

- [86] G. Hagen et al., Phys. Lett. B 656 (2007) 169.
- [87] S.K. Bogner et al., arXiv:nucl-th/0111042.
- [88] S.K. Bogner, R.J. Furnstahl and A. Schwenk, arXiv:0806.1365.
- [89] S.Y. Lee and K. Suzuki, Phys. Lett. B 91 (1980) 173 .
- [90] K. Suzuki and S.Y. Lee, Prog. Theor. Phys. 64 (1980) 2091.
- [91] M. Hjorth-Jensen, T.T.S. Kuo and E. Osnes, Phys. Rept. 261 (1995) 125.
- [92] S. Okubo, Prog. Theor. Phys. 12 (1954) 603.
- [93] S. Bayegan, M. Harzchi and M.R. Hadizadeh, Nucl. Phys. A 814 (2008) 21.
- [94] S. Bayegan, M. Harzchi and M.A. Shalchi, arXiv:0908.2304.
- [95] S.B. Liao, J. Polonyi and M. Strickland, Nucl. Phys. B 567 (2000) 493.
- [96] K. Hebeler, A. Schwenk and B. Friman, Phys. Lett. B 648 (2007) 176.
- [97] K. Hebeler et al., Phys. Rev. C 80 (2009) 044321.
- [98] S.D. Glazek and K.G. Wilson, Phys. Rev. D 48 (1993) 5863.
- [99] F. Wegner, Ann. Phys. (Leipzig) 3 (1994) 77.
- [100] S. Szpigel and R.J. Perry, in Quantum Field Theory, A 20th Century Profile, Ed. A.N. Mitra, Hindustan Publishing Company, New Delhi, 2000, arXiv:hep-ph/0009071.
- [101] R. Roth et al., Phys. Rev. C 72 (2005) 034002.
- [102] S. Kehrein, The Flow Equation Approach to Many-Particle Systems (Springer, Berlin, 2006).
- [103] S.D. Glazek and R.J. Perry, Phys. Rev. D 78 (2008) 045011.
- [104] E. Anderson et al., Phys. Rev. C 77 (2008) 037001.
- [105] E.L. Gubankova, H.C. Pauli and F.J. Wegner, arXiv:hep-th/9809143.
- [106] E. Gubankova, C.R. Ji and S.R. Cotanch, Phys. Rev. D 62 (2000) 074001.
- [107] R. Roth, S. Reinhardt and H. Hergert, Phys. Rev. C 77 (2008) 064003.
- [108] W.C. Haxton and T. Luu, Phys. Rev. Lett. 89 (2002) 182503.
- [109] T.C. Luu et al., Phys. Rev. C 70 (2004) 014316.
- [110] W.C. Haxton, arXiv:nucl-th/0608017.
- [111] W.C. Haxton, arXiv:arXiv:0710.0289.
- [112] H. Feldmeier et al., Nucl. Phys. A 632 (1998) 61.
- [113] R. Roth et al., Nucl. Phys. A 745 (2004) 3.
- [114] R. Roth et al., Phys. Rev. C 73 (2006) 044312.

- [115] H. Hergert and R. Roth, Phys. Rev. C 75 (2007) 051001.
- [116] H. Hergert and R. Roth, private communication.
- [117] P. Navratil, J.P. Vary and B.R. Barrett, Phys. Rev. C 62 (2000) 054311.
- [118] A. Nogga et al., Phys. Rev. C 73 (2006) 064002.
- [119] S. Fujii, R. Okamoto and K. Suzuki, J. Phys. Conf. Ser. 20 (2005) 83.
- [120] S. Fujii, R. Okamoto and K. Suzuki, Phys. Rev. C 69 (2004) 034328.
- [121] S. Fujii, R. Okamoto and K. Suzuki, Prog. Theor. Phys. 104 (2000) 123.
- [122] S. Fujii, R. Okamoto and K. Suzuki, Phys. Rev. Lett. 103 (2009) 182501.
- [123] M. Baldo, in Nuclear Methods and the Nuclear Equation of State, International Review of Nuclear Physics, Vol. 8, World Scientific, 1999.
- [124] W.H. Dickhoff and C. Barbieri, Prog. Part. Nucl. Phys. 52 (2004) 377.
- [125] E. Braaten and A. Nieto, Phys. Rev. B 56 (1997) 14745.
- [126] H.W. Hammer and R.J. Furnstahl, Nucl. Phys. A 678 (2000) 277.
- [127] U. van Kolck, Phys. Rev. C 49 (1994) 2932.
- [128] E. Epelbaum et al., Phys. Rev. C 66 (2002) 064001.
- [129] D.R. Entem and R. Machleidt, arXiv:nucl-th/0303017.
- [130] S. Ishikawa and M.R. Robilotta, Phys. Rev. C 76 (2007) 014006.
- [131] V. Bernard et al., Phys. Rev. C 77 (2008) 064004.
- [132] A. Schwenk, J. Phys. G 31 (2005) S1273.
- [133] A. Nogga, private communication.
- [134] S.C. Pieper et al., Phys. Rev. C 64 (2001) 014001.
- [135] W. Glöckle, The Quantum Mechanical Few-Body Problem (Springer-Verlag, Berlin, 1983).
- [136] P. Navratil and B.R. Barrett, Phys. Rev. C 54 (1996) 2986.
- [137] S.K. Bogner, R.J. Furnstahl and R.J. Perry, Annals Phys. 323 (2008) 1478.
- [138] E.D. Jurgenson and R.J. Furnstahl, Nucl. Phys. A 818 (2009) 152.
- [139] D. Gazit, S. Quaglioni and P. Navratil, Phys. Rev. Lett. 103 (2009) 102502.
- [140] P. Navratil, Few Body Syst. 41 (2007) 117.
- [141] S. Bogner, in preparation.
- [142] K. Tsukiyama, S. Bogner and A. Schwenk, in preparation.
- [143] S.R. White, J. Chem. Phys. 117 (2002) 7472.

- [144] I. Stetcu et al., Phys. Rev. C 71 (2005) 044325.
- [145] P. Navratil, G.P. Kamuntavicius and B.R. Barrett, Phys. Rev. C 61 (2000) 044001.
- [146] E. Anderson et al., in preparation.
- [147] R.J. Furnstahl and H.W. Hammer, Phys. Lett. B 531 (2002) 203.
- [148] A. Gezerlis and J. Carlson, Phys. Rev. C 77 (2008) 032801.
- [149] S. Giorgini, L.P. Pitaevskii and S. Stringari, Rev. Mod. Phys. 80 (2008) 1215.
- [150] M. Bender, P.H. Heenen and P.G. Reinhard, Rev. Mod. Phys. 75 (2003) 121.
- [151] J.M. Lattimer and M. Prakash, Astrophys. J. 550 (2001) 426.
- [152] A. Mezzacappa, Ann. Rev. Nucl. Part. Sci. 55 (2005) 467.
- [153] C.J. Horowitz and A. Schwenk, Nucl. Phys. A 776 (2006) 55.
- [154] G. Röpke, L. Münchow and H. Schulz, Nucl. Phys. A 379 (1982) 536.
- [155] B.L. Friman, J. Niskanen and E.M. Nyman, Nucl. Phys. A 383 (1982) 285.
- [156] B.D. Day, Rev. Mod. Phys. 39 (1967) 719.
- [157] J. Kuckei et al., Nucl. Phys. A 723 (2003) 32.
- [158] H.S. Kohler, arXiv:nucl-th/0511030.
- [159] P. Bozek, D.J. Dean and H. Muther, Phys. Rev. C 74 (2006) 014303.
- [160] J. Margueron, E.N.E. van Dalen and C. Fuchs, Phys. Rev. C 76 (2007) 034309.
- [161] P. Gogelein et al., Phys. Rev. C 79 (2009) 024308.
- [162] L.W. Siu et al., Phys. Rev. C 79 (2009) 054004.
- [163] E.N.E. van Dalen and H. Muther, Phys. Rev. C 80 (2009) 037303.
- [164] A. Lejeune, U. Lombardo and W. Zuo, Phys. Lett. B 477 (2000) 45.
- [165] M. Lutz, B. Friman and C. Appel, Phys. Lett. B 474 (2000) 7.
- [166] N. Kaiser, S. Fritsch and W. Weise, Nucl. Phys. A 697 (2002) 255.
- [167] S. Fritsch, N. Kaiser and W. Weise, Nucl. Phys. A 750 (2005) 259.
- [168] N. Kaiser, M. Muhlbauer and W. Weise, Eur. Phys. J. A 31 (2007) 53.
- [169] S.K. Bogner, R.J. Furnstahl and L. Platter, Eur. Phys. J. A 39 (2009) 219.
- [170] L. Tolos, B. Friman and A. Schwenk, Nucl. Phys. A 806 (2008) 105.
- [171] D.W.E. Blatt and B.H.J. McKellar, Phys. Rev. C 11 (1975) 614.
- [172] S.A. Coon et al., Nucl. Phys. A 317 (1979) 242.

- [173] J.W. Holt, N. Kaiser and W. Weise, Phys. Rev. C 81 (2010) 024002.
- [174] A.W. Steiner et al., Phys. Rept. 411 (2005) 325.
- [175] A. Schwenk, G.E. Brown and B. Friman, Nucl. Phys. A 703 (2002) 745.
- [176] A. Schwenk, B. Friman and G.E. Brown, Nucl. Phys. A 713 (2003) 191.
- [177] A. Schwenk and B. Friman, Phys. Rev. Lett. 92 (2004) 082501.
- [178] A. Schwenk, Int. J. Mod. Phys. B 20 (2006) 2724.
- [179] D.G. Yakovlev and C.J. Pethick, Ann. Rev. Astron. Astrophys. 42 (2004) 169.
- [180] D. Blaschke, H. Grigorian and D.N. Voskresensky, Astron. Astrophys. 424 (2004) 979.
- [181] D. Page et al., Astrophys. J. Suppl. 155 (2004) 623.
- [182] E.M. Cackett et al., Mon. Not. Roy. Astron. Soc. 372 (2006) 479.
- [183] E.M. Cackett et al., Astrophys. J. 687 (2008) L87.
- [184] E.F. Brown and A. Cumming, Astrophys. J. 698 (2009) 1020.
- [185] W. Zuo et al., Phys. Lett. B 595 (2004) 44.
- [186] M. Baldo et al., Phys. Rev. C 58 (1998) 1921.
- [187] J. Wambach, T.L. Ainsworth and D. Pines, Nucl. Phys. A 555 (1993) 128.
- [188] T. Duguet and T. Lesinski, AIP Conf. Proc. 1165 (2009) 243.
- [189] A. Sedrakian et al., Phys. Lett. B 576 (2003) 68.
- [190] N. Kaiser, T. Niksic and D. Vretenar, Eur. Phys. J. A 25 (2005) 257.
- [191] S. Baroni, A.O. Macchiavelli and A. Schwenk, arXiv:0912.0697.
- [192] A. Gezerlis and J. Carlson, Phys. Rev. C 81 (2010) 025803.
- [193] L.P. Gorkov and T.K. Melik-Barkhudarov, Sov. Phys. JETP 13 (1961) 1018.
- [194] H. Heiselberg et al., Phys. Rev. Lett. 85 (2000) 2418.
- [195] F. Barranco et al., Eur. Phys. J. A 21 (2004) 57.
- [196] A. Pastore et al., Phys. Rev. C 78 (2008) 024315.
- [197] R. Shankar, Rev. Mod. Phys. 66 (1994) 129.
- [198] D. Page et al., Astrophys. J. 707 (2009) 1131.
- [199] G. Hagen et al., Phys. Rev. Lett. 101 (2008) 092502.
- [200] R.J. Bartlett and M. Musiał, Rev. Mod. Phys. 79 (2007) 291.
- [201] J.R. Gour et al., Phys. Rev. C 74 (2006) 024310.



- [202] G. Hagen et al., Phys. Rev. C 76 (2007) 034302.
- [203] L.B. Wang et al., Phys. Rev. Lett. 93 (2004) 142501.
- [204] M. Brodeur et al., in preparation.
- [205] P. Mueller et al., Phys. Rev. Lett. 99 (2007) 252501.
- [206] V.L. Ryjkov et al., Phys. Rev. Lett. 101 (2008) 012501.
- [207] A.P. Zuker, Phys. Rev. Lett. 90 (2003) 042502.
- [208] J.E. McAninch et al., Phys. Lett. B 307 (1993) 13.
- [209] A. Deltuva, A.C. Fonseca and S.K. Bogner, Phys. Rev. C 77 (2008) 024002.
- [210] H. Witała et al., Phys. Rev. C 63 (2001) 024007.
- [211] A. Kievsky, M. Viviani and S. Rosati, Phys. Rev. C 64 (2001) 024002.
- [212] J. Kuros-Zolnierz et al., Phys. Rev. C 66 (2002) 024004.
- [213] A. Deltuva, R. Machleidt and P.U. Sauer, Phys. Rev. C 68 (2003) 024005.
- [214] A. Deltuva, A.C. Fonseca and P.U. Sauer, Phys. Rev. Lett. 95 (2005) 092301.
- [215] A. Deltuva, A.C. Fonseca and P.U. Sauer, Phys. Rev. C 72 (2005) 054004.
- [216] A. Deltuva, A.C. Fonseca and P.U. Sauer, Phys. Rev. C 71 (2005) 054005.
- [217] A. Deltuva and A.C. Fonseca, Phys. Rev. C 75 (2007) 014005.
- [218] G.G. Raffelt, Stars as Laboratories for Fundamental Physics: The Astrophysics of Neutrinos, Axions, and Other Weakly Interacting Particles (University of Chicago Press, Chicago, 1996).
- [219] M. Prakash et al., Ann. Rev. Nucl. Part. Sci. 51 (2001) 295.
- [220] G.I. Lykasov, C.J. Pethick and A. Schwenk, Phys. Rev. C 78 (2008) 045803.
- [221] S. Bacca et al., Phys. Rev. C 80 (2009) 032802.
- [222] S. Hannestad and G. Raffelt, Astrophys. J. 507 (1998) 339.
- [223] P. Navratil, S. Quaglioni and R. Roth, in preparation.
- [224] S. Quaglioni and P. Navratil, Phys. Rev. Lett. 101 (2008) 092501.
- [225] S. Quaglioni and P. Navratil, Phys. Rev. C 79 (2009) 044606.
- [226] S. Bogner, T.T.S. Kuo and L. Coraggio, Nucl. Phys. A 684 (2001) 432.
- [227] S. Bogner et al., Phys. Rev. C 65 (2002) 051301.
- [228] G. Hagen, M. Hjorth-Jensen and N. Michel, Phys. Rev. C 73 (2006) 064307.
- [229] N. Michel et al., J. Phys. G 36 (2009) 013101.
- [230] K. Tsukiyama, M. Hjorth-Jensen and G. Hagen, Phys. Rev. C 80 (2009) 051301.

- [231] T. Otsuka et al., arXiv:0908.2607.
- [232] Y. Utsuno et al., Phys. Rev. C 60 (1999) 054315.
- [233] Y. Utsuno et al., Phys. Rev. C 70 (2004) 044307.
- [234] B.A. Brown and W.A. Richter, Phys. Rev. C 74 (2006) 034315.
- [235] G.F. Bertsch, B. Sabbey and M. Uusnakki, Phys. Rev. C 71 (2005) 054311.
- [236] M. Kortelainen et al., Phys. Rev. C 77 (2008) 064307.
- [237] R. Fukuda et al., Prog. Theor. Phys. 92 (1994) 833.
- [238] M. Valiev and G.W. Fernando, Phys. Lett. A 227 (1997) 265.
- [239] S.J. Puglia, A. Bhattacharyya and R.J. Furnstahl, Nucl. Phys. A 723 (2003) 145.
- [240] A. Bhattacharyya and R.J. Furnstahl, Nucl. Phys. A 747 (2005) 268.
- [241] A. Bhattacharyya and R.J. Furnstahl, Phys. Lett. B 607 (2005) 259.
- [242] R.J. Furnstahl, J. Phys. G 31 (2005) S1357.
- [243] J. Polonyi and K. Sailer, Phys. Rev. B 66 (2002) 155113.
- [244] A. Schwenk and J. Polonyi, arXiv:nucl-th/0403011.
- [245] N. Kaiser, S. Fritsch and W. Weise, Nucl. Phys. A 724 (2003) 47.
- [246] T. Lesinski and T. Duguet, private communication.
- [247] S.R. Beane, arXiv:0812.1236.
- [248] T. Hatsuda, arXiv:0909.5637.
- [249] R.D. Amado, Phys. Rev. C 19 (1979) 1473.
- [250] J.L. Friar, Phys. Rev. C 20 (1979) 325.
- [251] O. Benhar and V.R. Pandharipande, Phys. Rev. C 47 (1993) 2218.
- [252] L. Frankfurt, M. Sargsian and M. Strikman, Int. J. Mod. Phys. A 23 (2008) 2991.
- [253] L. Frankfurt, M. Sargsian and M. Strikman, AIP Conf. Proc. 1056 (2008) 322.
- [254] R. Schiavilla et al., Phys. Rev. Lett. 98 (2007) 132501.
- [255] M. Alvioli, C. Ciofi degli Atti and H. Morita, Phys. Rev. Lett. 100 (2008) 162503.
- [256] F.G. Perey and B. Buck, Nucl. Phys. A 32 (1962) 353.
- [257] T.S. Walhout, Phys. Rev. D 59 (1999) 065009.
- [258] B.J. Schaefer et al., Phys. Rev. C 73 (2006) 011001.
- [259] M. Kohno et al., Phys. Rev. C 76 (2007) 064002.
- [260] H. Dapo, B.J. Schaefer and J. Wambach, Eur. Phys. J. A 36 (2008) 101.